AAAS
Ultrafast Science
Volume 2022, Article ID 9895418, 51 pages
https://doi.org/10.34133/2022/9895418

Ultrafast Science
A SCIENCE PARTNER JOURNAL

Review Article

Nature-Inspired Superwettability Achieved by Femtosecond Lasers

Jiale Yong,[1] Qing Yang,[2] Xun Hou,[1] and Feng Chen[1]

[1]*State Key Laboratory for Manufacturing System Engineering and Shaanxi Key Laboratory of Photonics Technology for Information, School of Electronic Science and Engineering, Xi'an Jiaotong University, Xi'an 710049, China*
[2]*School of Mechanical Engineering, Xi'an Jiaotong University, Xi'an 710049, China*

Correspondence should be addressed to Feng Chen; chenfeng@mail.xjtu.edu.cn

Received 10 September 2021; Accepted 3 November 2021; Published 7 February 2022

Wettability is one of a solid surface's fundamental physical and chemical properties, which involves a wide range of applications. Femtosecond laser microfabrication has many advantages compared to traditional laser processing. This technology has been successfully applied to control the wettability of material surfaces. This review systematically summarizes the recent progress of femtosecond laser microfabrication in the preparation of various superwetting surfaces. Inspired by nature, the superwettabilities such as superhydrophilicity, superhydrophobicity, superamphiphobicity, underwater superoleophobicity, underwater superaerophobicity, underwater superaerophilicity, slippery liquid-infused porous surface, underwater superpolymphobicity, and supermetalphobicity are obtained on different substrates by the combination of the femtosecond laser-induced micro/nanostructures and appropriate chemical composition. From the perspective of biomimetic preparation, we mainly focus the methods for constructing various kinds of superwetting surfaces by femtosecond laser and the relationship between different laser-induced superwettabilities. The special wettability of solid materials makes the femtosecond laser-functionalized surfaces have many practical applications. Finally, the significant challenges and prospects of this field (femtosecond laser-induced superwettability) are discussed.

1. Introduction

Wettability is one of the physical and chemical properties of a solid surface. In particular, the surface with special wettability is beautiful [1–10]. Over billions of years of evolution, many organisms in nature have exhibited unique surface wettability [11–13]. For example, lotus leaves have the self-cleaning function [14, 15]. Water striders can walk on water [16]. Butterflies can fly in the rain [17]. Mosquito eyes can prevent fog [18]. Fish cannot be contaminated by oil underwater [19, 20]. Desert beetles [21], cacti [22], and spider silk [23] can collect water mist. It was not until the late twentieth and early twenty-first century that the causes of these extreme wettabilities were understood with the development of microscopy and microanalysis techniques. The study shows that the wettability of the material surface mainly depends on the chemical composition and the microstructure of the solid surface [24–28]. Due to its key role in solving the problems related to energy, environment, resources, and health, superwettability has become one of the hot research directions in materials and micro/nanomanufacturing [29–33]. Nature is the best teacher for scientists and engineers, inspiring countless ideas to design new materials and develop new technologies. Inspired by these extreme wetting phenomena in nature, a series of super wettabilities has been achieved based on different micro/nanomachining methods, such as mechanical processing method, lithography, chemical etching, template method, plasma etching method, vapor deposition method, electrochemical method, sol-gel method, electrospinning method, electrochemical deposition, self-assembly, and spray/dip coating [1–10]. The developed superwettability has been widely applied in antiliquids [34, 35], self-cleaning [14, 36, 37], manipulation of liquid droplets [38, 39], oil/water separation [40–43], lab chip [44, 45], anti-icing/fogging/snowing [46, 47], cell engineering [48, 49], antifouling [50], water harvesting [51, 52], liquid patterning [53], anticorrosion [54, 55], microfluidics [56, 57], drag reduction [58, 59], buoyancy enhancement

[60, 61], and so on. Although the most traditional micro/nanoprocessing methods can be used to achieve superwettability, these methods are more or less subject to certain inherent limitations, such as complex preparation steps, limited to specific materials, and lack of flexibility. It is still a great challenge to develop a versatile and simple tool/method to produce various superwetting microstructures on any solid substrates.

The laser is one of the greatest inventions of the 20th century. With the development of ultrafast science [62], the interaction between ultrafast laser and matter has become a research hotspot [63]. Femtosecond (10^{-15} s) laser, as an advanced ultrashort pulsed laser, has two features of ultra-short pulse width and extremely high peak intensity [64–67]. In recent years, the femtosecond laser has become an essential tool for modern extreme and ultra-precision manufacturing. Femtosecond laser processing has the characteristics of high spatial resolution, small heat-affected zone, and noncontact manufacturing [64–67]. In particular, the femtosecond laser can ablate almost any material, resulting in microstructures on the material's surface. Femtosecond laser also has advantages in the fine design of micro/nanostructure. Because the surface microstructure has a significant effect on the wettability of solid substrates, femtosecond laser processing is used to form special microscale and nanoscale structures on substrate surfaces and obtain various superwettabilities [68–71]. Femtosecond laser shows a powerful ability to design and modify the wettability of materials.

This review will summarize the research progress of the superwettability achieved by femtosecond laser processing (Figure 1). The basic concepts and the typical wetting models in the field of surface wettability and the characteristics of femtosecond laser microfabrication are introduced as background (Section 2). Inspired by nature, a series of superwettabilities have been obtained on different substrates by combing the femtosecond laser-induced microstructure and appropriate chemical composition. The extreme wettability to water includes superhydrophilicity and superhydrophobicity (Section 3). The superhydrophilic structure can be thoroughly wetted by water, and the superhydrophobic surface has a robust repulsive effect on water. There are two completely different types of superoleophobic surfaces (Section 4). The superamphiphobic surfaces can repel oils in the air, and the underwater superoleophobic surfaces only repel oil in water. The bubble wettability of solid surfaces in water is then introduced (Section 5). The underwater superaerophobic surface and the underwater superaerophilic surface can repel or absorb bubbles in an aqueous liquid, respectively. The slippery liquid-infused porous surface (SLIPS) also exhibits excellent repellence against various pure or composite liquids by forming a trapped lubricating film on the porous structure (Section 6). The repellence of the laser-induced microstructures to other special fluids such as liquid polymer and liquid metal is also introduced (Section 7). The concepts of underwater superpolymphobicity and supermetalphobicity were put forward only in the past two years. In addition to the detailed preparation methods, we also show the rich applications of these superwetting surfaces. Finally, the current challenges and prospects for the realization and application of different femtosecond laser-induced superwettabilities are briefly discussed (Section 8).

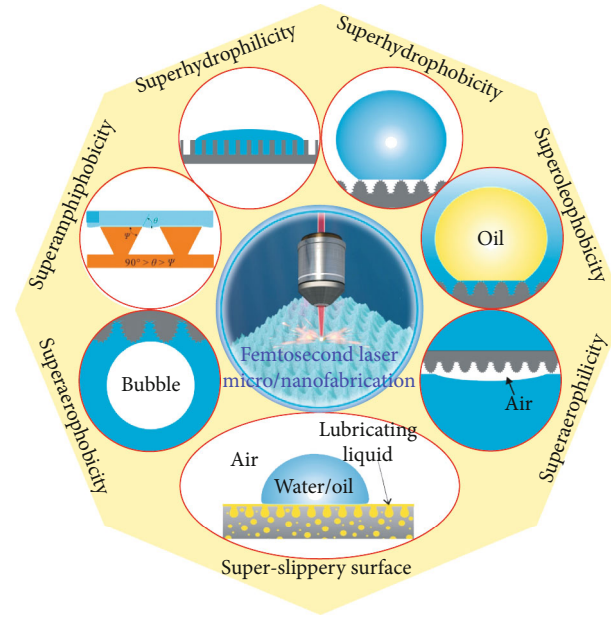

FIGURE 1: Various femtosecond laser-induced extreme wettabilities.

2. Background

2.1. Basic Wetting Theory. When a liquid droplet comes in contact with a solid surface in the air, a three-phase contact line is formed at the junction of the solid, liquid, and gas phases. The contact line continues to expand outward until the droplet reaches a static state. For a droplet on the solid surface, the angle formed between the solid-liquid contact surface and the tangent line of the droplet at the three-phase line is called contact angle (CA) [72–74]. Taking water droplets as an example, when CA is less than 90°, the surface is hydrophilic; when CA is greater than 90°, the surface is hydrophobic. In the extreme state, the CA of droplets on the superhydrophilic surface is less than 10°, while the CA of droplets on the superhydrophobic surface is more than 150°. The CA value can reflect the static wetting characteristics of the solid surface. On the other hand, dynamic wettability is usually characterized by a sliding angle (SA). The sample is gradually tilted until the droplet can roll away or slide down. The tilted angle is called SA [72–74]. The surface with large SA value has high adhesion to liquid. In contrast, the surface with low SA has very low adhesion to liquid.

Young described the effect of the interface energy on the wettability of an ideally smooth surface. As shown in Figure 2(a), the CA (θ) of the liquid droplet on the smooth surface can be expressed as [75, 76]:

$$\cos\theta = \frac{\gamma_{SA} - \gamma_{SL}}{\gamma_{LA}}, \tag{1}$$

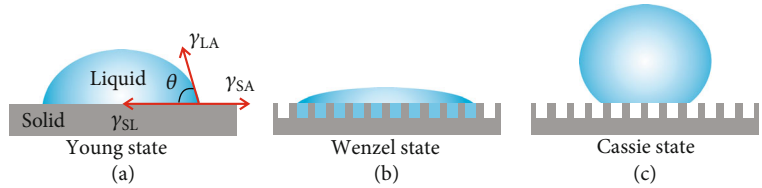

FIGURE 2: Typical wetting state of a liquid droplet on a solid surface. (a) Droplet on a flat substrate. (b) Droplet on the rough substrate and the liquid fills in the surface microstructures. (c) Droplet on the rough substrate and the liquid cannot penetrate in the surface microstructures.

where γ_{SA}, γ_{SL}, and γ_{LA} are the surface free energies at the solid/air interface, solid/liquid interface, and liquid/air interface, respectively.

Most surfaces are not smooth and have roughness. The rough surface microstructure has an essential effect on the wettability of the solid surface. Wenzel pointed out that the rough structure can significantly increase the contact area between liquid and the solid surface when the solid surface is wetted by the liquid (Figure 2(b)) [77]. He improved Young's formula by introducing the roughness factor (R, the ratio of total surface area to projected area). In Wenzel state, the CA (θ^*) of droplets on the rough surface can be described as [72, 78]:

$$\cos\theta^* = \frac{R(\gamma_{SA} - \gamma_{SL})}{\gamma_{LA}} = R\cos\theta, \quad (2)$$

where θ is Young's CA of the droplet on the corresponding smooth surface. In this wetting state, the liquid thoroughly fills the gaps in the rough microstructure. Because the actual surface area of a rough solid surface is greater than its apparent surface area ($R > 1$), it can be concluded from this formula that rough microstructure can amplify the intrinsic surface wettability of the solid substrate [72, 75].

Cassie et al. proposed an alternative model that reflects the contact state between a liquid and a rough surface when the liquid cannot penetrate the concave cavity of the rough microstructure (Figure 2(c)) [76, 79]. The liquid is on a composite surface consisting of solid and air. The space of the surface microstructure is filled with air, creating a layer of air trapped beneath the liquid. The apparent CA (θ^*) of the liquid droplet on the composite interface satisfies the following formula [72, 79]:

$$\cos\theta^* = f\cos\theta + f - 1, \quad (3)$$

where θ is Young's CA and f is the area fraction of the solid surface in contact with the liquid. Since the trapped air cushion significantly reduces the solid/gas contact area and disconnects the contact line, the surface in the Cassie state has very low adhesion to the liquid droplet.

2.2. Ultrafast Laser Microfabrication. Ultrafast laser has an extremely short pulse width. Among the laser pulses with different duration/widths, femtosecond (10^{-15} s) laser has been proven to be an effective and powerful tool in advanced microfabrication and nanofabrication. Because the laser pulse is compressed to a very short femtosecond magnitude, the femtosecond laser has a very high peak power, which can reach 10^{14} W [64–67]. The ultrashort pulse width and ultrahigh peak power density are the two main features of femtosecond laser [64, 65]. When the femtosecond laser pulses are focused on an area of space smaller than the diameter of a human hair, the light intensity can reach the magnitude of 10^{22} W/cm^2. The ultrahigh peak power fluence makes the interaction between the femtosecond laser and the solid material very different from that of the traditional lasers [66, 67].

The unique features of ultrashort pulse width and extremely high peak intensity enable femtosecond laser microfabrication to have many definite advantages against the traditional laser processing techniques, such as a minimal heat-affected zone formation around the ablated area, noncontact manufacturing, high spatial resolution, and versatility in terms of the materials that can be processed. The femtosecond laser can directly excite the material to the plasma state, resulting in the "cold" etching of the material. This process dramatically reduces the photothermal effect which usually causes the low-machining-accuracy and bad-material-selectivity problems. The interaction between femtosecond laser and the solid substrate is a complex nonlinear process. Only in the limited region near the center of the focal spot, the area where the laser energy is higher than the threshold of multi-photon reaction can be processed, thereby achieving superfine micro/nanoprocessing of the material. Figures 3(a) and 3(b) show the morphology of the laser-drilled microhole structures on the steel foil (thickness of 100 μm). The samples were ablated by a nanosecond laser (pulse width of 3.3 ns) and a femtosecond laser (pulse width of 200 fs), respectively [80]. Severe swelling resulted from melting forms around the nanosecond laser-induced microhole (Figure 3(a)). In contrast, the edge of the femtosecond laser-induced microhole was very sharp, and its wall was steep (Figure 3(b)). The contrast effect can also be verified on the transparent material surfaces. As shown in Figures 3(c) and 3(d), the quality of the produced microstructure on the NaCl surface by 300 fs laser is much better than that produced by 16 ns [81]. The results demonstrate a limited heat-affected zone and high precision during femtosecond laser micromachining. The nonlinear process (such as multiphoton absorption or tunneling ionization) also allows the femtosecond laser to ablate a wide range of materials, no matter the opaque or the transparent materials, including semiconductors, metals, polymers, brittle materials (e.g., glasses), ceramics, and biomaterials (e.g., tissues) [82–88]. Microscale and nanoscale structures can be directly

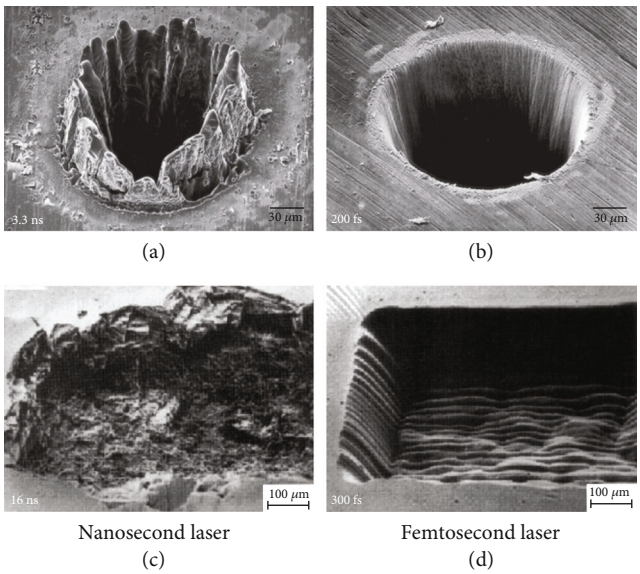

FIGURE 3: Morphology of the laser-drilled microhole structures. (a, b) Steel foil with thickness of 100 μm: (a) pulse width of 3.3 ns and (b) pulse width of 200 fs. (c, d) Monocrystalline sodium chloride (NaCl) surface: (c) pulse width of 16 ns and (d) pulse width of 300 fs. Reproduced from [80, 81] with the permission.

prepared on the sample surface through one-step laser ablation. Femtosecond laser microfabrication has already been successfully applied in high-quality, high-precision surface micro/nanomachining, such as drilling, cutting, nanograting, surface patterning and texturing, and micro/nanostructuring [64–67].

Figures 4(a) and 4(b) schematically depict the laser processing systems [89, 90]. The former system is based on an objective lens, and the latter is based on a plane-convex lens. The samples are fixed on a program-controlled translation platform. The laser beam is focused onto the sample surface by the optical lens. A variable attenuator is used to adjust the energy of the focused laser. An electromechanical shutter is used to control the off/on of the laser beam. The line-by-line scanning manner is often adopted to ensure that the whole surface of the substrate is ablated by the focused laser beam, as shown in Figure 4(c). The interaction between femtosecond laser and matter is a nonlinear process. Taking the silicon substrate as an example, when the laser pulses are irradiated on the sample surface, the nonlinear absorption triggers the multiphoton/avalanche ionization [91, 92]. Part of laser energy is absorbed by electrons. The absorbed energy is further transferred from electrons to the crystal lattice and then diffuses into the material. The temperature of the focal spot is extremely high because of the absorption of the laser energy. On the other hand, the generated plasma is restricted to a limited region, resulting in very high plasma pressure. As the plasma with high pressure and high temperature instantaneously expands and bursts out of the ablation spot, the ionized materials are removed from the substrate surface. The ejection of the ablated material results in permanent damage of the substrate and generates various rough surface microstructures on the substrate (Figure 4(d)). When part of the ejected molten particles fall back, fine nanoprotrusions will further self-assembly cover on the ablated surface after the solidification of the ejected particles, known as the resolidification/crystallization/casting process [92]. As a result, micro/nanostructures are formed on the sample surface after femtosecond laser processing.

Hierarchical micro/nanoscale structures can be created directly on the surface of various materials by simple femtosecond laser ablation. Because the laser processing position, the scanning speed, and the scanning track can be precisely controlled by the program, various 2D patterns and 3D microstructures can be easily designated and produced without expensive masks, as shown in Figure 5. Since the surface morphology and chemical composition mainly determine the surface wettability, these patterned microstructures usually exhibit various unique wettabilities. Femtosecond laser microfabrication has been successfully applied in surface science to design and change the surface wettability of solid materials in the past decade. The crucial parameters in laser processing include laser energy, scanning speed, and the interval/shift of the scanning lines. Table 1 shows the main parameters adopted to fabricate superwetting surfaces introduced in this review.

3. Superhydrophilicity and Superhydrophobicity

3.1. Superhydrophilic Surfaces. Surface wettability determines the behavior of liquids on solid surfaces. Vorobyev and Guo improved the surface wettability of metal substrates by using high-intensity femtosecond laser pulses to construct metal surfaces [96]. The laser pulses are horizontally polarized and focused on the surface of the platinum plate. The scanning manner was used to extend the structured area of the laser beam horizontally, followed by a vertical shift. Multiple parallel microgrooves were formed on the metal sample surface (Figure 6(a)). The period of the microgrooves is 100 μm, corresponding to the interval between two scanning lines. The ridges and valleys of the microgrooves are covered with porous micro/nanostructures (Figure 6(b)). The nanoprotrusions and nanocavities aggregate into microscale structures. The microcavities and the microscale aggregates are fused on the metal surface (Figures 6(c) and 6(d)). With the formation of the micro/nanoscale hierarchical structure, the optical properties of the metal surface change significantly due to the rough microstructure, resulting in the black surface of the metal. Figure 6(e) shows the wetting process of a large methanol droplet contacting with the structured platinum. The liquid quickly spreads and flows along the microgrooves. Interestingly, when the sample is placed vertically at 90°, the fluid can move uphill against gravity. Different from the grooved structure, methanol droplet spread uniformly in all directions on the platinum sample with orthogonally crossed microgrooves.

Microgroove array can also be produced on the silicon surface by femtosecond laser processing (Figure 6(f)) [97]. The surface of the microgroove is covered with micro/nanostructures. When a water droplet is dripped onto the treated area of the silicon surface, the droplet spreads and quickly

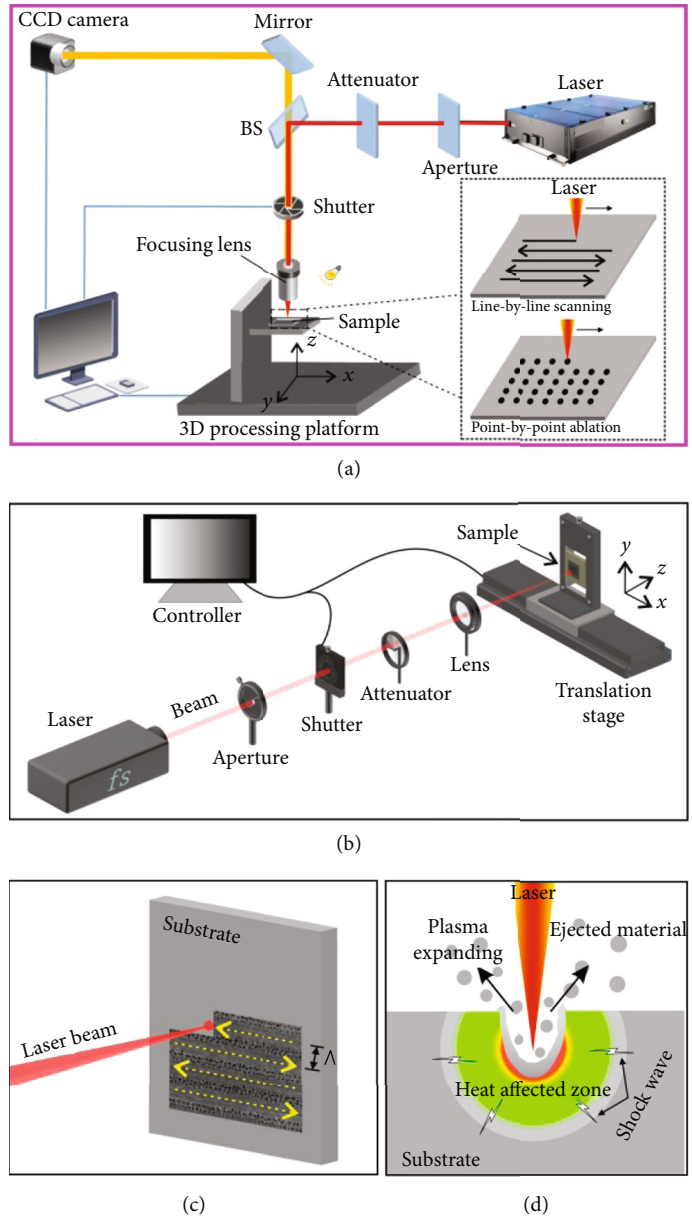

FIGURE 4: Schematic of the laser processing system. (a) Using an objective lens to focus the laser beam. (b) Using a plane-convex lens to focus the laser beam. (c) The line-by-line laser scanning manner. (d) The interaction between femtosecond laser and solid substrate. Reproduced from [89, 90, 93] with the permission.

wets the surface. The water can move 22 mm forward along the microgrooves in about 0.6 s. When a drop of water comes in contact with the bottom of the vertically placed sample, the water immediately spreads upward at a high velocity on the silicon surface, as shown in Figure 6(g).

The water-uphill process was also observed on the femtosecond laser-structured glass surface [98]. The glass surface is originally hydrophilic. The CA of a water droplet on the smooth glass surface is 15°. When the multiple parallel microgrooves were prepared on the glass surface (Figure 6(h)), water droplets can thoroughly wet the rough structures with a water CA (WCA) of 0°. The water droplet can also move uphill along the microgrooves of the glass surface when the surface is vertical (Figure 6(i)).

The results demonstrate that femtosecond laser-induced micro/nanostructures turn metals, silicon, and glass superhydrophilic for volatile liquids and water. Liquids can easily wet the laser-structured surface. These substrates are inherently hydrophilic. According to the Wenzel equation, the rough surface microstructure can enhance the natural wettability of a solid surface [72]. The hydrophilicity is amplified to superhydrophilicity by the surface micro/nanostructures. Therefore, the laser-ablated hydrophilic substrates usually exhibit strong superhydrophilicity.

3.2. Superhydrophobic Surfaces. In the eyes of Asians, lotus leaves (Figure 7(a)) are a symbol of sanctity because they grow on the silt but are not imbrued. Raindrops and

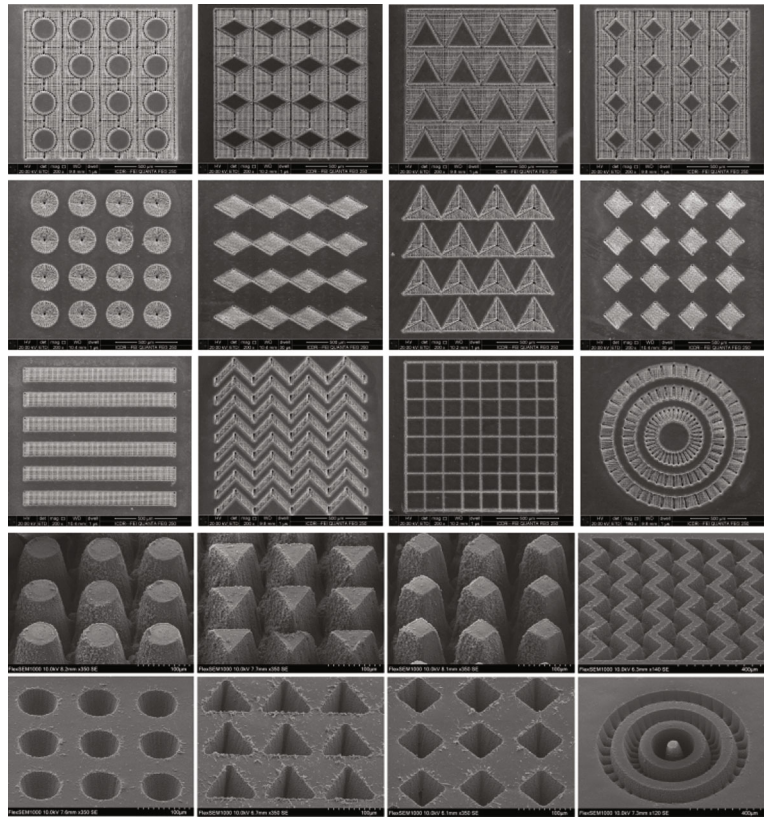

Figure 5: Various 2D patterns and 3D microstructures fabricated by femtosecond laser. Reproduced from [94, 95] with the permission.

dewdrops can curl into a small ball shape on the lotus leaf. When the lotus leaf has a slight shake, the liquid droplets will freely roll down and take the contaminants away from the surface. This phenomenon is called the "self-cleaning effect" or "lotus leaf effect" [14, 36, 37]. The self-cleaning effect is ascribed to the excellent superhydrophobicity of the lotus leaf [14, 15]. Superhydrophobicity generally refers to that water droplet on a solid substrate has a WCA larger than 150°. Figure 7(d) shows the shape of a tiny water droplet on the lotus leaf. The WCA reaches up to 160°. Water droplets can easily roll on the lotus leaf, and the water SA (WSA) is only 2° (Figure 7(e)) [60, 121]. In 1997, Barthlott and Neinhuis revealed the microstructure of the surface of the lotus leaf through a scanning electron microscope (SEM) [14]. It was found that a large number of microscale papillae with a diameter of about 10 μm are randomly distributed on the surface of the lotus leaf (Figure 7(b)) [121]. Each microscale papillae is further covered with rich nanoscale branch-like protrusions with a diameter of ~120 nm, forming a micro/nanoscale hierarchical structure (Figure 7(c)). In addition, the whole surface is coated with a layer of hydrophobic wax crystals which has very low surface energy. The hierarchical microstructure can hold the water droplet up when the water droplet is dripped onto the lotus leaf. An air cushion forms underneath the water droplet, which has excellent repellence to water droplet. The trapped air cushion remarkably reduces the effective contact area between the water droplet and the lotus leaf. The water droplet only touches the top part of the hierarchical microstructure but cannot wet such surface structure, as shown in Figure 7(f). Therefore, the lotus leaf offers excellent water resistance and has superhydrophobicity. The contact between the water droplet and lotus leaf is at the Cassie wetting state [72, 73, 75, 76]. The superhydrophobicity of lotus leaf reveals that the synergistic effect between hierarchical microstructure and low-surface-energy chemical composition results in the superhydrophobicity and extremely low water adhesion.

Two routes are mainly adopted to fabricate superhydrophobic surfaces by imitating the lotus leaf [136–139]. For a hydrophilic substrate, rough microstructures should be created on the material surface first. And, the surface further needs to be modified with the low-surface-energy molecular layer to obtain superhydrophobicity. If the substrate is an intrinsically hydrophobic material, superhydrophobicity can be directly achieved by constructing proper rough microstructures on the material surface.

3.2.1. Silicon Surface. In 2006, Baldacchini et al. obtained superhydrophobicity on silicon surface by femtosecond laser treatment [99]. The *n*-doped Si(100) wafer was firstly fixed in a processing chamber filled with reactive SF_6 gas. Then, the femtosecond laser beam was focused on the silicon surface by a plane-convex lens with a focal length of 25 cm. They found that rough microstructures were formed under femtosecond laser ablation. The height of the microstructures increased with increasing the laser fluence. As the fluence increased to larger than 4.0 kJ/m^2, separated high-

Table 1: Crucial parameters for fabricating superwetting surfaces introduced in this review.

Section in this review	Samples		Parameters of laser system			Processing parameters			References
	Material	Wettability	Pulse duration/ width	Central wavelength	Repetition rate	Laser power	Scanning speed	Interval of scanning lines	
3.1	Platinum, gold	Superhydrophilicity	65 fs	800 nm	1 kHz	1.1 mJ/pulse		100 μm	[96]
3.1	Silicon	Superhydrophilicity	65 fs	800 nm	1 kHz	8.5 J/cm^2	1 mm/s	100 μm	[97]
3.1	Glass	Superhydrophilicity	65 fs	800 nm	1 kHz	1.1 mJ/pulse		100 μm	[98]
3.2	Silicon	Superhydrophobicity	100 fs	800 nm	1 kHz	0.9 J/cm^2			[99]
3.2	Silicon	Superhydrophobicity	180 fs	800 nm	1 kHz	0.37~2.47 J/cm^2			[100]
3.2	Silicon	Superhydrophobicity	30 fs	800 nm	1 kHz	15 mW	2 mm/s	2 μm	[101]
3.2	PDMS	Superhydrophobicity	50 fs	800 nm	1 kHz	30 mW	4 mm/s	10 μm	[102]
3.2	PTFE	Superhydrophobicity, superoleophilicity	50 fs	800 nm	1 kHz	20 mW	5 mm/s	5 μm	[103]
3.2	SMP	Superhydrophobicity	50 fs	800 nm	1 kHz	10 mW, 30 mW	6 mm/s, 4 mm/s	6 μm, 2 μm	[104]
3.2	Different steel and titanium alloys	Superhydrophobicity	150 fs	800 nm	1 kHz	0.78, 2.83, 5.16 J/ cm^2	0.25 mm/s	Spot overlap = 50%, spot size = 30 μm	[105]
3.2	Stainless steel	Superhydrophobicity	130 fs	800 nm	1 kHz	2.4 J/cm^2	1 mm/s	30 μm	[106]
3.2	Platinum, titanium, brass	Superhydrophobicity	65 fs	800 nm	1 kHz	9.8 J/cm^2, 7.6 J/cm^2, 3.9 J/cm^2		100 μm	[107]
3.2	Zinc	Superhydrophobicity	50 fs	800 nm	1 kHz	15 mW	2 mm/s	2 μm	[108]
3.2	K9 glass	Superhydrophobicity	130 fs	800 nm	1 kHz	100~200 mW			[109]
3.2	Soda-lime glass	Superhydrophobicity	183 fs	786 nm	1 kHz	21 mW	5 mm/s	10 μm	[110]
3.2	Silica glass	Superhydrophobicity	800 fs	1030 nm	200 kHz	20-100 μJ/pulse			[111]
4.1	Photoresist	Superamphiphobicity	100 fs	780 nm	80 MHz	50 mW	30 mm/s		[112]
4.1	Copper	Superamphiphobicity	800 fs	1030 nm	200 kHz	30 μJ/pulse (2.65 J/ cm^2)	500 mm/s	40 μm	[113]
4.2	Silicon	Underwater superoleophobicity	50 fs	800 nm	1 kHz	20 mW	2 mm/s	2 μm	[114]
4.2	Silicon	Underwater superoleophobicity	104 fs	800 nm	1 kHz	60 mW	1 mm/s	50 μm	[115]
4.2	Titanium	Underwater superoleophobicity	50 fs	800 nm	1 kHz	15 mW	2 mm/s	2 μm	[95]
4.2	Aluminum, copper, iron, molybdenum, stainless steel	Underwater superoleophobicity	50 fs	800 nm	1 kHz	10 mW	2 mm/s	2 μm	[116]
4.2	Nickel	Underwater superoleophobicity	104 fs	800 nm	1 kHz	190 mW	1 mm/s	50 μm	[117]
4.2	Silica glass	Underwater superoleophobicity	50 fs	800 nm	1 kHz	20 mW	4 mm/s	4 μm	[118]

Table 1: Continued.

Section in this review	Samples		Parameters of laser system			Processing parameters			References
	Material	Wettability	Pulse duration/ width	Central wavelength	Repetition rate	Laser power	Scanning speed	Interval of scanning lines	
4.2	Glass slide	Underwater superoleophobicity	50 fs	800 nm	1 kHz	10 mW, 15 mW	2 mm/s	2 μm	[119, 120]
4.2	PDMS	Underwater superoleophobicity	50 fs	800 nm	1 kHz	40 mW	5 mm/s	5 μm	[89]
5.1	Silicon, aluminum	Underwater superaerophobicity	50 fs	800 nm	1 kHz	15 mW, 30 mW	2 mm/s, 5 mm/s	2 μm, 5 μm	[121]
5.1	Aluminum	Underwater superaerophobicity	67 fs	800 nm	1 kHz	200 mW	2 mm/s	40 μm	[122]
5.1	Stainless steel	Underwater superaerophobicity	67 fs	800 nm	1 kHz	500 mW	1 mm/s	80 μm	[123]
5.1	PDMS	Underwater superaerophobicity	50 fs	800 nm	1 kHz	40 mW, 50 mW	5 mm/s, 8 mm/s	5 μm, 8 μm	[89, 124]
5.2	PDMS	Underwater superaerophilicity	50 fs	800 nm	1 kHz	30 mW	4 mm/s	4 μm	[121]
5.2	PTFE	Underwater superaerophilicity	50 fs	800 nm	1 kHz	30 mW	4 mm/s, 5 mm/s	4 μm, 5 μm	[121, 125]
5.2	Aluminum	Underwater superaerophilicity	67 fs	800 nm	1 kHz	200 mW	2 mm/s	40 μm	[122]
5.2	Stainless steel	Underwater superaerophilicity	67 fs	800 nm	1 kHz	500 mW	1 mm/s	80 μm	[123]
5.2	Silicon	Underwater superaerophilicity	67 fs	800 nm	1 kHz	500 mW	1 mm/s	100 μm	[126]
6.2	PA6	Super-slippery property	50 fs	800 nm	1 kHz	25 mW	4 mm/s	4 μm	[127]
6.2	Epoxy polymer	Super-slippery property	50 fs	800 nm	1 kHz	20 mW	8 mm/s	8 μm	[128]
6.2	PET	Super-slippery property	50 fs	800 nm	1 kHz	30 mW	4 mm/s	4 μm	[129]
6.2	NiTi alloy	Super-slippery property	400 fs	1030 nm	2.5 MHz	4.3 μJ/pulse	12 mm/s	6 μm	[130]
6.2	Stainless steel	Super-slippery property	50 fs	800 nm	1 kHz	80 mW	2 mm/s	2 μm	[131]
6.2	Aluminum alloy	Super-slippery property	104 fs	800 nm	1 kHz	300 mW	1 mm/s	100 μm	[132]
7.1	Stainless steel	Underwater superpolymphobicity	67 fs	800 nm	1 kHz	500 mW	2.5 mm/s	80 μm	[90]
7.1	Silicon, glass, aluminum, copper	Underwater superpolymphobicity	67 fs	800 nm	1 kHz	500 mW	2.5 mm/s	60 μm	[133]
7.2	Silicon, PDMS	Supermetalphobicity	50 fs	800 nm	1 kHz	20 mW	2 mm/s, 4 mm/s	2 μm, 4 μm	[134]
7.2	PDMS	Supermetalphobicity	50 fs	800 nm	1 kHz	20 mW	8 mm/s	8 μm	[135]

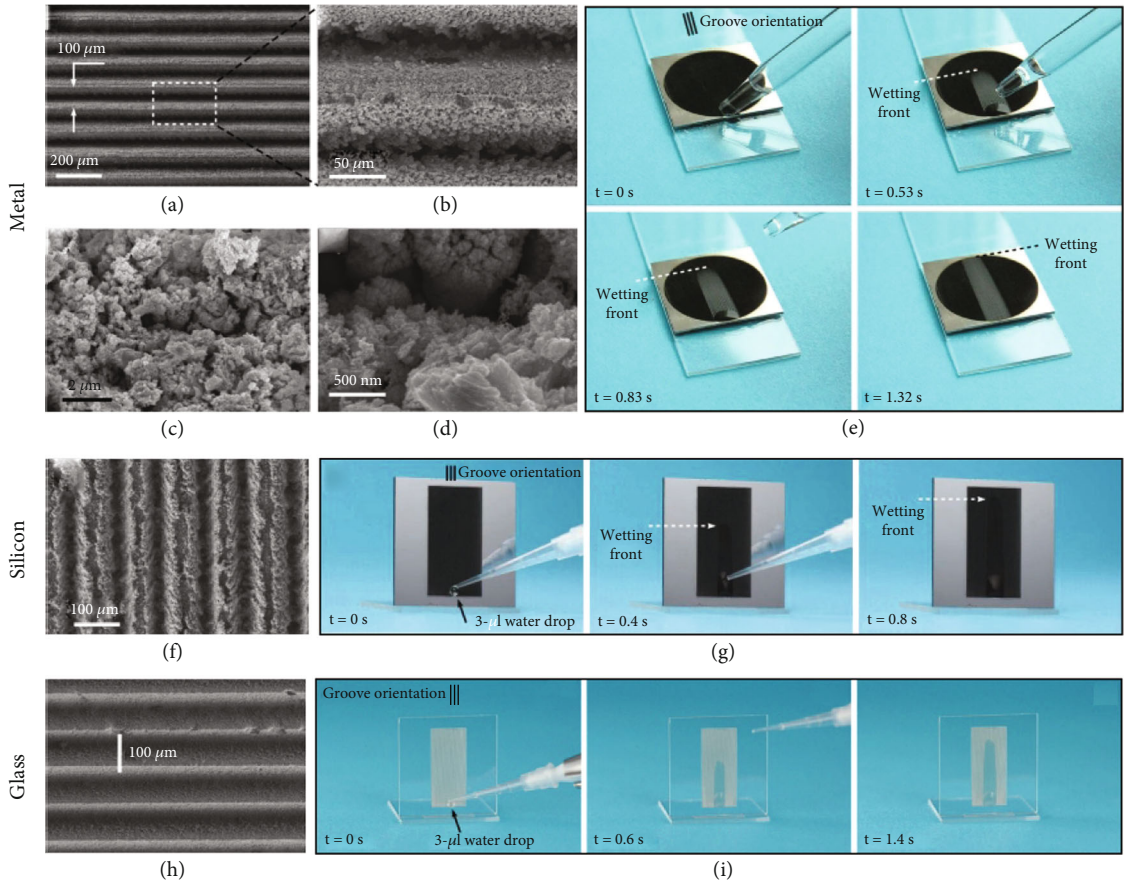

FIGURE 6: Superhydrophilicity of the (a–e) platinum, (f, g) silicon, and (h, i) glass surfaces after femtosecond laser treatment. (a–d) Laser-induced multiple parallel microgrooves on the platinum surface. (e) Methanol quickly wetting the structured metal surface. (f) Laser-induced microstructure on the silicon surface. (g) Water wetting and spreading uphill on the structured silicon surface. (h) Laser-induced microstructure on the glass surface. (i) Water wetting and spreading uphill on the structured glass surface. Reproduced from [96–98] with the permission.

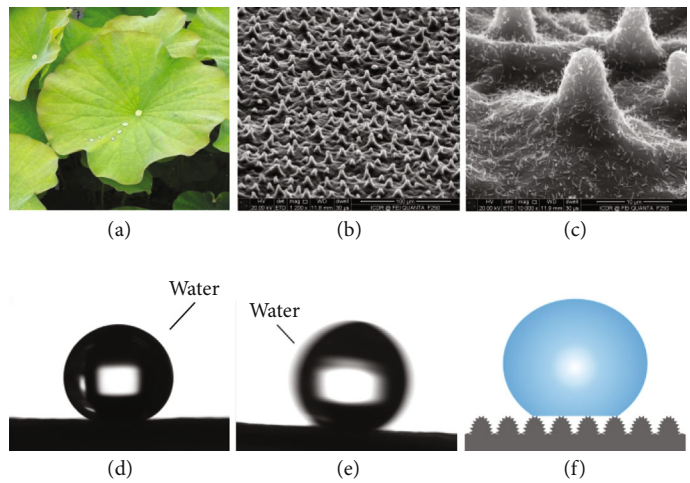

FIGURE 7: Superhydrophobicity of lotus leaf. (a) Photography of a lotus leaf. (b, c) SEM images of the surface microstructure of a lotus leaf. (d) Water droplet on the lotus leaf. (e) Water droplet rolling on a lotus leaf. (f) Cassie wetting state between water droplet and the surface microstructure of a lotus leaf. Reproduced from [121] with the permission.

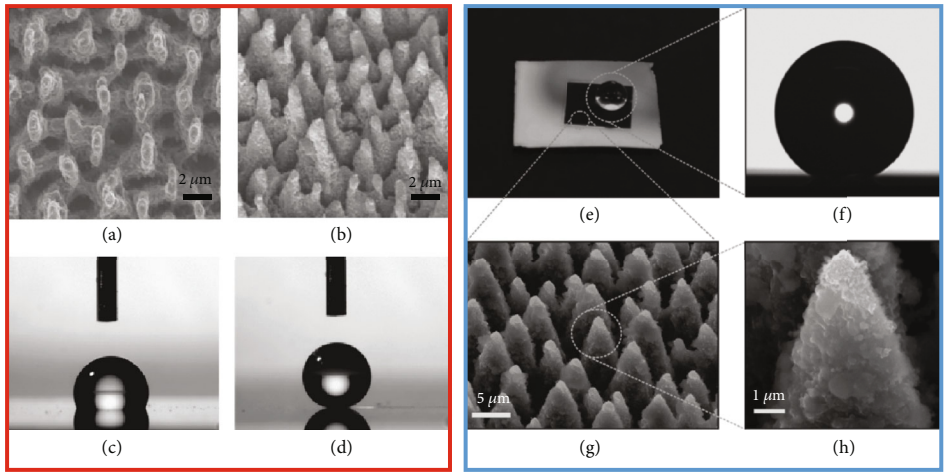

FIGURE 8: Different superhydrophobic silicon surfaces prepared by femtosecond laser ablation under the reactive SF_6 gas. (a, b) SEM images of the laser-structured silicon microstructure. (c, d) Water droplet on the fluoroalkylsilane-modified (c) flat silicon surface and (d) textured silicon surface. (e) Photography of a water droplet on the femtosecond laser-structured superhydrophobic black silicon surface. (f) Shape of the water droplet in (e). (g, h) Surface microstructure of the black silicon in (e). Reproduced from [99, 100] with the permission.

aspect-ratio protrusions started to appear. With continuing to grow the laser fluence, a kind of well-defined conical-shaped spikes could finally be fabricated on the silicon surface (Figures 8(a) and 8(b)). The laser-structured surface was further lowered surface free energy by the modification of fluoroalkylsilane molecules. The resultant surface showed excellent superhydrophobicity and very low water adhesion. Water droplets on the superhydrophobic surface had a WCA of 160° (Figure 8(d)) and a very small contact angle hysteresis (<3°). By contrast, the intrinsic WCA for a fluoroalkylsilane-modified smooth silicon surface was only 115° (Figure 8(c)).

Similarly, Zorba et al. also used the femtosecond laser to create superhydrophobic silicon microstructures under the SF_6 gas (Figure 8(e)) [100, 140]. After laser ablation, the sample surface was entirely covered by uniform microscale conical spikes with a size of 10 μm and an aspect ratio of 4 (Figure 8(g)). The surface of every conical spike was also covered by abundant nanoscale protrusions (Figure 8(h)). Such hierarchical rough microstructure is very similar to a natural lotus leaf and is usually called "black silicon" because the sample surface looks very dark (Figure 8(e)). After the fluoroalkylsilane modification, a water droplet on the sample surface could bead up to form a nearly spherical shape with a WCA of 154° (Figure 8(f)). It could easily roll off a 5° tilted surface.

Superhydrophobicity was successfully achieved on silicon surface by femtosecond laser ablation under SF_6 gas, but the SF_6 processing environment also made the experimental equipment and the operation step very complex. Chen's group developed the method for constructing superhydrophobic silicon surface by simple femtosecond laser ablation in the atmosphere [101, 141–143]. In ambient conditions, the laser beam was directly focused on the silicon surface by an objective lens (20×, NA = 0.45). The diameter of the focal spot was about 10 μm. The line-by-line scanning was adopted with the laser power, scanning speed, and interval of 15 mW, 2 mm/s, and 2 μm, respectively. The femtosecond laser treatment generated a rough micro/nanoscale binary structure on the silicon surface (Figures 9(a)–9(d)) [101]. The laser-structured surface is uniformly covered by an array of periodic microscale mountains with a period of 10 μm. The height and the diameter of the micromountains are ~2.9 and 6 μm, respectively. In addition, there are plenty of nanoscale protrusions upon the surface of the micromountains. Every micromountain is also surrounded by four deep microholes. The measured surface roughness reaches up to 2.46 μm. The as-prepared microscale and nanoscale structures result from the femtosecond laser pulse-induced ablation and the recrystallization of ejected particles [92]. Such rough hierarchical microstructure is helpful to achieve superhydrophobicity. Following the ablation process, the rough silicon surface was further modified with a fluoroalkylsilane monolayer. Figures 9(e) and 9(f) show a tiny water droplet on the as-prepared surface, which maintains a spherical shape with a WCA of 158°. With slightly tilting or shaking the sample, the droplet could easily roll away. The measured water WSA was as low as 4°. A water droplet that free-fell onto the as-prepared surface could rebounce numerous times with a rebound coefficient of 0.9. The extremely high WCA and low WSA values reveal that the femtosecond laser-induced silicon microstructure possesses outstanding features of superhydrophobicity and ultralow adhesion to water. Water droplet on such ultralow adhesive superhydrophobic surface is at the Cassie state and can only contact the peak of the rough micromountains. The trapped air between the surface microstructure and the droplet gives rise to the excellent water repellency of the femtosecond laser-structured silicon surface.

By adjusting the parameters during femtosecond laser ablation or designing the unique micropatterned surface structure, even the anisotropic wettability or the tunable water-adhesion can be appended to the as-prepared superhydrophobic surfaces [141–143]. The anisotropic or adhesion-

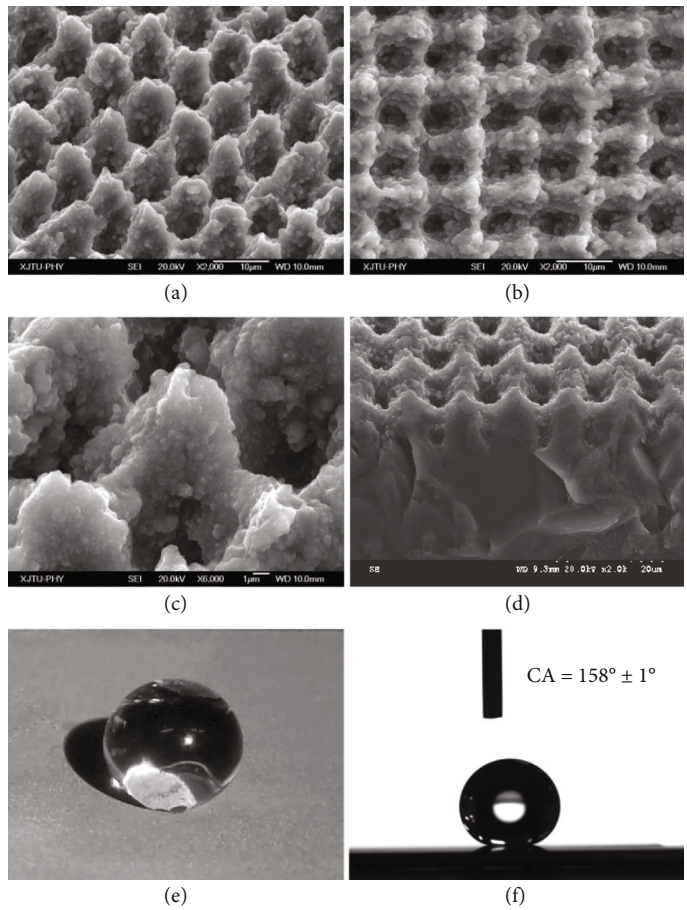

FIGURE 9: Superhydrophobic silicon surface fabricated by femtosecond laser ablation in the atmosphere. (a–d) SEM images of the femtosecond laser-ablated silicon surface: (a) side view, (b) top view, (c) higher resolution image, and (d) cross-sectional image. (e, f) Shape of a small water droplet on the superhydrophobic silicon surface. Reproduced from [101] with the permission.

tunable superhydrophobic surfaces have great applications in manipulating liquid droplets.

3.2.2. Polymers. As far as the inherently hydrophilic substrate, the sample needs to be further lowered surface free energy to obtain superhydrophobicity after forming enough rough surface microstructures. However, superhydrophobic microstructures can be directly created on an intrinsically hydrophobic substrate without additional chemical modification. Polydimethylsiloxane (PDMS) has many features such as flexibility, thermal stability, optical transparency, nontoxicity, and good biocompatibility [144, 145]. In addition, it is also a common hydrophobic substrate. Yong et al. used the one-step femtosecond laser ablation to fabricate various superhydrophobic PDMS surfaces [102, 124, 146, 147]. A microgroove with a width of 12.17 μm and a depth of 8.57 μm could be formed on the PDMS surface after the scan by a focused femtosecond laser beam (energy/pulse of 30 μJ) at the scanning speed of 4 mm/s (Figure 10(a)) [102]. A periodic microgroove array was further generated by the line-by-line scanning, as shown in Figure 10(a). There are a lot of irregular nanoparticles randomly covering the wall and rim of the microgrooves. With decreasing the period (D) of the microgrooves array, the femtosecond-laser-induced microgrooves got near each other (Figures 10(a) and 10(b)). Finally, a new homogeneous rough microstructure appeared because of the strong overlap of the adjacent microgrooves when $D \leq 10\,\mu$m (Figure 10(c)). The femtosecond laser-ablated PDMS surface was characterized by numerous microscale coral-like microstructures (Figure 10(d)). The size of the coral-like structures was about several micrometers, and their surface was randomly and entirely distributed with nanoprotrusions, forming a hierarchical microstructure. Water droplets on the uniform hierarchical microstructure showed a WCA of 157.5° (Figure 10(e)) and could easily roll away on a 1° tilted substrate (Figure 10(f)). Therefore, the rough PDMS surface exhibits ultralow adhesive superhydrophobicity even without any modification because the laser-induced microstructure directly allows the water droplet to be at the Cassie state on the PDMS surface.

Because of the advantages of low cost, strong chemical resistance, and environmental stability, polytetrafluoroethylene (PTFE) is widely used in numerous industrial fields. The surface morphology and chemical composition of the PTFE substrate almost do not change regardless of the storage in harsh environments (e.g., strong acid and alkali solutions, very low or high temperature (-180°C to +250°C), and even organic solvents) for a long time. This remarkable stability

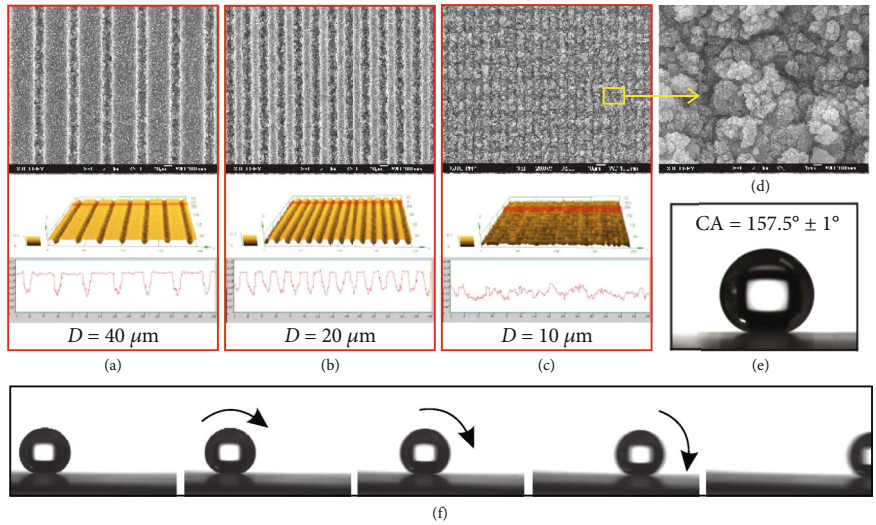

FIGURE 10: Surface microstructure and wettability of the femtosecond laser-structured PDMS surfaces. (a–c) SEM images and 3D and cross-sectional profiles of the femtosecond laser-induced microgrooves array with different periods (D): (a) 40 μm, (b) 20 μm, and (c) 10 μm. The basic microgrooves in (c) are destroyed due to the strong overlap of the adjacent microgrooves. (d) SEM image of the surface microstructure in (c) at high magnification. (e) Static shape of a water droplet on the homogeneous rough PDMS substrate. (f) Dynamic sequence of a water droplet rolling on the rough PDMS surface tilted at 1°. Reproduced from [102] with the permission.

is a double-edged sword, which also brings many difficulties to create a rough texture on the PTFE surface. Many conventional methods (e.g., chemical etching, thermal treatment, coating, template replication) are not suited for achieving superhydrophobicity on the PTFE surface because those methods cannot roughen the PTFE substrate. However, building micro/nanoscale texture on PTFE substrate becomes an easy thing via femtosecond laser ablation. Yong et al. obtained a superhydrophobic PTFE surface by a one-step femtosecond treatment [103, 148]. After laser ablation, there were abundant pores and protrusions forming on the PTFE surface (Figures 11(a)–11(c)). The pores are interconnected with each other, like an ant nest. The protrusions are 300 nm to 2 μm in size. Water droplets on the laser-structured PTFE showed a WCA of 155.5° (Figures 11(d) and 11(e)) and could roll off once the sample was tilted 2.5° (Figure 11(f)), indicating that the hydrophobicity of the PTFE material was amplified by the laser-induced surface roughness. Such femtosecond laser-structured surface exhibits both superhydrophobicity and ultralow adhesion to water droplets because water droplets are at the Cassie wetting state on the microstructures. In general, rough microstructures can amplify the surface wettability of solid materials, so the PTFE substrate was changed from intrinsic hydrophobicity (WCA = 111.5°) to contrasting superhydrophobicity after femtosecond laser treatment.

The advantage of the chemical stability of the PTFE material ensures the durability of the superhydrophobicity of the laser-ablated PTFE surfaces [103, 148]. When the aqueous droplets with pH ranging from 1 to 13 were placed on the rough PTFE sheet, the measured WCAs were larger than 150° and the WSAs were smaller than 10° for no matter acid water droplets or alkaline water droplets. Therefore, the femtosecond laser-structured PTFE surface could also maintain its ultralow adhesive superhydrophobicity to various strong acid/alkaline solutions [103]. Similarly, when the sample was stored in the aqueous solution with different pH, the superhydrophobicity showed no change after a whole day, demonstrating that the surface had strong repellence to acid/alkaline solutions. In addition, the surface microstructure is also able to withstand heat. Even though the sample was heated at 200°C for one day, no significant decrease of the measured WCA and increased WSA occurred. The result also revealed that the structured PTFE surface kept its superhydrophobicity when stored in various harsh environments for one day, including high temperature (250°C), 40% hydrofluoric acid, concentrated sulfuric acid, 10 M sodium hydroxide solution, and even aqua regia [148]. Such durable property is intimately linked to the inherent chemical inertness of the PTFE substrate and the laser-induced microstructure. Chemical inertness leads to an ultralow damage speed for the aspects of no matter surface chemical composition or the topography. The rough surface microstructure amplifies this effect by significantly reducing the contact area between corrosive liquids and the PTFE surface.

Shape-memory polymer (SMP) is a smart material that can transform between permanent and deformed shapes under external stimuli [149–151]. Due to the unique shape-memory property, reversible wettability can be realized on the SMP surface by designing appropriate micro/nanostructures. Recently, Bai et al. created micropillar structures on the thermal-responsive SMP surface by femtosecond laser ablation [104]. The surface showed excellent low-adhesive superhydrophobicity after fluoroalkylsilane treatment. When the surface was pressed by force, all the SMP micropillars would lean to one side with the decline of surface superhydrophobicity. Interestingly, the surface morphology and wettability could completely recover to the original states through a simple heating process. The surface

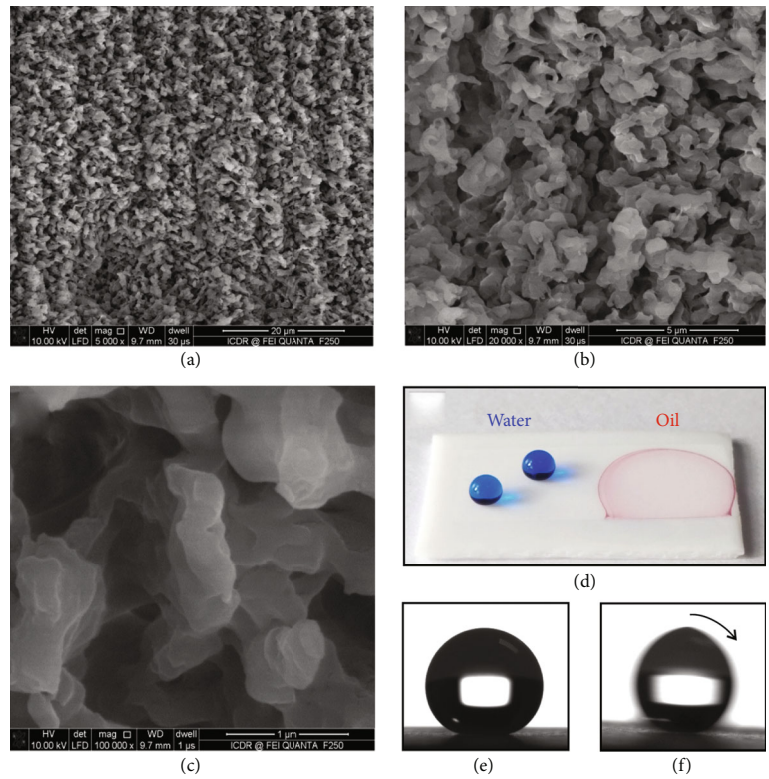

FIGURE 11: Superhydrophobicity of the PTFE surface after femtosecond laser ablation. (a–c) Surface microstructure. (d) Photography of water (blue color) droplets on the as-prepared PTFE surface. (e) Static shape and (f) roll behavior of a water droplet on the laser-structured surface. Reproduced from [103] with the permission.

microstructures and wettability of the SMP micropillars could be reversibly regulated by repeatedly pressing and heating the samples.

3.2.3. Metals. Metals are widely applied in daily life, industry, military, and agricultural production, such as building, automobile, machine, rope, airplane, ship, and weapon. However, those metal-based devices usually suffer from contamination, corrosion, rusting, oxidation, and freezing. For example, the rust of industrial machines causes enormous economic losses every year [152]. In the past, several plane crashes were ascribed to the ice formation on the wings [153]. Fortunately, endowing the metal surfaces with superhydrophobicity is an effective way to solve the problems as mentioned above [46, 47, 54, 55, 154]. Kietzig et al. prepared specific rough double-scale microstructures on different metal alloys by femtosecond laser ablation [105]. As long as the treated surfaces were stored in air for 30 days, the wettability of those surfaces would switch from superhydrophilicity to superhydrophobicity because the laser-induced microstructures were inclined to absorb carbon-containing compounds in the atmosphere.

Wu et al. used a femtosecond laser to ablate the AISI 316L stainless steel at different laser fluences [106]. The laser beam was focused on the sample surface with a spot diameter of 180 μm in a vacuum chamber under vacuum (3.5×10^{-3} Pa). For the case of low laser fluence (e.g., 0.08 J/cm^2), a periodic nanoscale structure was formed on the sample surface, known as the laser-induced periodic surface structure (LIPSS), as shown in Figure 12(a). The direction of the LIPSS was perpendicular to the polarization of the laser beam. The period of the LIPSS was ~500 nm. The width and the height of the ripples were both about 350 nm. LIPSS is a unique characteristic only possessed by laser irradiation, which is generally caused by the interference between the incident laser pulse and the scattered tangential wave originating from previous pulses [64–67]. As the laser fluence increases, separated protrusions with bigger width than the LIPSS were generated. For the higher laser fluence (e.g., 2.4 J/cm^2), the separated protrusions turned to conical-shaped spikes with the size of several micrometers (Figure 12(b)). The top of the spikes was also covered with the typical LIPSS, forming a hierarchical micro- and nanoscale structure. Only LIPSS was formed at low laser intensity. As far as the case of high laser intensity, the high central fluence allowed the material in the spot center to melt. Such liquid metal would further undergo extreme heat-induced phase explosion, cool rapidly, and freeze. Microscale roughness was generated during this instantaneous process. As the spot center moved, the low-fluence spot fringe built the LIPSS on the microscale protrusions. It was found that both the size and the distance between the spikes increased with the increase of the laser fluence. When different sample surfaces were silanized by silane reagent, the flat stainless steel surface exhibited weak hydrophobicity with a WCA of 113.0°. The surface with only nanoscale LIPSS showed a WCA of 150.3° (inset of Figure 12(a)). Still, water droplets could not roll off on such substrate. In contrast, the surface with double-scale

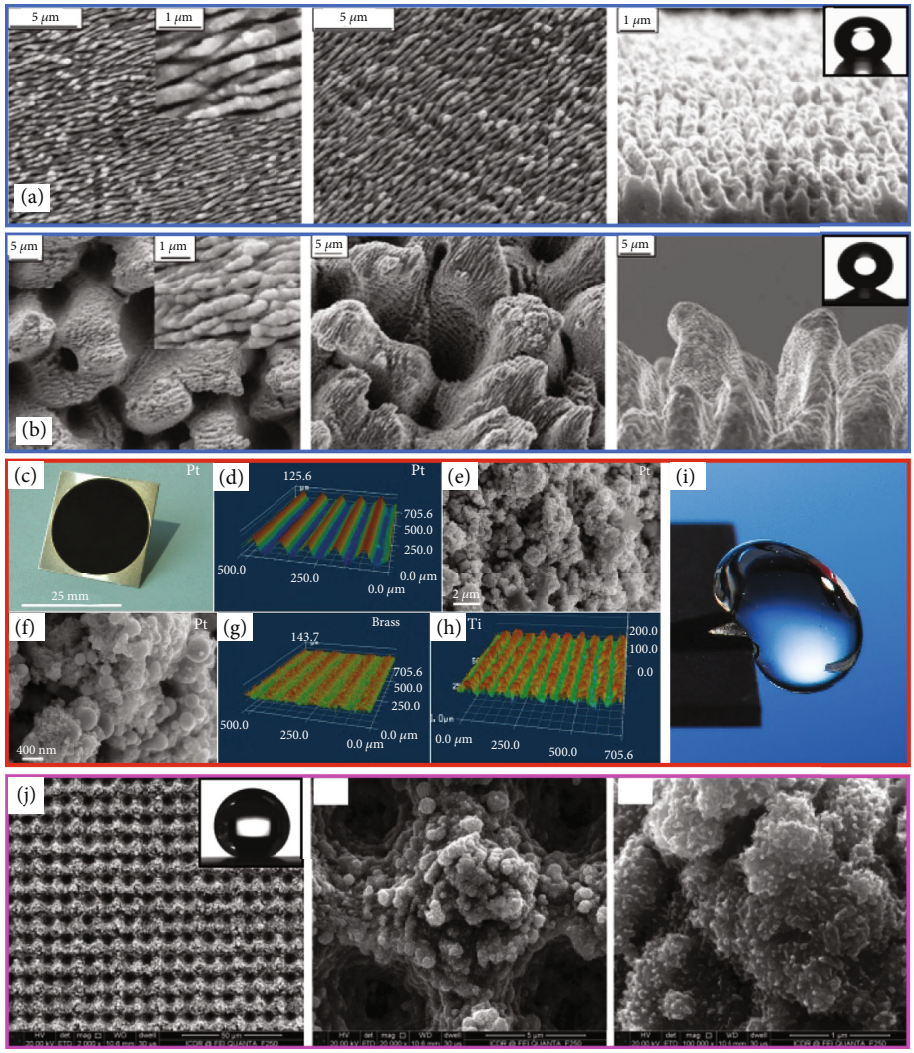

FIGURE 12: Different superhydrophobic metals fabricated by the femtosecond laser. (a, b) Top (left column), side (middle column) views, and profiles (right column) of the surface microstructures of the stainless steel surfaces ablated by femtosecond laser at different laser fluences: (a) low fluence = 0.08 J/cm^2 and (b) high fluence = 2.4 J/cm^2. Insets: water droplets on the silanized surfaces. (c) Photography of the laser-ablated platinum surface. (d) 3D profile of the microstructure of the black platinum surface. (e, f) SEM images of the rough platinum surface. (g, h) Femtosecond laser-induced superhydrophobic microstructures on (g) the brass surface and (h) the titanium surface. (i) Water repellence of the as-prepared superhydrophobic black metal. (j) Surface microstructures of the zinc surface after femtosecond laser treatment. The inset shows a water droplet on the zinc sample after dark storage. Reproduced from [106–108] with the permission.

microstructure presented superhydrophobicity and very low adhesion to water droplets with a WCA of 166.3° (inset of Figure 12(b)) and a WSA of 4.2°, respectively.

Vorobyev and Guo obtained various black metals by femtosecond treatment [107]. As shown in Figure 12(c), laser ablation resulted in that the platinum surface became velvet black. The platinum surface was ablated by a laser beam at the laser fluence of 9.8 J/cm^2. The enhanced optical absorption reveals that microstructures are formed on the platinum surface. The laser-treated surface is characterized by a uniform hierarchical surface microstructure. An array of parallel microgrooves with a depth of 75 μm and a space of 100 μm was generated on the sample surface (Figure 12(d)). The microgrooves were interspersed with many nanoparticles whose smallest feature was only 5-10 nm (Figures 12(e) and 12(f)). As the treated surface was exposed to air for enough period, superhydrophobicity was exhibited by the rough black platinum surface. The measured WCA of a tiny water droplet on the surface was 158°. Regarding the dynamic property, the water droplet could easily roll off as the superhydrophobic surface was tilted to 4°, demonstrating the excellent water repellency of the as-prepared black metal (Figure 12(i)). The superhydrophobic microstructures were also fabricated on the brass and titanium substrates by femtosecond laser ablation at the laser fluence of 3.9 J/cm^2 and 7.6 J/cm^2, respectively (Figures 12(g) and 12(h)). The laser-induced superhydrophobic metallic surfaces have a low light reflectance. The hierarchical surface microstructures cause that the reflectance decreases to 3.3%-4.1% (platinum surface), 1.3%-3.5% (brass surface), and 4.2%-4.5% (titanium

surface) in the visible wavelengths, respectively. The collision of metal blackening and superhydrophobicity can produce many colorful fireworks. The black metals with high optical absorption have potential applications in light collection and solar cells. The water repellence and the self-cleaning function can improve the performance and reduce the maintenance of the devices that use those surfaces.

Yong et al. fabricated a superhydrophobic zinc surface with switchable wettability by femtosecond laser processing [108]. Figure 12(j) shows the SEM images of the sample surface after femtosecond laser ablation. The surface morphology is a typical micro/nanoscale hierarchical structure. Uniform micromountains are arranged on the zinc surface as an array. The size of the micromountains is about 8 μm, and the average distance between those micromountains is about 10 μm. The center domain between adjacent four micromountains develops to a deep microhole. The surface of every micromountain is also coated with abundant irregular nanoprotrusions. The untreated bare flat zinc consists of Zn element with an atomic proportion of 100%. In contrast, the atomic proportion of Zn decreases to 67.56%, and new element O with an atomic proportion of 32.44% appear in the sample surface after laser ablation. The result reveals that oxidation also occurs during femtosecond laser treatment, leading to a thin rough ZnO layer coating on the original Zn substrate. The rough ZnO microstructure exhibits superhydrophobicity after dark storage, with the measured WCA and WSA of 159.5° and 8° to a water droplet, respectively (inset of Figure 12(j)).

3.2.4. Glass. Glass is one of the typical difficult-to-process materials because of its high hardness and brittleness, but femtosecond laser is an effective tool to process glass surfaces. Zhou et al. applied a femtosecond laser to build a double-scale structure on a K9 glass surface [109]. The microraster was formed by the repeated laser scans on the sample surface. The groove depth, groove width, and ridge width of the microraster are 50 μm, 210 μm, and 20 μm, respectively. A large number of regular submicron structures also exist in the microgrooves. The resultant glass surface showed great superhydrophobicity after lowering the surface free energy of the double-scale rough raster structure by fluoroalkylsilane modification. On the sample surface, the WCA and WSA of a water droplet were 152.3° and 4.6°, respectively. By comparison, the water droplet on the silanized smooth K9 glass had a WCA of just 114.7°. Ahsan et al. also achieved superhydrophobicity on a soda-lime glass surface by laser microfabrication [110]. The laser scanning led to periodic microgratings with a period of 10 μm on the glass surface. Each track was ablated twice by the laser beam. The periodic microgratings were 8 μm in width. Meanwhile, micropillars with a width of 2 μm were also evolved as the boundary of adjacent microgratings. There were periodic self-assembled microripples and nonuniform nanostructures at the bottom of the microgratings. Such laser-structured glass surface presented a WCA ranging from 152° to 155° as long as the rough surface was further chemically treated with fluoroalkylsilane.

Lin et al. prepared a transparent superhydrophobic surface by directly writing an array of micropits on the surface of silica glass using a femtosecond laser [111]. Figure 13(a) shows the microstructure of the laser-induced micropits. The micropits are arranged uniformly and periodically. The micropits are 20 μm in diameter and 30 μm in spacing. The inner surface of the micropits is characterized by submicrometer ripples. A larger number of nanorods and nanoparticles are also formed on the ripple structures. After chemical modification to reduce the surface free energy, the surface of the structured glass exhibits excellent superhydrophobicity, with a WCA of 161.2 ± 0.4° and a WSA of 2 ± 1° (Figure 13(b)). Interestingly, the hierarchical micropits do not strongly affect the light transmittance of the glass (Figure 13(c)). The transparency of the superhydrophobic glass is higher than 92% in visible and near-infrared wavelengths (Figure 13(d)). The appropriate micropits with self-organized nanostructures provide the essential roughness for the entire surface to achieve superhydrophobic, while the sufficient unirradiated areas (over 65%) between the micropits ensure the high transparency of the laser-ablated glass.

3.3. Applications of Superhydrophobic/ Superhydrophilic Surfaces

3.3.1. Water Superwicking. Superhydrophilic microstructure can enhance the wetting effect of water on solid materials. Water fully spreads out on the superhydrophilic surface, which dramatically increases the contact area between the liquid and the solid substrate. The superwicking property can allow fluids to wet a tilted surface against gravity (Figures 6(e), 6(g), and 6(i)) [96–98]. The driving forces of the liquid spreading are the supercapillary effect and superhydrophilic force. The superwicking property can be widely applied in liquid drive, evaporation, heat transfer, microfluidic, fuel cell, and catalyst. For example, Singh et al. created superhydrophilic microstructures on an aluminum surface [155]. The super-wicking and super-light-absorbing properties enable the functional surface to be applied in efficient solar-based water sanitation. The superhydrophilic microstructure can drive the contaminated water to the solar absorber, even if the device is tilted at any angle for directly facing the sun. Sunlight is absorbed by the metal, heating the metal surface and causing water to evaporate. The femtosecond laser-induced superhydrophilic microstructure shows a remarkable ability to purify contaminated water, with evaporation efficiency exceeding 100% of an ideal device.

3.3.2. Liquid Repellence. Liquid repellence is a natural property of superhydrophobic surfaces. Superhydrophobic materials are difficult to be wetted by water [99–111, 124, 140–154]. Water droplets roll easily on the superhydrophobic surface. The water droplets, such as raindrops, can bounce off when they impact superhydrophobic surfaces (Figure 12(i) and Figure 14(a)) [103]. The superhydrophobic materials can keep clean and dry in the rain and other humid environments. The liquid repellence is the basics of the broad applications of superhydrophobic materials.

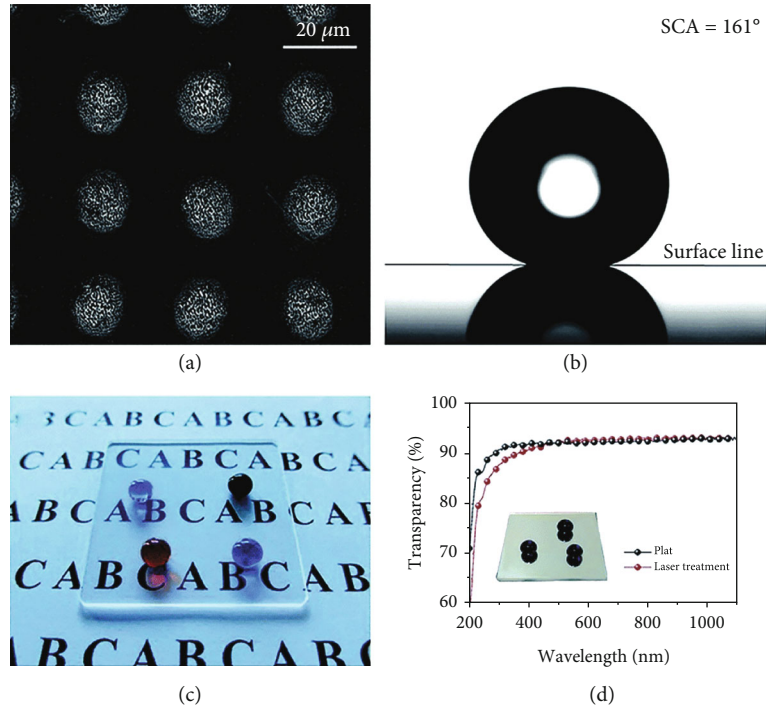

FIGURE 13: Transparent superhydrophobic glass surface prepared by femtosecond laser. (a) Laser-induced hierarchical micropits on glass surface. (b) Water droplet on the superhydrophobic glass surface. (c) Photograph of the as-prepared glass on a paper. (d) Transparency of the laser-structured glass. Reproduced from [111] with the permission.

3.3.3. Self-Cleaning. Like lotus leaf, the femtosecond laser-induced artificial superhydrophobic surfaces also have excellent self-cleaning ability (Figure 14(b)) [101, 102, 140]. When a superhydrophobic surface is contaminated with solid dust particles, water droplets (such as raindrops) that fall on the sample surface will roll off freely and collect all the dust particles in their path. The contaminated surface looks very messy, but the path of the water droplets becomes clean, leaving no pollutions behind. Compared with a common smooth surface, water droplets on the superhydrophobic surface remain quasi-spherical and can easily roll off. The droplets can pick up foreign dirt particles during the rolling process because water has a stronger affinity for most dust than solid surfaces. The self-cleaning function enables the artificial superhydrophobic materials to be applied to outdoor buildings, car housings, mobile phone screens, solar panels, and other fields to reduce the number of cleaning of these materials.

3.3.4. Manipulation of Tiny Droplets. Unlike the superhydrophobicity of lotus leaves, rose petals are superhydrophobic but have high adhesion to water droplets. Chen et al. proposed different strategies to adjust the water adhesion of the femtosecond laser-induced superhydrophobic surfaces [102, 141, 144, 145, 148]. For example, they fabricated a series of patterns consisting of the untreated and the laser-structured regions [38, 102, 141]. The untreated region has high adhesion to water, while the laser-structured region shows superhydrophobicity with ultralow adhesion. The adhesion of the resultant superhydrophobic surface can be tuned from extremely low to extremely high by changing the area fraction of these two regions. Water droplets can be manipulated in different ways based on the controllable adhesion of the as-prepared superhydrophobic surfaces. As shown in Figure 14(c), the superhydrophobic surface with high adhesion can be used as a "mechanical hand" to pick up a droplet from an ultralow-adhesive substrate [38]. The droplet can be transported and placed on the surface with higher water adhesion. The contact area between the droplet and the mechanical hand is very small, so there is almost no liquid loss in the whole process of droplet transportation. Loss-less droplet transportation has a broad application prospect in liquid manipulation, microchemical reaction, and bioengineering. Free-falling water droplets can bounce many times on superhydrophobic surfaces with ultralow adhesion. With the increase of the adhesion, the rebounding number of droplets gradually decreases [38]. For the highly adhesive superhydrophobic surface, the water droplets adhere tightly to the solid surface after impacting on the sample and cannot rebound. The property of the controllable droplet bounce can be used for inkjet printing. When small high-adhesive points are embedded on the low-adhesive superhydrophobic surface, water droplets roll across the surface and eventually attach to the designed points. This pattern can quickly capture and locate droplets.

Bai et al. fabricated a superhydrophobic SMP surface with anisotropic wettability by femtosecond laser etching microgroove array on the SMP surface [94]. By integrating the switchable adhesion and anisotropic wettability, the femtosecond laser-structured SMP microgroove array could be used as a multifunctional platform for liquid manipulation, such as directional liquid transportation, directional self-

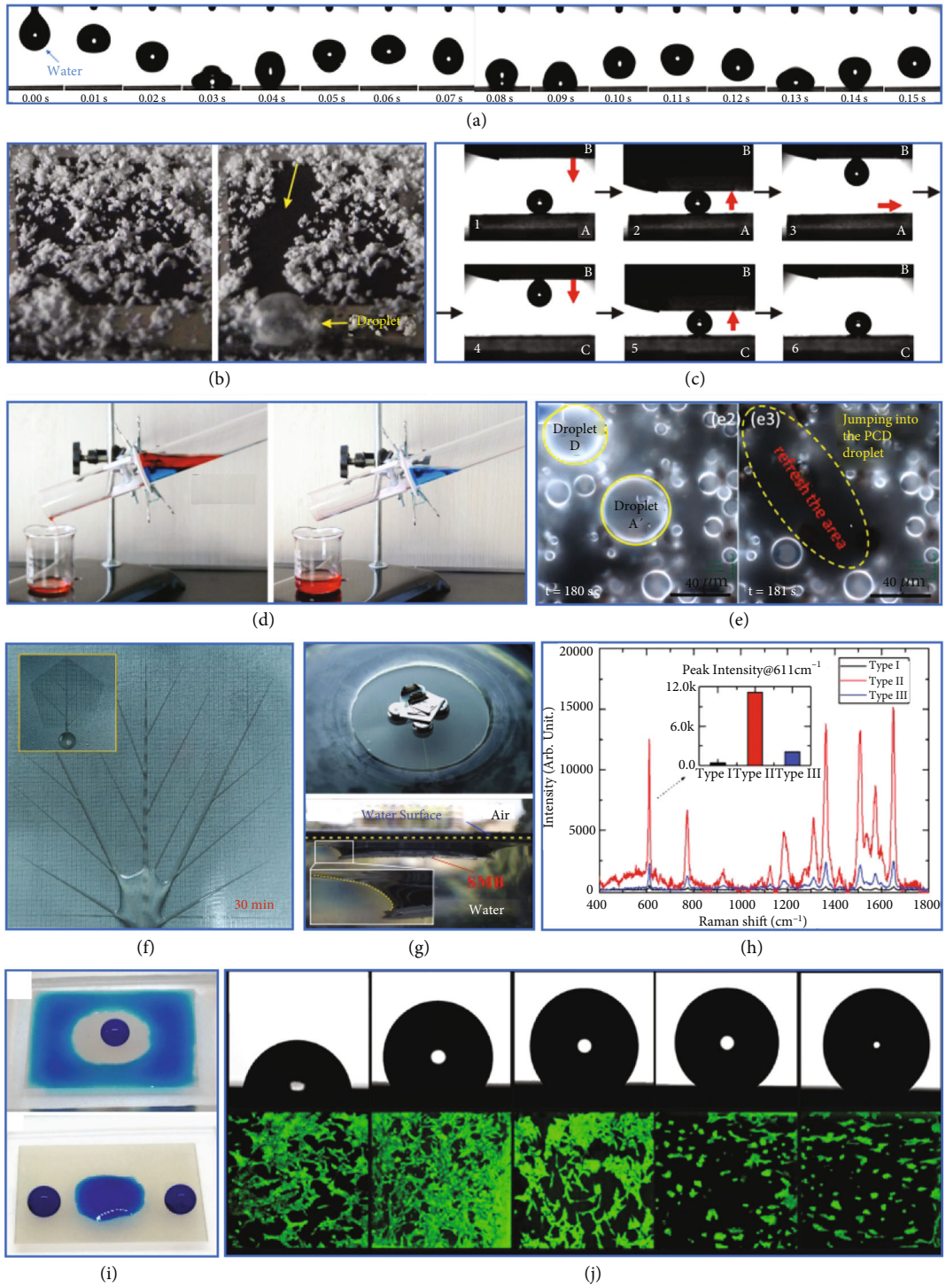

FIGURE 14: Application examples of the superhydrophilic surfaces and superhydrophobic surfaces fabricated by femtosecond laser. (a) Liquid repellence: water droplet rebounding on the superhydrophobic surface. (b) Self-cleaning: water droplets rolling away and taking up foreign dirt particles on a superhydrophobic surface. (c) Droplet manipulation: transferring a tiny water droplet by using a superhydrophobic surface with controllable adhesion. (d) Separating the mixture of water (blue) and oil (red) by a porous superhydrophobic PTFE sheet. (e) The anti-icing and icephobic property of the triple-scale superhydrophobic microstructure. (f) Superhydrophilic-superhydrophobic venation network for collecting water fog. (g) Superhydrophobicity making PDMS sheet with heavy load floating on water surface. (h) Enhance Raman spectroscopy after concentrating the solution droplet on the superhydrophobic substrate. (i) Patterning liquid by the superhydrophobic and superhydrophilic microstructures. (j) Cell culture on the laser-structured surfaces with different wettability. Reproduced from [38, 60, 89, 101, 103, 156–159] with the permission.

cleaning, liquid pattern, droplet-based microreactor, and gas sensing. Meanwhile, these functions could be repeatedly realized on the same sample surface by continuously "writing" and "erasing" the pattern of standing/inclined microgrooves.

3.3.5. Oil/Water Separation. Frequent oil leakage accidents and discharge of oily industrial wastewater cause substantial economic losses and seriously pollute the natural ecological environment [40–43, 160]. Yong et al. proposed a method for separating oil-water mixtures via the femtosecond laser-structured superhydrophobic porous PTFE sheet (Figure 14(d)) [103]. A femtosecond laser firstly ablated the surface of a PTFE sheet to form a hierarchical microstructure on the sheet. A series of open microholes were then created in the sheet by mechanical drilling. The as-prepared porous sheet is superhydrophobic and strongly repels water. However, oil can thoroughly wet the surface of the sheet and permeate through the micropores. When the mixture of water and oil is poured onto the superhydrophobic and superoleophilic porous sheet, the superoleophilicity allows the oil phase to penetrate and pass through the sheet. In contrast, the water repellence makes the superhydrophobic sheet intercept water; that is, the water phase cannot pass through the sheet. Finally, the oil-water mixture is successfully separated into the water portion above the sheet and the oil portion under the sheet. Because of the durability of the superhydrophobicity of the laser-ablated PTFE, the superhydrophobic porous PTFE sheet can even separate the mixtures of oils and strong acid/alkali solutions.

3.3.6. Fog/Water Harvesting. Ren et al. prepared a Janus foil by femtosecond laser drilling, low surface energy modification, and laser removal [161]. The laser drilling process generated a set of micropores on the aluminum foil. The laser-incident side is defined as the bottom surface, and the opposite is defined as the top surface. The resultant micropores are conical because of the cone shape and the Gaussian power distribution of the focused laser beam. The diameter of the pores on the bottom surface is larger than that on the top surface, forming a conical gradient structure. The drilled aluminum foil shows superhydrophilicity due to the formation of surface microstructure. After low-surface-energy modification, both sides of the aluminum foil become superhydrophobic. Finally, a laser was used to scan the bottom surface of the porous foil. After the removal of modified fluoroalkyl silane, the superhydrophilic state of the bottom surface was restored. The top surface remained superhydrophobicity. It was found that droplets could automatically pass through the hydrophilic/hydrophobic Janus membrane from the top surface to the bottom surface. This process is driven by gradient wetting force and Laplace pressure of the conical micropores. This Janus foil can be used to collect fog from the atmosphere, efficiently transferring the collected water to the inside of the collector. Compared with the ordinary superhydrophilic membrane, the water collection efficiency of the Janus foil is improved by 209 %. Yin et al. fabricated a superhydrophobic-hydrophilic hybrid pattern by gluing together a superhydrophobic mesh and a hydrophilic copper sheet [162]. PTFE nanoparticles were deposited on the surface of copper mesh during the process of the femtosecond ablating the mesh on a PTFE substrate, making the mesh superhydrophobic. The hybrid surface has good performance and efficiency in fog harvesting. The hydrophilic region firstly absorbs the tiny droplets. The superhydrophobic structure enables the attached water droplets to fall off from the hybrid surface in time and drop into the collecting container when the diameter of the water droplets exceeds the pore size of the mesh. Liu et al. reported a novel water-collecting configuration of a superhydrophilic-superhydrophobic venation network (Figure 14(f)) [156]. Superhydrophobic microstructures were previously formed on the sample surface by femtosecond laser ablation. Then, the superhydrophilic venation network was integrated into the superhydrophobic area. The skeleton of the venation network is cascaded with the water-collecting microstructures. The fog drops attached to the sample surface can be self-driven and concentrated to a designated location. The venation network can perform water collection on a large-scale surface.

3.3.7. Anti-Icing. Pan et al. designed a triple-scale superhydrophobic microstructure with both anti-icing and icephobic capabilities [157]. Femtosecond laser ablation combined with chemical oxidation produced periodic hierarchical microcones on the copper sheets. The surface of the microcones is covered with nanograsses and microflowers. The surface shows stable superhydrophobicity under the Cassie state, and the critical Laplace pressure can reach 1450 Pa. The superhydrophobic surface has excellent anti-icing capability, mainly attributed to the rapid rolling-off of impacting droplets, excellent humidity resistance via hierarchical condensation, and a remarkable delay of heterogeneous nucleation at the solid-liquid interface under freezing conditions. When a droplet impacts the superhydrophobic surface, the droplet can rebound more than 20 times. The contact time between the droplet and sample surface is less than 9 ms, avoiding the complete contact between liquid and the solid surface. The condensed secondary droplets between the microcones can move upward and be continually absorbed into the condensed primary droplets at high humidity (Figure 14(e)), so the space between surface microstructures is filled with air instead of the condensed droplets. The trapped air within the surface microstructure acts like a thermal resistance layer and can significantly reduce the heat transfer between the solid surface and the liquid. The stable air pockets in the Cassie state result in a significant delay of the heterogeneous nucleation at the solid-liquid interface. In addition, the adhesion strength of ice on the superhydrophobic surface is only 1.7 kPa. The ice can even be removed by its weight. Therefore, the as-prepared superhydrophobic surface also has outstanding icephobic performance in addition to the anti-icing capability.

3.3.8. Buoyancy Enhancement. Superhydrophobicity allows tiny devices to float on water. Yong et al. designed five different PDMS wafers by femtosecond laser processing [60]. The surfaces of these wafers have different wettabilities. The

comparison shows that the wettability of the lower surface has little effect on the loading capacity of the wafers, while the superhydrophobicity of the upper surface, especially the edge of the upper surface, can significantly improve the loading capacity of the thin sheet (Figure 14(g)). This effect is known as the "superhydrophobic edge effect". It is difficult for water to wet the superhydrophobic structure on the upper edge of the thin sheet. The superhydrophobic structure and surface tension can bend the water surface even though the top of the sheet is already below the water level. The curved liquid meniscus increases the total displacement, thereby increasing the buoyancy acting on the sheet. The increased buoyancy gives the superhydrophobic sheet a greater load capacity. Zhan et al. demonstrated that superhydrophobicity can even make sheets of metal float on water [61]. Ordinary metals sink quickly to the bottom of water because they are denser than water. There are many important potential applications for tiny devices that can float on water, such as hydrology monitoring, water pollution monitoring, and support for aquatic robots.

3.3.9. Surface-Enhanced Raman Spectroscopy (SERS). The superhydrophobic surface also has important applications in biochemical analysis and detection. Wang et al. found that the superhydrophobic microstructures prepared by femtosecond laser ablation can enhance Raman spectroscopy [158]. Femtosecond laser ablation produced a large number of conical-spike-like microstructures on a silicon substrate. Then, a silver film with a thickness of 60 nm was deposited on the laser-induced structure by an electron beam evaporator. After absorbing low-surface-energy carbon compounds in the air, the structured surface shows superhydrophobicity and has extremely low adhesion to the aqueous solution. The superhydrophobicity allows the contact line of the solution droplet on the as-prepared surface to freely shrink inwards without the pinning effect during droplet evaporation. After evaporation, the area of the concentrated solution is reduced to 0.14 mm^2, which is 19.5 times less than that on the high-adhesion substrates. The concentration of the molecules is 88.1 times that of the original solution. The ultrahigh concentration of the molecules can make the Raman signal enhancement factor reach 6×10^6, which is far higher than the requirement of molecular-level detection (Figure 14(h)). The surface-enhanced Raman spectroscopy based on the laser-induced superhydrophobic substrate shows excellent performance in ultra-trace molecular detection.

3.3.10. Liquid Patterning. The superhydrophobic microstructure has strong liquid repellence, which can drive the liquid to other places. By using superhydrophobic microstructure to restrict the liquid, complex liquid patterns can be prepared. For example, Yong et al. prepared structured patterns on a PDMS substrate by femtosecond laser treatment and selective oxygen plasma treatment [89]. The pattern is composed of superhydrophilic region and superhydrophobic region. When water is distributed to the patterned surface, it only wets the superhydrophilic area but does not exist above the superhydrophobic region. Water is restricted to the superhydrophilic region and is difficult to spread to the superhydrophobic region because of its strong repulsive effect. As a result, the superhydrophilic area is entirely covered by water, and the superhydrophobic area remains clean, forming a liquid pattern (Figure 14(i)). The shape of the liquid pattern is consistent with the design of the superhydrophilic region surrounded by a superhydrophobic region. This method can pattern liquids to various complex shapes by using superhydrophilic-superhydrophobic microstructures.

3.3.11. Cell Engineering. The adhesion, growth, division, migration, and other behaviors of cells are closely related to the culture substrate. The surface roughness and chemical composition of biomaterials play a crucial role in the behavior of cells. In addition to the above two factors, wettability is another important factor that affects the cell behavior on solid substrates. The controllable wettability and roughness of the femtosecond laser-processed surface can be used to control the interaction between cells and biomaterials. Ranella et al. prepared many kinds of conical spike microstructures under different laser energy fluences [159]. These conical microstructures have different sizes, aspect ratios, and densities. The wettability of the structured surfaces varies from hydrophilic to superhydrophobic, resulting in markedly different responses of fibroblasts to these surfaces. It is found that these cells are more inclined to adhere to the hydrophilic substrate and are inhibited on the superhydrophobic surface (Figure 14(j)). For the laser-structured rough surface, the transition between cell rejection and cell affinity can be achieved by changing the surface from hydrophobic (modified with hydrophobic fluorosilane layer) to hydrophilic (modified with hydrophilic oxide layer).

3.3.12. Underwater Wettability. The underwater wettability is closely related to the wettability of the structured substrate in the air [26, 89]. Yong et al. experimentally and theoretically discussed the relationship and interconversion between six different superwetting states [89, 122, 123]. It is demonstrated that most superhydrophilic microstructures prepared by femtosecond laser are superoleophobic and superaerophobic in water, while most superhydrophobic microstructures are superoleophilic and superaerophilic in water. Therefore, superhydrophilicity and superhydrophobicity are the basis of various underwater superwettabilities.

4. Superoleophobicity

Although superhydrophobic surfaces can repel water, they are readily wetted by organic liquids because they usually have very low surface tension. When the CA of oil droplets on the surface is greater than 150°, the surface is superoleophobic. Superoleophobic surfaces can repel organic liquids even with surface tension as low as 20-30 mN/m [28, 32, 73]. It is more difficult to prepare a superoleophobic surface than a superhydrophobic surface. Two breakthroughs play an essential role in the development of superoleophobicity. First, Tuteja et al. pointed out the importance of the reentrant surface curvature for achieving superoleophobicity in the air [163, 164]. Another is that Liu et al. proposed the concept of underwater superoleophobicity [19]. Their

achievements were followed a rapid development in the field of superoleophobic materials.

4.1. Superamphiphobic Surfaces. The superhydrophobic surfaces can repel water, but low-surface-tension organic liquids usually wet them because the surface tension of organic liquids is much lower than that of water [28, 32, 73]. Interestingly, the springtails can prevent oils from penetrating the skin (Figure 15(a)) [165–167]. The superoleophobicity allows the insect to breathe even in many organic liquids with low surface tension. It is found that the skin of the springtail is characterized by mushroom-like reentrant microstructures [167]. A lot of bristles and rhombic meshes are distributed on the springtail skin (Figure 15(b)). The rhombic meshes are composed of interconnected nanogranules (Figure 15(c)). Both the ridges and granules have a negative overhang shape, forming a reentrant curvature. It is the reentrant microstructure that results in the superoleophobicity for the springtail skin.

Tuteja et al. first pointed out the importance of the reentrant microstructure in preparing a superoleophobic surface [163]. Young's CA of the liquids (such as oils and organic solvents) with ultralow surface tension on any flat surface is usually much less than 90° ($\theta < 90°$). As shown in Figure 15(d), when the liquid is in contact with the textured surface with the local geometric angle, ψ, less than the intrinsic CA of the liquid ($\theta < \psi$), the net traction at the liquid-gas interface is downward. The direction of the net traction promotes the liquid to penetrate the solid texture, so the liquid will thoroughly wet the rough microstructures of the solid surface. On the contrary, the net traction is upward in the case of $\theta > \psi$ (Figure 15(e)), which will drive the liquid-gas interface back to the top of the columns and lead to a composite solid-liquid-gas interface (Figure 15(f)). Therefore, only the condition of $\theta \geq \psi$ can support a stable Cassie state. According to this design constraint, the liquids with low surface energy tend to wet many trapezoid-shaped superhydrophobic microstructures ($\psi > 90°$). Only the inverted-trapezoid-shaped surfaces ($\psi < 90°$) with reentrant texture have the possibility to support oils in the Cassie state on a solid substrate (Figure 15(f)) [73, 164]. Therefore, in addition to sufficiently rough micro/nanostructure and strict chemical modification, a reentrant curvature structure is necessary to achieve superoleophobicity in air. The superoleophobic surface can even repel oil droplets with a surface tension of 20~30 mN/m with an oil CA (OCA) of 150° or greater.

Bioinspired reentrant microstructures are critical for achieving superoleophobicity in the air [28, 32, 73]. Usually, a superoleophobic surface also repels water because the surface tension of water is much less than that of oils. The surface that can repel both water and low-surface-tension liquids is called a superamphiphobic surface [168–172]. Ultrafast laser-induced two-photon polymerization is a microscopic 3D printing technology and can construct 3D microstructures with submicrometer resolution. Liu et al. used this method to successfully prepare triply reentrant structures on various substrates, as shown in Figure 15(g) [112]. The flat substrate was immersed into the negative photoresist. Then, the laser was focused into the photoresist and directly wrote microstructures layer by layer. The high laser intensity in the focal point can trigger the radical polymerization reaction along the laser scanning path. The oligomers at the laser focal point were thus transformed into a dense and cross-linked polymer network via photoinduced reaction. After the printing process, the residual photoresist was removed with propylene glycol methyl ether acetate and isopropyl alcohol. Figure 15(g) shows the microstructure of the as-prepared triply reentrant structures. The structure has a slight overhang at the bottom of the inner vertical overhang compared to the doubly reentrant microstructure. The third overhang structure significantly increases the maximum critical breakthrough pressure to low-surface-tension liquids. The triply reentrant structure shows strong repellence to water (with surface tension γ of 72.8 mN m^{-1}) and various organic liquids ($\gamma = 12.0 - 27.1$ mN m^{-1}), such as n-dodecane, ethanol, hexane, and silicone oil. Even the fluorinated solvents (e.g., n-perfluorooctane) can also not wet the as-prepared superamphiphobic surface. Notably, the superamphiphobic reentrant structures can be written on various substrates, such as rigid silicon wafer (Figure 15(h)) and flexible polyimide film (Figure 15(i)). This feature enriches the application of artificial superamphiphobic surfaces.

Although two-photon polymerization can produce perfect reentrant structures, this method is still limited by processing efficiency and cannot produce superamphiphobic microstructure on a large scale. The main reason is that each unit of reentrant microstructure is induced by a large number of scanning lines and scanning layers. Except for two-photon polymerization, the femtosecond laser is difficult to directly write reentrant microstructures on the material surface. Han et al. proposed a new strategy to prepare hierarchical reentrant microstructure by combining femtosecond laser ablation and chemical etching method, as shown in Figure 16(a) [113]. The femtosecond laser was focused on the surfaces of the copper plates and scanned the sample in a pattern of cross lines. After repeating 40 times, the scanning lines of the grid became deep grooves because material removal occurs along the laser scanning path. The unablated area between the grid forms a uniform microcone array. The height of the microcones reaches up to 50 μm. The spatial period of the microcone array is in agreement with the space of the scanning space (e.g., 40 μm). Nanoparticle clusters are also distributed on the surface of the microcones. The size of the clusters ranges from 50 nm to 500 nm. Chemical analysis reveals that a thin layer of Cu_2O is formed on the microcones. Although the copper surface with microcones can exhibit good superhydrophobicity after perfluorodecyltrimethoxysilane modification, the OCA of a hexadecane droplet on the modified surface is only 14°. Therefore, the microcones covered with convex nanoparticle clusters are not enough to achieve superoleophobicity because of rare reentrant geometries. In the second step of the hybrid method, nanograss structures were grown on the surface of each microcone by an oxidation process. The Cu plate with microcones was immersed into a solution of 2.5 mol L^{-1} NaOH and 0.13 mol L^{-1} $(NH_4)_2S_2O_4$ for 20 min at room

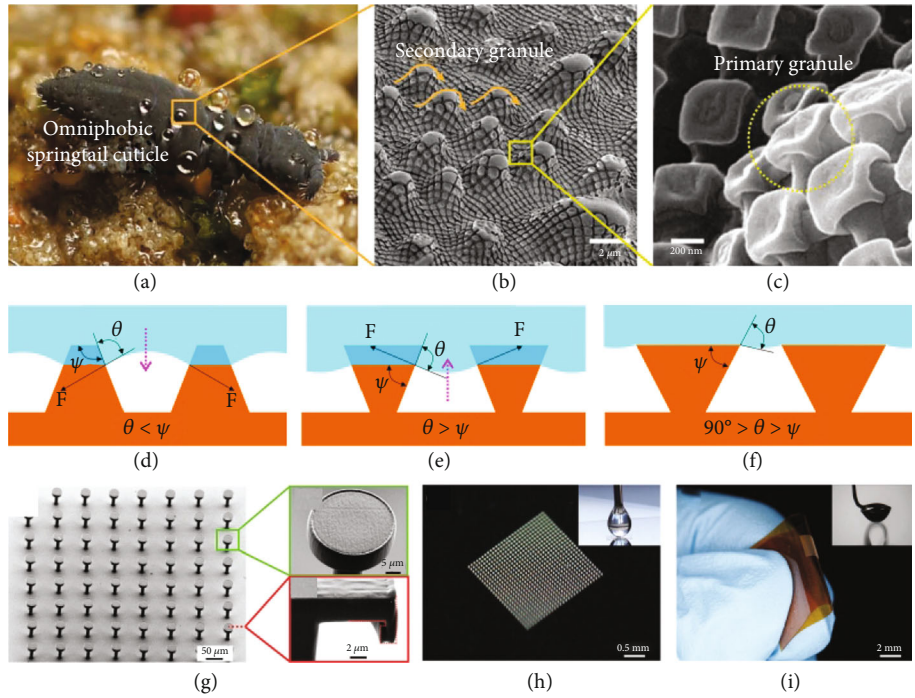

FIGURE 15: Achievement of superoleophobicity by designing reentrant structure. (a) Springtail. (b, c) Reentrant texture on the springtail skin. (d, e) Hypothetical solid-air-liquid interfaces on (d) a trapezoid texture and (e) an inverted-trapezoid texture. (f) Robust solid-liquid-gas interface of the liquid with low surface tension on the inverted-trapezoid (reentrant) texture. (g) Morphology of the triply reentrant structures prepared by two-photon polymerization. (h) Digital picture of triply reentrant structures on silicon wafer and its repellence to n-perfluorooctane (inset). (i) Digital picture of triply reentrant structures on flexible polyimide film and its repellence to n-perfluorooctane droplet (inset). Reproduced from [73, 112, 167] with the permission.

temperature. As a result, dense grass-like nanostructures were grown all over the surface of the microcones. The nanostructures are clusters of thin ribbons that are flexible and twisted with each other. The thickness of the ribbons is less than 10 nm, and the width of the ribbons is 40-80 nm. The nanograss structures are composed of CuO. As the ribbons are stacked layer by layer, the nanograss structures also result in porous features with plenty of local reentrant geometries. On the other hand, many upward convex nanostructures become sideward grown ones on the microcone surface, markedly enriching reentrant geometries. The hybrid method of femtosecond laser ablation and chemical bath produce a hierarchical structure with reentrant nanograss on microcones on the copper substrate (Figures 16(b)–16(d)). Finally, the Cu plate was immersed into an isopropyl alcohol solution of perfluorodecyltrimethoxysilane with a mass fraction of 0.5% for 2 h and then dried at 80°C for 2 h. A water droplet and a dodecane droplet can bead up on the resultant surface with a CA larger than 150°, so the enriched reentrant geometries endow the as-prepared surface with superamphiphobicity (Figure 16(e)).

The wettability of different liquids with the surface tensions ranging from 21.6 mN m^{-1} to 72.8 mN m^{-1} on the resultant surface was investigated, as shown in Figures 16(f) and 16(g). Before the liquid surface tension decreases to 27.5 mN m^{-1} (hexadecane), the CA and the SA of liquid droplets on the sample surface only have a slight change. The hexadecane droplet on the sample surface has an OCA of 157.7° and an oil SA (OSA) of 6°. With liquid surface tension further decreasing, the SA starts to increase rapidly. Regarding the dodecane with a surface tension of 25.4 mN m^{-1}, the surface still shows superamphiphobicity with an OCA of 154.7° and an OSA of 9.7°. However, an octane droplet (21.6 mN m^{-1}) can stick on the sample surface and cannot roll off at any tilting angle. Therefore, the as-prepared superamphiphobic surface can maintain excellent liquid repellence even the surface tension of liquid decreases to as low as 25.4 mN m^{-1} (dodecane). Compared to the 3D reentrant nanograss on microcones (sample 3D-NG@MC), the polished surface and the 2D nanograss on shallow microstructures (Sample 2D-NG@MC) are easy to lose liquid repellence to low-surface-tension liquids. The result demonstrates that the realization of the excellent superamphiphobicity is inseparable from the laser-induced ordered and deep microstructures and the reentrant nanostructures prepared by subsequent chemical etching. The hybrid method of the femtosecond laser ablation and chemical etching method successfully leads to superamphiphobicity for the copper plate.

4.2. Underwater Superoleophobic Surfaces. Fish can swim freely and keep their skin clean, even in oil-polluted waters. In 2009, Liu et al. revealed the root cause of underwater oil resistance of fish scales [19]. This property is mainly derived from the superoleophobicity of fish scales in water. Most fish skin is covered by fan-like scales,

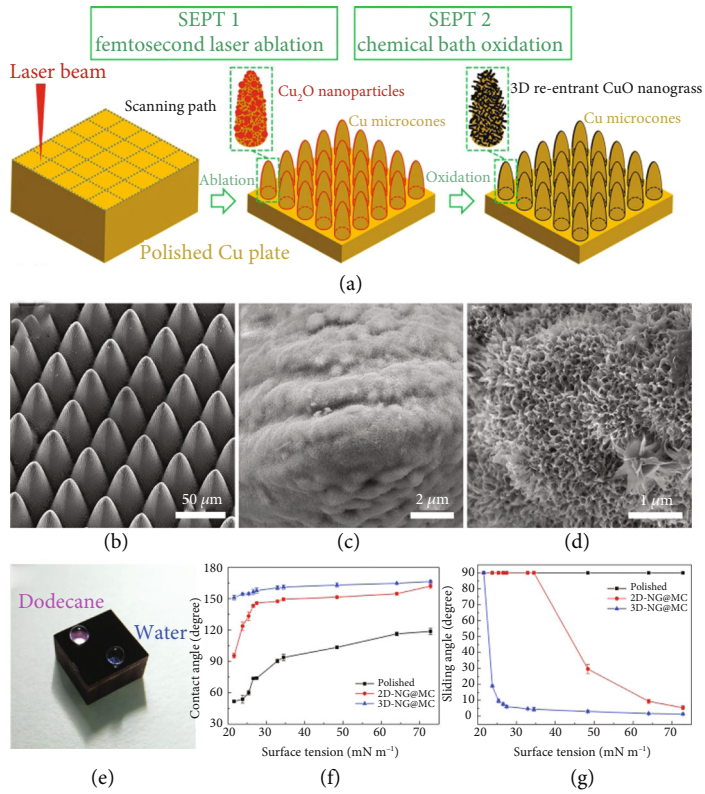

FIGURE 16: Realization of superamphiphobicity by the combination of femtosecond laser ablation and chemical etching method. (a) Schematic diagram of preparation process of superamphiphobic microstructure. (b–d) Morphology of the 3D reentrant nanograss on laser-structured microcones. (e) Photo of a water droplet and a dodecane droplet on the resultant surface. (f, g) Variation of the wettability of the as-prepared superamphiphobic surface on the surface tensions of different liquids. Reproduced from [113] with the permission.

such as carp (Figure 17(a)). There are many microscale hill-like protuberances orderly distributing on the surface of the fan-shaped fish scales along the fanning-out direction (Figure 17(b)) [20]. The protuberance microstructures are 100~300 μm in length and 30~40 μm in width (Figure 17(c)). The surface of each protuberance is further decorated with a large number of finer micro/nanoscale pimple structures (Figure 17(d)). In addition, fish scales consist mainly of hydrophilic calcium phosphate and protein skeletons and are also coated with a thin layer of mucous. Hydrophilic chemical composition and rough surface structure make fish scales have superhydrophilicity in air. The water droplets can spread out quickly on the surface of fish scales. By contrast, when the fish scales are immersed in water, the oil droplet on the scale surface can remain a spherical shape with an OCA of 156.4°, showing excellent underwater superoleophobicity (Figure 17(e)). In the water in which the fish lives, the surface microstructures on the scales are wetted by water, and the water fills in the space between the rough microstructures. A layer of trapped water forms on the surface of fish scales. When an underwater oil droplet is in contact with the fish scale, it is repelled by the trapped water layer and can only touch the tip of the rough microstructures. The trapped water cushion between the oil droplet and the fish scales results in an oil-water-solid three-phase system. This water cushion effectively prevents oil droplets from touching the solid substrate, resulting in enhanced oleophobicity. The oil droplet on the fish scales is at the underwater version of Cassie contact state, as shown in Figure 17(f). Therefore, the combination of hydrophilic chemical composition and rough surface morphology endows fish scales with excellent underwater superoleophobicity and oil-resistant property. Other organisms, such as clam shells, the lower surface of lotus leaves, seaweed, and filefish skin, also have underwater superoleophobic surfaces [69, 73]. The oil resistance of fish scales provides a feasible way of achieving superoleophobicity in a water medium by combining the high surface free-energy chemistry and suitable surface microstructures. Underwater superoleophobic surfaces can be easily prepared based on the effective route of "from in-air superhydrophilicity to underwater superoleophobicity" [173–177].

4.2.1. Silicon Surface. The first example of the femtosecond laser-induced underwater superoleophobic surface is the textured silicon surface [114]. The flat silicon surface presents hydrophilicity in the air with the intrinsic WCA of 60° (Figure 18(a)). When the flat silicon surface is placed in water, the 1,2-dichloroethane oil droplet on its surface shows an OCA of 124.6°, revealing underwater weak oleophobicity of the flat silicon (Figure 18(c)). Yong et al. fabricated an array of periodic hierarchical rough micromountains on the silicon surface through the single-step laser ablation, without additional chemical treatment [114]. Such morphology is

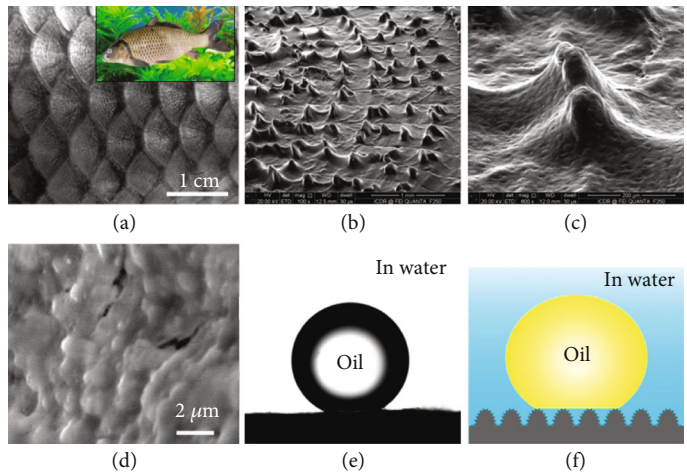

Figure 17: Underwater superoleophobicity of fish scales. (a) Photography of fish scales. (b, c) SEM images of the surface microstructure of a fish. (d) The fine structure on the protuberance microstructures of fish scales. (e) An oil droplet on the fish scale in water. (f) Underwater Cassie wetting state between oil droplet and the surface microstructure of a fish scale. Reproduced from [19, 20] with the permission.

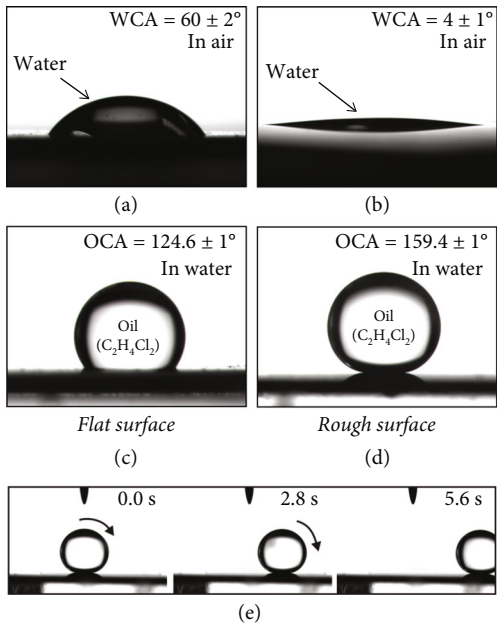

Figure 18: Wettability of the femtosecond laser-structured silicon surface compared to an untreated flat silicon surface. (a, b) Water droplet on (a) the untreated silicon substrate and (b) the structured silicon surface in air. (c, d) Oil droplet on (c) the untreated silicon surface and (d) the structured surface in a water medium. (e) Underwater oil droplet rolling away on the slightly tilted rough silicon surface. Reproduced from [114] with the permission.

very similar to that of the SEM images in Figure 9. The hydrophilicity of the sample surface was enhanced to superhydrophilicity by the laser-generated hierarchical microstructures. The water droplet dripped onto the rough surface could rapidly spread out, with a final WCA of 4° (Figure 18(b)). Like the fish scale, oil droplets could maintain an approximate sphere shape on the superhydrophilic silicon surface in water (Figure 18(d)). The measured OCA was as large as 159.4°. In addition, the underwater oil droplet would roll away once the sample was slightly tilted (e.g., 0.5°) or shaken, as shown in Figure 18(e). Such results indicate the underwater superoleophobicity and ultralow oil adhesion of the laser-ablated silicon.

The underwater superoleophobicity results from the underwater Cassie wetting of the oil droplet on the rough silicon surface in water [69, 73, 114]. Because of the superhydrophilicity, the laser-induced surface microstructure will be entirely wetted by water when the laser-ablated silicon is immersed in water. Of course, water also fills the valley of the hierarchical microstructures. When an oil droplet is further put on the underwater structured silicon surface, the oil droplet is prevented from effectively touching the silicon substrate by the trapped water in the microstructure. Such block effect is driven by the natural repulsive force between nonpolar oils and polar water. The oil droplet can just contact the top part of the rough microstructure. The trapped water cushion dramatically reduces the actual contact area between the silicon surface microstructure and the underwater oil droplet, thereby endowing the laser-treated surface with remarkable oil repellence as well as underwater superoleophobicity.

Li et al. ablated silicon surface in different liquid environments and obtained different surface microstructures by femtosecond laser [115]. They found that the physical property of the processing solution influenced the morphology of the laser-induced surface microstructures. When the silicon substrate was ablated in an ethanol solution using a femtosecond laser, microcones regularly covered the treated surface. By comparison, when the sample was ablated in a sucrose solution, a layer of micromolars was formed on the silicon surface. Both the viscosity and boiling point of the sucrose solution are higher than that of the ethanol solution. The heights of the laser-induced microcones and the micromolars were about 3.3 and 5.9 μm, respectively. The size of the resultant microcones and micromolars could be easily controlled by solutions and the energy of the laser pulses.

Both of the two kinds of rough surfaces treated by liquid-assisted laser ablation exhibited superhydrophilicity and underwater superoleophobicity. The underwater oil droplet showed an OCA of 157.76° on the microcones-structured surface (ablated in ethanol solution) and the droplet on the micromolars-structured surface (ablated in sucrose solution) showed an OCA of 169.21°.

4.2.2. Metals. Yong et al. used a femtosecond laser to ablate a titanium substrate, leading to rough surface morphology and surface oxidization [95]. After laser ablation, the typical hierarchical micromountains appeared on the substrate, with the surface color changing to black (Figures 19(a)–19(d)). In the aspect of the chemical composition, the laser-treated surface consisted of not only titanium but also a new oxygen element. The result indicates that the laser constructed a stratum of the rough TiO_2 layer on the original substrate. After UV treatment, the resultant surface became superhydrophilic in air, with a WCA of 2.5° to a water droplet (Figure 19(e)). Such in-air superhydrophilicity enabled underwater oil droplets (1,2-dichloroethane) to keep a spherical shape on the resultant surface with the OCA of 160.5° (Figure 19(f)) and to freely roll away with tilting the substrate at 1°. Although the sample will lose underwater superoleophobicity if stored in the dark for a long time, interestingly, the rough surface is able to reobtain superhydrophilicity as well as underwater superoleophobicity just by UV light irradiation again.

Zhang et al. prepared microscale and nanoscale textures and achieved underwater superoleophobicity on the surfaces of different metals through femtosecond laser ablation, including aluminum, copper, iron, molybdenum, and stainless steel [116]. The measured OCA values of underwater oil droplets (1,2-dichloroethane) on those laser-structured metals were 157° (aluminum), 155° (copper), 157° (iron), 152° (molybdenum), and 155.5° (stainless steel), respectively. Such high OCA values indicate the excellent underwater superoleophobicity of those structured metals. The treated metals also showed very low oil adhesion to the droplets of various oils in water, as the oil droplets on those samples could roll away by just microvibration. The ultralow oil-adhesive underwater superoleophobicity is ascribed to the inherent hydrophilicity of these metals and the formation of the laser-induced rough surface microstructures.

Li et al. enhanced the wettability of nickel surface from hydrophilicity to superhydrophilicity by femtosecond laser ablation [117]. The ablation was performed in a sucrose solution at the laser power of 0.19 mJ/pulse. Self-organized hierarchical microcones were uniformly generated on the sample surface during the solution-assisted laser ablation. The bottom of every microcone was 3 μm in diameter, and the surface of microcones was decorated entirely with villus-like structures with only 10-30 nm in size. The laser-induced hierarchical microcones made the treated nickel surface superhydrophilic in air and superoleophobic after the water immersion. The measured OCA and OSA were 166° and 2.2°, respectively, to the oil droplet on the laser-structured surface in water.

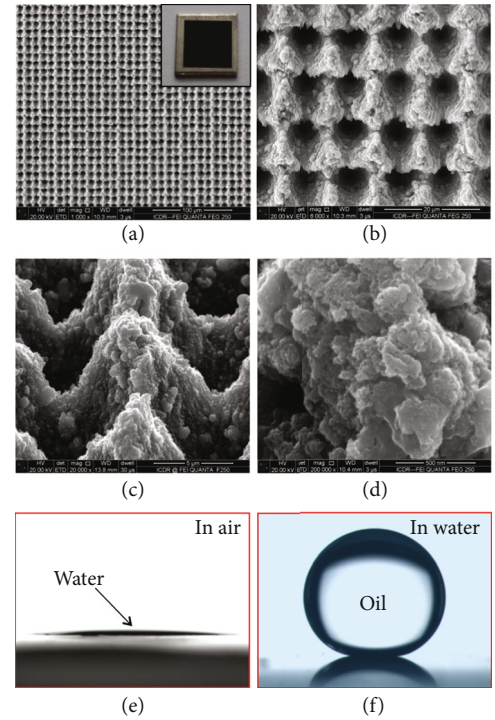

Figure 19: Surface microstructure and wettability of the femtosecond laser-ablated titanium substrate. (a–d) SEM images of the laser-induced hierarchical microstructure. Inset: image of the laser-treated titanium sheet. (e) Water droplet on the resultant surface in air. (f) Underwater oil droplet on the resultant surface. Reproduced from [95] with the permission.

4.2.3. Glass. Figure 20(a) shows a piece of silica glass after femtosecond laser ablation [118]. The treated glass looks opaque due to the existence of rough surface microstructure on the silica glass surface. There are full of nanoparticles with the size of tens to hundreds of nanometers randomly distributing on the sample surface (Figures 20(b)–20(d)). Plenty of nanoscale holes and grooves are also formed between the nanoparticles. The nanoscale structure is believed to have developed from the resolidification of the molten ejected particles that fell on the substrate surface and cooled down instantly during laser ablation. The nanostructured silica glass presents superhydrophilicity in the air. At the same time, it shows underwater superoleophobicity to a series of oils, including 1,2-dichloroethane, chloroform, hexadecane, crude oil, petroleum ether, sesame oil, and paraffin liquid. For example, the measured OCA of a 1,2-dichloroethane droplet on such surface in water is 160.2° (Figures 20(e) and 20(f)). This droplet also can freely roll away on a 1° tilted sample, meaning that the OSA is lower than 1°. Surprisingly, the laser-structured glass becomes transparent after the immersion in the water besides the underwater superoleophobicity (Figure 20(e)). The black letters behind the glass can be seen. The transmittance of the aquatic sample is close to that of untreated silica glass, reaching up to 91.6% at the wavelength of 632 nm. The existence of the water environment improves transparency. In a water medium, the laser-induced nanostructure of the silica glass surface is thoroughly wetted by water, resulting in a glass/

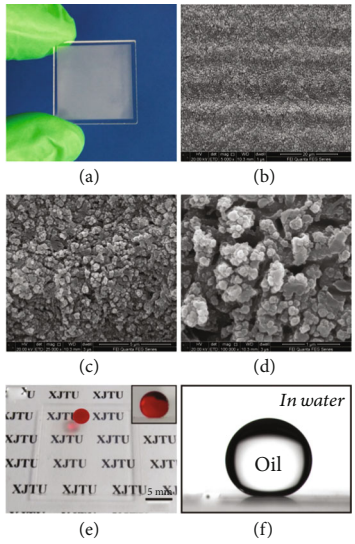

FIGURE 20: Underwater superoleophobicity and high transparency of the silica glass after femtosecond laser treatment. (a) Photography of a piece of the treated silica glass. (b–d) Surface microstructure of the laser-ablated silica glass. (e) Photography of an oil droplet (red color) on the as-prepared glass in water. (f) Underwater oil droplet on the rough glass surface. Reproduced from [118] with the permission.

water interface. In general, if two different media have closer refractive indices, a more negligible reflectance will occur at the interface of such two media. Because the refractive index difference between silica glass and water is smaller than that between silica glass and air, the Mie scattering and the reflectance of the rough silica glass are weakened by the water medium, endowing the laser-ablated surface with good underwater transparency.

In addition to the silica glass, underwater superoleophobic microstructures also can be generated on the surface of more common and cheap glass. Yong et al. and Huo et al., respectively, used the femtosecond laser to induce different microstructures or micropatterns on the surface of glass slides [119, 120]. The resultant surfaces showed superoleophobicity in water because of the formation of rough microstructures and the intrinsically water-loving chemistry of the glass substrate. Furthermore, the adhesion of the laser-structured glass surfaces to underwater oil droplets could be adjusted from ultralow to ultrahigh by changing the morphology of the laser-induced microstructures or micropatterns. The ultralow oil-adhesive superoleophobic glass surfaces had excellent oil resistance in the water. In contrast, the glass surfaces with very high oil adhesion were successfully applied in the no-loss transportation of tiny oil droplets, the fusion of oil/organic microdroplets, and the rapid capture of oil droplets.

4.2.4. Polymers. Polymers are considered one of the most challenging substrate materials for achieving underwater superoleophobicity because most polymer materials are inherently hydrophobic and dissolve easily in oils and organic solutions. Yong et al. reported a novel method to switch the oil wettability of the femtosecond laser-structured rough PDMS surface from underwater superoleophilicity to underwater superoleophobicity [89]. The laser ablation process created a kind of hierarchical microstructure on the PDMS substrate (Figures 21(a) and 21(b)). The original laser-treated PDMS surface was superhydrophobic in the air due to the rough surface microstructure and the hydrophobic nature of the PDMS material. The measured WCA and WSA of a water droplet on the surface were 155.5° and 2°, respectively (Figure 21(c)). A silver mirror-like reflectance could be seen as the PDMS surface was dipped into water, demonstrating the existence of a thin layer of trapped air between the PDMS surface and the surrounding water. At present, when an underwater oil (1,2-dichloroethane) droplet was made in contact with the PDMS surface, it would rapidly spread out along the trapped air layer after just contacting with the PDMS surface, resulting in the final OCA of this droplet being only 6.5° (Figure 21(d)). This process was driven by capillary action and pressure. Therefore, the original laser-structured superhydrophobic PDMS surface showed superoleophilicity underwater. Interestingly, the wettability of the laser-ablated PDMS surface could be reversed just through oxygen plasma irradiation for a short time. After the rough PDMS sample suffering from oxygen plasma treatment for 30 s (55 W), the surface turned superhydrophilic in air. Water could thoroughly wet the sample surface with a WCA of 4.5° (Figure 21(e)). Likewise, underwater superoleophobicity was presented by the plasma-irradiated rough PDMS surface. Underwater oil droplets on such a surface had an OCA of 158° (Figure 21(f)). They could roll off when the surface was angled at 3° (Figure 21(g)), revealing strong oil-repellent ability and ultralow oil adhesion of the PDMS substrate in a water medium. The switch from underwater superoleophilicity to superoleophobicity results from the oxygen plasma-induced chemical change of the laser-treated PDMS surface [178]. Oxygen plasma irradiation is one of the most used methods for activating PDMS material. The original -CH_3 of the PDMS substrate can be replaced by the -OH group during the short-time plasma irradiation, resulting in the formation of hydrophilic radical silanol group (-SiOH) on the PDMS surface (Figure 21(h)) [89, 124, 179]. The surface morphology of the PDMS sample was almost unchanged due to the short exposure time. As a result, the laser-induced rough microstructure and the oxygen plasma-induced hydrophilic chemistry allowed the PDMS surface to show superhydrophilicity in air and underwater superoleophobicity.

4.3. Applications of Superoleophobic Surfaces. Superoleophobic materials have strong repellence to oil, making them widely applied in the use and treatment of oils. Superamphiphobic materials also have superhydrophobicity, so most applications of superhydrophobic materials are also applicable to superamphiphobic materials. On the other hand, the applications of underwater superoleophobic materials are often limited to water mediums.

4.3.1. Antioil Contamination. When optical devices work in a water medium, they are easily polluted by oil contaminations, which leads to the degradation of optical performance.

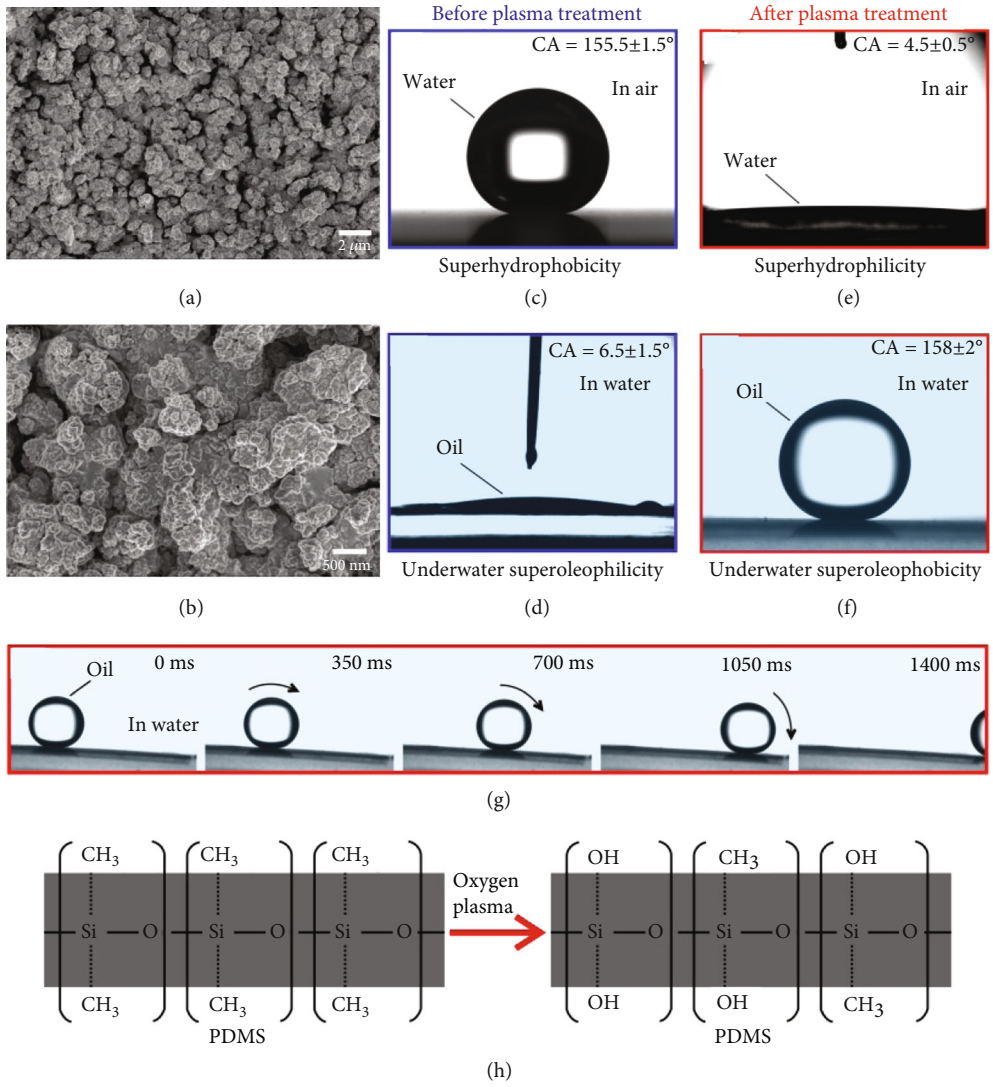

FIGURE 21: Underwater superoleophobicity of the femtosecond laser-structured PDMS surface after oxygen plasma irradiation. (a, b) SEM images of the ablated PDMS surface. (c) Water droplet (in air) and (d) oil droplet (in water) on the rough PDMS surface before plasma treatment. (e) Water droplet (in air) and (f) oil droplet (in water) on the rough PDMS surface after plasma treatment. (g) Oil droplet rolling on the tilted underwater superoleophobic PDMS sample in water. (h) Oxygen plasma-induced chemical change of the PDMS surface. Reproduced from [89] with the permission.

Yong et al. prepared underwater superoleophobic microstructures on a glass surface by femtosecond laser ablation [119]. When the organic pollutant was poured over the sample in a water medium, the pollutant adhered to the untreated areas. By contrast, the laser-treated area was kept clean and free from contamination (Figure 22(a)). Li et al. prepared a microlens array on K9 glass via femtosecond laser wet etching technique [180]. The femtosecond laser direct writing method was used to process the entire surface of the microlens array, and fine micro/nanoparticles were formed on the surface of each microlens. The formation of micro/nanostructure does not affect the optical properties of the microlens array in water. The textured microlens array still shows remarkable underwater imaging capability. In addition, the micro/nanoparticles enable the microoptical device to have underwater superoleophobicity. The microlens array greatly repels oils in the water, preventing this device from contaminating with oil or grease underwater. The underwater microlens array also has a self-cleaning function. When an oil-contaminated device is dipped into water, the oil molecules in the surface structure are replaced by water due to the underwater superoleophobicity (Figure 22(b)). Since the device is completely submerged in water, all oil contaminants are cleaned without any residue.

4.3.2. Manipulation of Oil Droplets. The oil loss caused by the residue in the process of manipulating tiny oil droplets can be avoided by using underwater superoleophobic materials. Yong et al. controlled the oil adhesion of the femtosecond laser-induced underwater superoleophobic glass surface by changing the surface morphology [119]. As the average distance of each pulse-ablated position increases, the oil

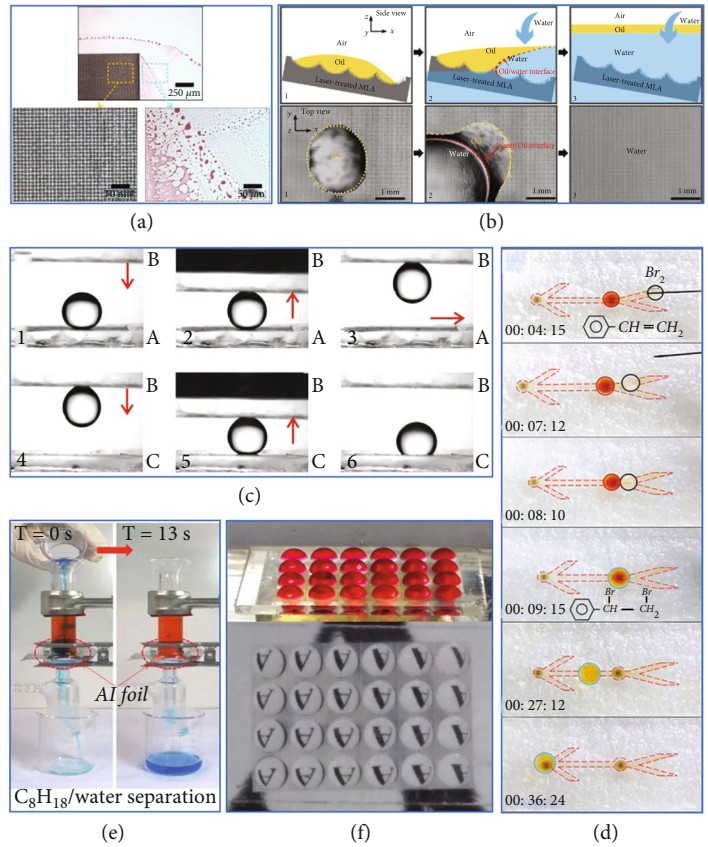

FIGURE 22: Application examples of the femtosecond laser-structured superoleophobic surfaces. (a) Underwater superoleophobicity preventing substrate from being polluted by oil contaminations in water. (b) Self-cleaning oil contaminants on an underwater superoleophobic surface after immersion in water. (c) Transferring tiny oil droplet by using an underwater superoleophobic surface as a "mechanical hand". (d) Guiding oil droplets to move along the designed tracks. (e) Separation the mixture of water (blue) and oil (red) by using the prewetted porous underwater superoleophobic sheet. (f) Restricting oil in the special region by the underwater superoleophobic microstructures. Reproduced from [119, 180–183] with the permission.

adhesion can be tuned from ultralow to ultrahigh. The oil droplets roll away easily on the surface with very low oil adhesion, while the oil droplets stick firmly on the surface with very high oil adhesion. The controllable oil adhesion enables the as-prepared underwater superoleophobic surfaces to manipulate oil droplets in an aqueous environment. For example, the ultrahigh oil-adhesive superoleophobic surface can pick up an oil droplet from a low oil-adhesive surface because the oil droplets tend to adhere to the surfaces with stronger oil adhesion. The oil droplet can be further released onto an ordinary oleophobic surface that has the highest oil adhesion. In this way, the oil droplet is successfully transferred from the surface with lower oil adhesion to the surface with higher oil adhesion (Figure 22(c)). The oil transportation process has almost no oil loss because of the underwater superoleophobicity of the "mechanical hand".

4.3.3. Guiding the Movement of Oil Droplets. The underwater superoleophobic track can be used for the dynamic migration of oil droplets. Cheng et al. used the femtosecond laser etching method to fabricate deep grooves on the PDMS substrate [181]. Multiple laser ablation was performed in the groove domain. For example, an array of period groove-like tracks with a width of 200 μm and a height of 88 μm was prepared. The top and bottom of the tracks are covered with laser-induced rough microstructure. After oxygen plasma treatment, the tracks exhibit underwater anisotropic superoleophobicity. Although the adhesion of the resultant surface to oils in water is low, the oil droplets are more likely to roll along the tracks with an OSA of 1° rather than along the perpendicular direction with an OSA of 6°. The track can guide the movement of the oil droplets underwater with no oil attached. When a drop of styrene in carbon tetrachloride and a drop of bromine in carbon tetrachloride solution were guided to contact with each other by the resultant tracks underwent, the two droplets joined together, triggering the additional reaction between the styrene and bromine droplets (Figure 22(d)). The result shows that the microdroplet reaction with a small amount of reactants can be realized based on the underwater anisotropic superoleophobic tracks.

4.3.4. Oil/Water Separation. The underwater superoleophobic surface usually has superhydrophilicity. The inverse wettability of underwater superoleophobic materials to oil and water allows them to separate the mixture of water and oils. For example, Li et al. fabricated an array of regular

micropores on an ultrathin aluminum foil via femtosecond laser perforation [182]. The diameter of the laser-perforated pores is as low as 2.4 μm. Both the edges and the inner walls of the micropores are covered with rich rough nanostructures. The hierarchical structure composed of microspores and nanoscale roughness makes the resultant porous foil superhydrophilic and underwater superoleophobic. When the mixture of water and oil was poured onto the as-prepared porous foil prewetted with water, the water phase easily permeated through the foil because of the superhydrophilicity of the pores. In contrast, the underwater superoleophobicity enabled the foil to repel the oil so that the oil phase was intercepted by the foil and could not pass through the porous foil. The oil always stayed on the top of the foil. As a result, the oil-water mixture was successfully separated (Figure 22(e)). Yin et al. created underwater superoleophobic nanostructure directly on the surface of stainless steel mesh by femtosecond laser processing [183]. The mesh has an inherent porous microstructure. The underwater superoleophobic mesh can also separate the mixture of water and oil as it just lets the water pass through.

4.3.5. Oil Patterning. The liquid repellence enables the superoleophobic microstructures to pattern the liquid. In a composite pattern composed of the superoleophobic domain and ordinary domain, oil is only allowed to contact with the ordinary domain, so it is restricted in this domain by the surrounding superoleophobic structure. Therefore, a variety of liquid patterns can be implemented. Yong et al. prepared a pattern of an array of circles on the glass substrate using a femtosecond laser to ablate the glass surface selectively [184]. The pattern consists of inner unablated flat circles and a surrounding laser-induced microstructure. Smooth glass surfaces are oleophobic, while the laser-induced microstructures exhibit superoleophobicity underwater. In water, when oil is dripped on a circle, the oil covers the entire circle and cannot spread to the structured area. The underwater superoleophobic microstructures confine oil in the untreated circles, forming an array of underwater oil droplets (Figure 22(f)). Surface tension causes the oil droplets to appear as convex lens shapes, and the array of oil droplets forms a lens system with the surrounding water environment. The liquid lens array has excellent imaging capability.

5. Underwater Superaerophobicity and Superaerophilicity

Bubbles can usually be present in liquids. Like the wettability of water and oil, if the wetting behavior of bubbles on solid materials can be designed, these materials can be used to manipulate bubbles in the water. There are also two extreme states of underwater bubbles on the solid surfaces [185–188]. The surface shows underwater superaerophobicity to bubbles when the bubble has a bubble CA (BCA) larger than 150° on the material surface. On the contrary, if the BCA of the bubble on the material surface is less than 10°, the surface is underwater superaerophilic. Controlling the bubble wettability of a solid substrate has a broad application prospect, which is helpful to make rational use of bubbles and avoid the damage caused by bubbles in the liquid.

5.1. Underwater Superaerophobic Surfaces. In nature, it is difficult for bubbles to adhere to the fish skin, and the adhesion of bubbles will adversely affect fish survival. If the bubbles stick mainly to one side of the fish, the fish will be difficult to maintain balance, especially for little fish. Attached air bubbles also increase drag underwater, and fish cannot swim fast enough to become easy prey. Through evolution and natural selection, fish have evolved perfectly versatile surfaces adapted to the liquid living environment and resistant to bubble adhesion [121]. Fish scales are hydrophilic in the air because they are composed of hydrophilic chemical composition and have a hierarchical surface microstructure. When the fish scale is immersed in the water, and a small bubble is released on the surface of the scale, the bubble remains spherical with a BCA of 155° (Figure 23(a)). Once the fish scale is slightly tilted by 9°, the bubble will be free to roll from the surface (Figure 23(b)). The results show that the fish scales have superaerophobicity and low adhesion to bubbles in the water. This underwater superaerophobicity gives the fish scales the ability to repel bubbles, preventing them from sticking to the fish's skin.

Figures 23(c)–23(f) reveal the formation mechanism of the underwater superaerophobicity of fish scales. When the fish scale is immersed into water, its surface microstructure is thoroughly wetted by water because of its hydrophilicity (Figures 23(c) and 23(d)). The trapped water filled in the surface microstructure exerts a repulsive force on the bubbles due to the incompatibility of water and air. When a bubble is released on the fish scale in the water, the bubble is repelled by the trapped water and only touches the peak of the surface microstructure of the scale in the underwater Cassie contact state (Figures 23(e) and 23(f)) [1, 73, 121]. This wetting state is very stable, allowing the bubble remain spherical over time. The effective contact between the gas and the fish scale is significantly reduced so that the fish scales have excellent repulsion and superaerophobicity to the bubbles in the water. Inspired by fish scales, underwater superaerophobicity can be easily obtained by producing micro/nanostructures on a hydrophilic (high-surface-energy) substrate [189–192]. In general, underwater superaerophobic materials have a strong ability to repel gas in water.

5.1.1. Silicon. Mimicking fish scales, Yong et al. used femtosecond laser treatment to achieve underwater superaerophobicity on the silicon surface [121]. Silicon is essentially hydrophilic, similar to the chemistry of fish scales. After ablation by femtosecond laser, micro/nanoscale structures are formed on the silicon substrate (Figures 24(a) and 24(b)). Micromountains of 7-8 μm in size are evenly distributed on the silicon surface. The surface of each micromountain is covered with nanoparticles. The rough hierarchical microstructure makes the silicon surface superhydrophilic in air. Water droplets can rapidly wet the surface structure of the silicon and disperse (Figure 24(d)). The WCA of water is 5° ± 1°. To study the wettability of underwater bubbles on

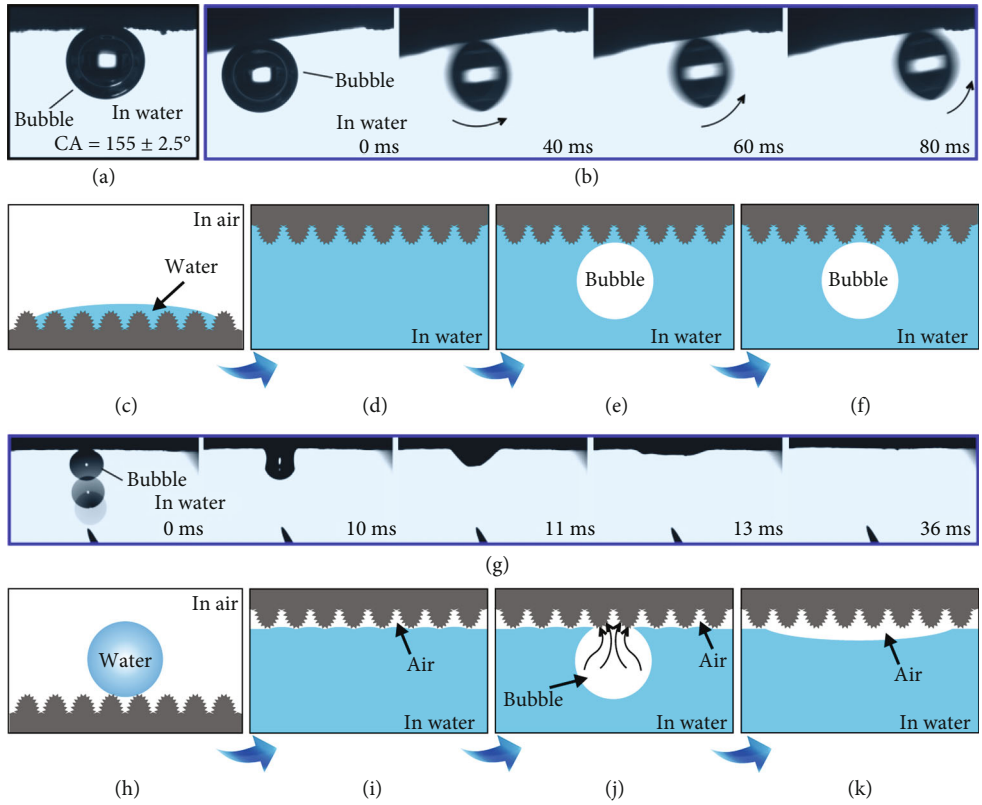

FIGURE 23: Underwater superaerophobicity of fish scale and underwater superaerophilicity of lotus leaf. (a) Small bubble on the fish scale in water. (b) Process of an underwater bubble rolling off a fish scale. (c–f) Formation mechanism of the underwater superaerophobicity: (c) water wetting the hierarchical microstructure of fish scale, (d) fish scale in water, (e) releasing a bubble onto the surface of the fish scale in water, and (f) after a period of time. (g) Process of a bubble spreading out on a lotus leaf in water. (h–k) Formation mechanism of the underwater superaerophilicity of lotus leaf: (h) water siting on the hierarchical microstructure of lotus leaf, (i) lotus leaf in water, (j) releasing a bubble onto the surface of the lotus leaf in water, and (k) after a period of time. Reproduced from [121] with the permission.

the silicon surface, the sample was immersed in water, and the bubbles were released on the surface of the samples. The untreated smooth silicon surface has an underwater aerophobicity, and a tiny bubble on this surface has a BCA of 125° ± 2°. The bubble can firmly adhere to the smooth surface at any tilted angle, indicating the silicon surface has high adhesion to the bubble. In contrast, the laser-structured silicon surface can support the bubble as a spherical shape with the BCA of 162° ± 2° (Figure 24(c)). As long as the surface is tilted by 2°, the bubble will quickly roll away from the sample surface, so the rough silicon surface shows ultralow adhesion to the bubbles (Figure 24(e)). Therefore, the femtosecond laser-induced surface microstructure endows the silicon surface with underwater superaerophobicity. The underwater superaerophobic silicon surface has a strong ability to repel bubbles in water and is very similar to fish scales.

5.1.2. Metals. Most metals are hydrophilic. Underwater superaerophobicity can be achieved on the metal surface by forming a proper surface microstructure. For example, Yong et al. obtained underwater superaerophobicity on the aluminum substrate by femtosecond laser processing [122]. Each laser scanning line produced a single groove. Microgroove array was fabricated on the aluminum surface by the line-by-line scanning process (Figures 25(a) and 25(b)). The width and the depth of the laser-induced microgrooves are about 35.2 μm and 20.9 μm, respectively. The surface of the ridges between the microgrooves is also randomly decorated with abundant nanoparticles (Figures 25(c) and 25(d)). The microgrooves are mainly caused by laser-induced material removal, and the nanoparticles come from the resolidification of the ejected particles during laser ablation. The micro/nanoscale hierarchical structure makes the laser-ablated surface exhibit superhydrophilicity in air. The rough surface shows a WCA of 1.7 ± 1.8° to water droplet. When the aluminum is dipped into water, the laser-ablated area is fully wetted by water (Figure 25(e)). A small bubble can keep a spherical shape on the rough aluminum surface in water (Figure 25(g)). The BCA of the bubble is 154 ± 1°, revealing the underwater superaerophobicity of the laser-structured surface. The underwater superaerophobic aluminum surface also shows ultralow adhesion to air bubbles in the water. The bubble can easily roll away once the surface is slightly tilted.

Yong et al. ablated the stainless steel surface by a femtosecond laser and induced a three-level hierarchical microstructure consisting of microgrooves, microspikes, and nanoripples [123]. Before laser treatment, the stainless steel surface exhibits hydrophilicity. The water droplet on the

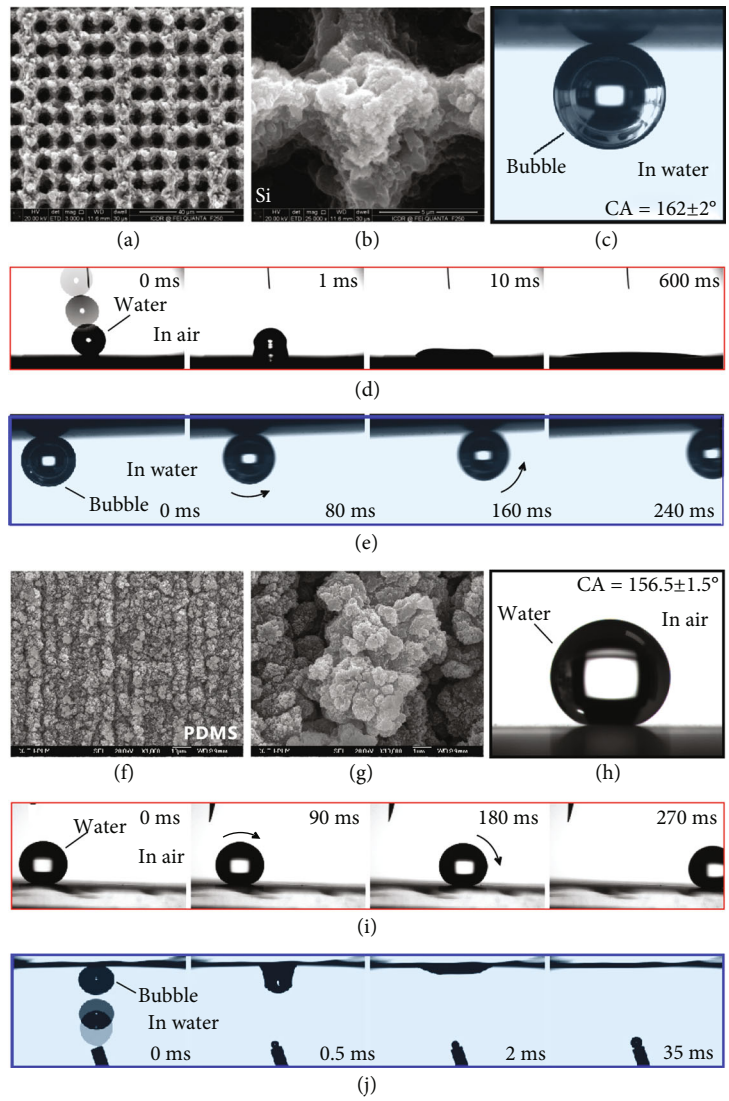

FIGURE 24: Underwater superaerophobicity of silicon surface and underwater superaerophilicity of PDMS surface achieved by femtosecond laser processing. (a, b) Surface microstructure of the silicon substrate after laser ablation. (c) Bubble on the structured silicon surface in water. (d) Water droplet falling onto the structured silicon surface in air. (e) Underwater bubble rolling away the structured silicon surface. (f, g) Surface microstructure of the PDMS substrate after laser ablation. (h) Water droplet on the structured PDMS surface in air. (i) Water droplet rolling off the structured PDMS surface. (j) Releasing a bubble onto the structured PDMS surface in water. Reproduced from [121] with the permission.

untreated stainless steel has a WCA of $79.8 \pm 1.6^{\circ}$. The BCA of a bubble on the smooth stainless steel is $111.9 \pm 4.6^{\circ}$ in water, so the surface is underwater aerophobic before laser treatment. The hierarchical microstructure produced by femtosecond laser ablation can enhance the underwater bubble wettability of the stainless steel. Interestingly, the laser-ablated surface strongly repels bubbles in the water. An underwater bubble on the structured stainless steel has a BCA of $152.4 \pm 1.6^{\circ}$ and can easily roll off with a bubble SA (BSA) of $1.1 \pm 0.9^{\circ}$. Therefore, femtosecond laser treatment endows the stainless steel surface with underwater superaerophobicity and excellent bubble repellence in water.

5.1.3. Polymers. Yong et al. obtained underwater superaerophobicity on the PDMS surface by the femtosecond laser processing and novel plasma irradiation [89, 124]. A kind of micro/nanoscale hierarchical structure was created on the PDMS substrate through one-step femtosecond laser ablation. The cooperation of the rough binary structures and hydrophobic chemical composition results in excellent superhydrophobicity for the PDMS surface. Usually, the surface-free energy of PDMS can be increased by oxygen plasma irradiation. Plasma irradiation can convert the original $-CH_3$ groups on the PDMS surface into the hydrophilic silanol radical group (-SiOH) [178, 179]. After oxygen plasma irradiation, the laser-structured surface is superhydrophilic in air. Water droplets can easily wet the laser-ablated area with a final WCA of $6 \pm 1.5^{\circ}$. In a water medium, the plasma-treated rough PDMS surface can repel bubbles. The BCA of the spherical bubbles on the resultant

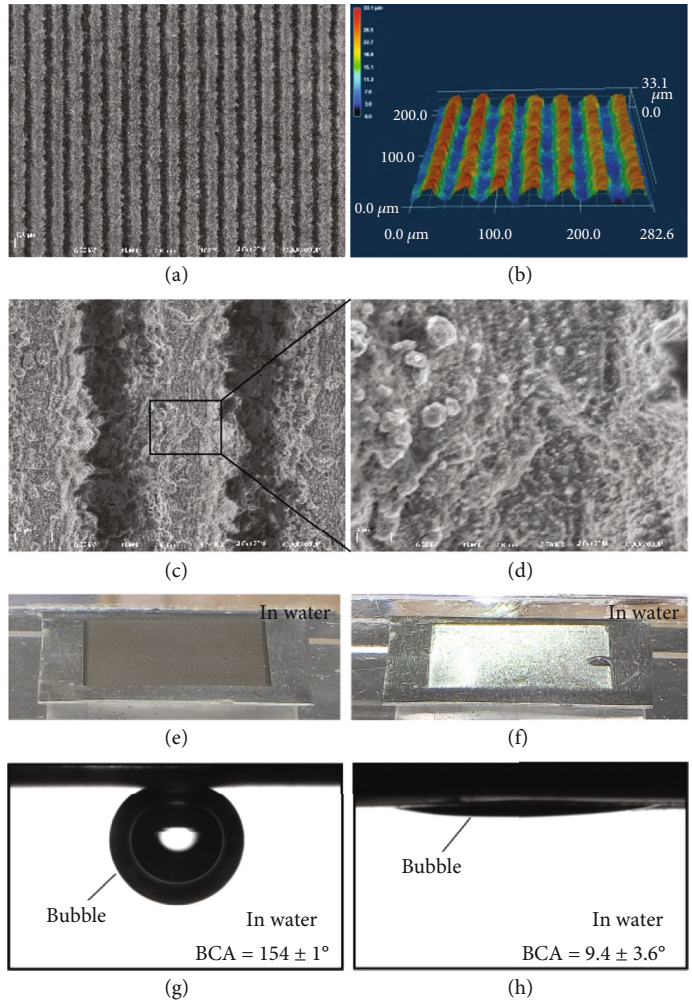

Figure 25: Underwater superaerophobicity and superaerophilicity of the femtosecond laser-structured aluminum surface. (a) Laser-induced hierarchical microgrooves on the aluminum surface. (b) 3D profile of the hierarchical microgrooves. (c, d) High-magnification SEM images of the microstructure produced by femtosecond laser ablation. (e) Laser-structured surface in water. (f) Fluorinated rough aluminum surface in water. (g) Bubble on the laser-structured surface underwater. (h) Bubble on the fluorinated rough aluminum surface underwater. Reproduced from [122] with the permission.

PDMS surface reaches up to 156 ± 1.5°. As long as the surface is tilted by 2°, the bubbles will roll away rapidly. These results indicate that the PDMS surface shows superaerophobicity in water after femtosecond laser ablation and oxygen plasma irradiation.

5.2. Underwater Superaerophilicity. Water spiders and flies can breathe in water [193, 194]. When they dive into the water to feed, a layer of air forms around their bodies. Even underwater, they can breathe oxygen from this layer of air. This type of breathing is commonly referred to as "physical gill breathing" or "breastplate breathing." The floating ferns *Salvinia* can also capture air in water, with the ability to retain air for a long time [195]. The surface of these creatures has the ability to absorb gases in water, showing great underwater superaerophilicity. It is worth noting that the abovementioned underwater superaerophilic surfaces are superhydrophobic in air. The most famous superhydrophobic surface is the lotus leaf, whose superhydrophobicity is due to the synergistic effect of hierarchical surface microstructure and low-surface-energy chemical composition. When the lotus leaf is immersed in water, the silver-mirror-like light reflection around the lotus leaf can be directly observed with the naked eye, indicating that a layer of air is trapped between the surface of the lotus leaf and the water. As shown in Figure 23(g), once a bubble is released below the lotus leaf in the water, it rises and touches the lotus leaf. It is found that the bubble spreads rapidly on the lotus leaf surface after contacting with the lotus leaf and is finally absorbed by the lotus leaf. The BCA of the bubble is close to 0°, so the superhydrophobic lotus leaf has excellent underwater superaerophilicity [121].

Figures 23(h)–23(k) describe the formation mechanism of the underwater superaerophilicity of the lotus leaf. The contact between lotus leaves and water is in the Cassie state (Figure 23(h)). When the superhydrophobic lotus leaf is immersed in water, water cannot wet the surface microstructure of the lotus leaf due to its excellent superhydrophobicity.

A layer of air is formed between the water medium and the surface microstructure of the lotus leaf (Figure 23(i)). If a gas bubble rises and touches the lotus leaf in the water, the gas in the bubble is easily pushed by the water pressure into the air layer around the lotus leaf (Figure 23(j)) [26, 121]. Finally, the gases in the bubble and in the trapped air layer merge (Figure 23(k)). The gas bubble appears to be absorbed by the superhydrophobic lotus leaf. Therefore, the lotus leaves show underwater superaerophilicity. Inspired by lotus leaves, underwater superaerophilicity can be easily obtained by producing micro/nanostructures on a hydrophobic (low-surface-energy) substrate [93, 196–199]. The materials with underwater superaerophilicity have a remarkable ability to absorb and capture gas bubbles underwater.

5.2.1. Polymers. PDMS is a kind of natural hydrophobic material. Yong et al. used a femtosecond laser to prepare hierarchical rough micro/nanostructures on the surface of the PDMS substrate (Figures 24(f) and 24(g)) [121]. The surface wettability of the PDMS is enhanced from hydrophobicity to superhydrophobicity by laser ablation (Figures 24(h) and 24(i)). In water, once a bubble touches the laser-structured surface, the bubble will spread rapidly over the PDMS surface within 35 ms (Figure 24(j)). The structured surface completely absorbs the bubble with a BCA of ~0°. Therefore, the PDMS surface is superaerophilic in water. Like lotus leaf, the underwater superaerophilic PDMS surface has the function of absorbing gas in water.

Huo et al. achieved underwater superaerophilicity on the PTFE surface by femtosecond laser ablation [125]. The laser-structured surface is characterized by a coral-forest-like dual-scale morphology consisting of a large number of microscale protrusions and fine nanoscale protuberances. In water, the BCA of a bubble is only 8.5° on the structured PTFE surface. The bubble can be merged with the prior-existing air cushion over the microstructures within 0.12 s.

5.2.2. Metals. Yong et al. used fluoroalkylsilane (1H,1H,2H,2H-perfluorodecyltriethoxysilane) to modify the laser-ablated aluminum substrate [122]. The aluminum maintained its hierarchical surface microstructure, while the modification treatment turned the sample from superhydrophilic to superhydrophobic. Water droplet on the modified surface has a WCA of $155.3 \pm 1.2°$ and WSA of $6.3 \pm 1.2°$. In water, the structured area reflects mirror-like light because a thin layer of trapped air exists on the superhydrophobic surface (Figure 25(f)). A bubble can spread out on the sample surface within 40 ms. The BCA of the bubble is only $9.4 \pm 3.6°$, demonstrating the underwater superaerophilicity of the laser-structured aluminum surface after fluoroalkylsilane modification (Figure 25(h)). Similarly, when the surface energy of the femtosecond laser-structured stainless steel is reduced, the surface can also present superaerophilicity underwater [123]. After femtosecond laser treatment, the rough stainless steel was immersed into a 0.01 M ethanol solution of stearic acid for 12 h. The resultant surface is superhydrophobic in air. Water droplet on the sample surface has a WCA of $156.3 \pm 0.8°$ and a WSA of $2.3 \pm 0.3°$. When a bubble comes in contact with the resultant surface in water, the bubble will rapidly spread out after just contacting the stainless steel surface and be absorbed by the sample surface. The stainless steel surface shows underwater superaerophilicity with a BCA of $1 \pm 1°$ to bubbles in the water.

5.2.3. Silicon. Although the laser-structured silicon surface shows underwater superaerophobicity, the bubble wettability can be changed to superaerophilicity by chemical modification. Yong et al. reduced the surface free energy of the femtosecond laser-ablated silicon surface by fluoroalkylsilane modification [126]. The resultant surface shows superhydrophobicity in air. When the surface is submerged in water, quasi-superaerophilicity is exhibited by the modified rough silicon surface. The BCA of bubbles on the silicon surface is as low as $12.2 \pm 0.7°$.

5.3. Applications of Underwater Superaerophobic/Superaerophilic Surfaces

5.3.1. Underwater Antibubbles and Bubble Absorption. The behavior of a bubble on a solid surface depends on the wettability of the solid surface to bubbles [26, 89, 121]. The underwater superaerophobic surface has the function of resisting bubbles in the water. It is difficult for bubbles to adhere to such a surface. In contrast, bubbles are easy to spread over an underwater superaerophilic surface and are eventually absorbed by the surface in the water. The unique bubble wettability endows the underwater superaerophobic and superaerophilic materials with significant advantages in manipulating bubbles in the aqueous environment.

5.3.2. Manipulation of Underwater Bubbles. Huo et al. fabricated microstructures on a thermally responsive shape-memory polymer by femtosecond laser ablation [200]. The original smooth substrate is inherently aerophobic and shows high adhesion to bubbles underwater. When the substrate is turned over or upright, the bubbles are constantly pinned to this polymer surface. After ablation by femtosecond laser, the polymer surface exhibits superaerophobicity and ultralow bubble adhesion underwater. The bubble rolls easily over the sample surface when the substrate is tilted at an angle of 3°. Square pattern arrays were prepared on the polymer surface using a femtosecond laser to selectively ablate the partial domain of the sample surface. The hybrid pattern is composed of a low-adhesive structured domain and a high-adhesive smooth domain. By adjusting the area fraction of the structured domain to the whole surface, the apparent adhesion of the sample surface to the underwater bubble can be changed from low to high. Picking up and releasing bubbles at particular locations were achieved by using the patterned surface with different bubble adhesions in the liquid. Using a surface with medium adhesion as a "mechanical hand", bubbles on the surface with low bubble adhesion could be easily picked up. The picked bubble could also be transferred from the mechanical hand to the surface with high bubble adhesion. There was no gas residue on the "mechanical hand" during the whole process of the lossless bubble transportation. The patterned surface can be used to split a bubble into smaller ones. When a large bubble

was pressed onto the aerophobic/superaerophobic pattern and then lifted, a super-small bubble was left on the surface of the sample due to the high adhesion of the smooth region between the structured domains to the bubble. A set of tiny bubbles were obtained by shifting the sample and repeating the pressing-lifting process. When the square-patterned film was bended, the smooth domain of the bended area was stretched, providing a larger area for bubbles to attach. At this point, the underwater bubble could adhere tightly to the bended area. Interestingly, when the folded film was heated, the film gradually returned to its planar shape because of the significant shape-memory effect of the polymer substrate. With the decrease of the stretched area, the adhesion of the film to bubbles decreased gradually. When the bubble adhesion could not resist the buoyancy, the bubbles detached from the polymer film and were released in situ.

5.3.3. Selective Passage of Bubbles. The bubble wettability has an important effect on the passage of bubbles through porous plates in liquid. Yong et al. combined open microholes with the femtosecond laser-induced superwetting microstructures to prepare a series of underwater superaerophobic and superaerophilic porous sheets (Figures 26(a) and 26(d)) [121, 124, 126]. When the air bubbles are continuously released below the underwater superaerophobic porous sheet in the water, all the bubbles are intercepted by the porous sheet. They cannot pass through the sheet (Figures 26(b) and 26(c)). The gas-repellent property of the underwater superaerophobic microstructure endows the porous sheet with the ability to intercept bubbles. For the underwater superaerophilic porous sheet, when the first bubble contacts the porous sheet in water, it is instantly absorbed by the porous sheet because of the superaerophilicity of the laser-induced microstructure. With the continuous release of bubbles below the sheet, all the bubbles are absorbed by the lower side of the sheet, and the absorbed gas gradually bulges above the upper side of the sheet. The air bulge gradually grows. Once the buoyancy of the gas bulge is sufficient to overcome the adhesion of the sheet, the air bulge will detach from the porous sheet and rise again in the form of a new large bubble. As the air bulges leave one by one from the upper side of the sheet, all the bubbles successfully pass through the underwater superaerophilic porous sheet (Figures 22(e) and 22(f)). Underwater superaerophilicity and open microholes play a crucial role in the permeability of the bubbles through the porous sheet. Therefore, the underwater superaerophobic porous membrane can intercept bubbles, while the underwater superaerophilic porous membrane can allow bubbles to pass through it in the water.

5.3.4. Bubble Collection. Superhydrophobic materials can resist water, while bubbles can pass through the underwater superaerophilic porous sheets. Yong et al. designed a bubble-collection device that can collect gas bubbles in the water [124]. As shown in Figures 27(b) and 27(c), a bottomless cavity is the main body of the collection device. The bottom of the cavity is covered with an underwater superaerophilic porous sheet (Figure 27(a)) that is the core component of the device. Femtosecond laser was used to form microstructures on the PDMS sheet. The underwater superaerophilic sheet is also superhydrophobic. The superhydrophobicity can prevent water from flowing into the collection cavity. When the gas bubbles rise one by one and come in contact with the bottom of the designed collection device, the bubbles can be fully absorbed by the porous sheet and enter the internal space of the device through the underwater superaerophilic porous sheet (Figure 27(d)). As a result, the gas bubbles are successfully collected by the device. The collected gas can be transported in time through a pipe connected to the enclosed cavity. The device can collect a wide variety of bubbles, regardless of the gas species. For example, the collection device can potentially capture bubbles of self-seeping methane on the seafloor.

Zhu et al. prepared a bubble Janus based on the copper foam [202]. Firstly, superhydrophobic silica nanoparticles were coated on the branches of the copper foam. Then, a femtosecond laser was used to ablate the whole surface of one side of the copper foam. The unablated side remains superhydrophobicity and underwater aerophilicity. However, the laser-treated side switches to hydrophilic and superaerophobic underwater. The bubbles in the liquid can pass directly from the laser-ablated side to the unablated side of the Janus foam, but they cannot pass through the foam in the opposite direction. A gas-collection device based on the unidirectional bubble-transportation property of the Janus foam is designed, which allows carbon dioxide bubbles to enter the collecting chamber.

5.3.5. Water/Gas Separation. Yong et al. proposed a method to remove bubbles from water flow by using underwater superaerophobic and superaerophilic porous mesh [201]. The hierarchical microstructure was prepared on the surface of the stainless steel mesh (Figure 27(e)), making the mesh superhydrophilic and superaerophobic in water. The structured mesh switches to exhibit superhydrophobicity and underwater superaerophilicity when it is modified with a low-surface-energy monomolecular layer. An underwater superaerophobic mesh is inserted into the water pipe and placed vertically to the pipeline. In front of the inserted mesh, a small hole is prepared on the pipe wall and covered with an underwater superaerophilic mesh. The superhydrophilicity of the inserted mesh allows water to wet and flow through the mesh. As shown in Figure 27(f), when the bubbles in the water reach the inserted mesh with the water flow, the bubbles are intercepted by the mesh because of the tremendous repulsive effect of the underwater superaerophobic mesh on the bubbles. All the bubbles stop forward and rise to the underwater superaerophilic mesh on the pipe wall by buoyancy. The liquid repellence of the superhydrophobicity of the mesh on the sidewall ensures that the water in the pipe will not flow out of the pipeline. Instead, the bubbles can be absorbed into this mesh and quickly pass through the mesh. All the bubbles in the water flow are completely removed as they penetrate from the inside of the pipe to the outside and are eventually released into the atmospheric environment (Figure 27(g)). Both the collection manner and the removal manner successfully achieve water/gas separation.

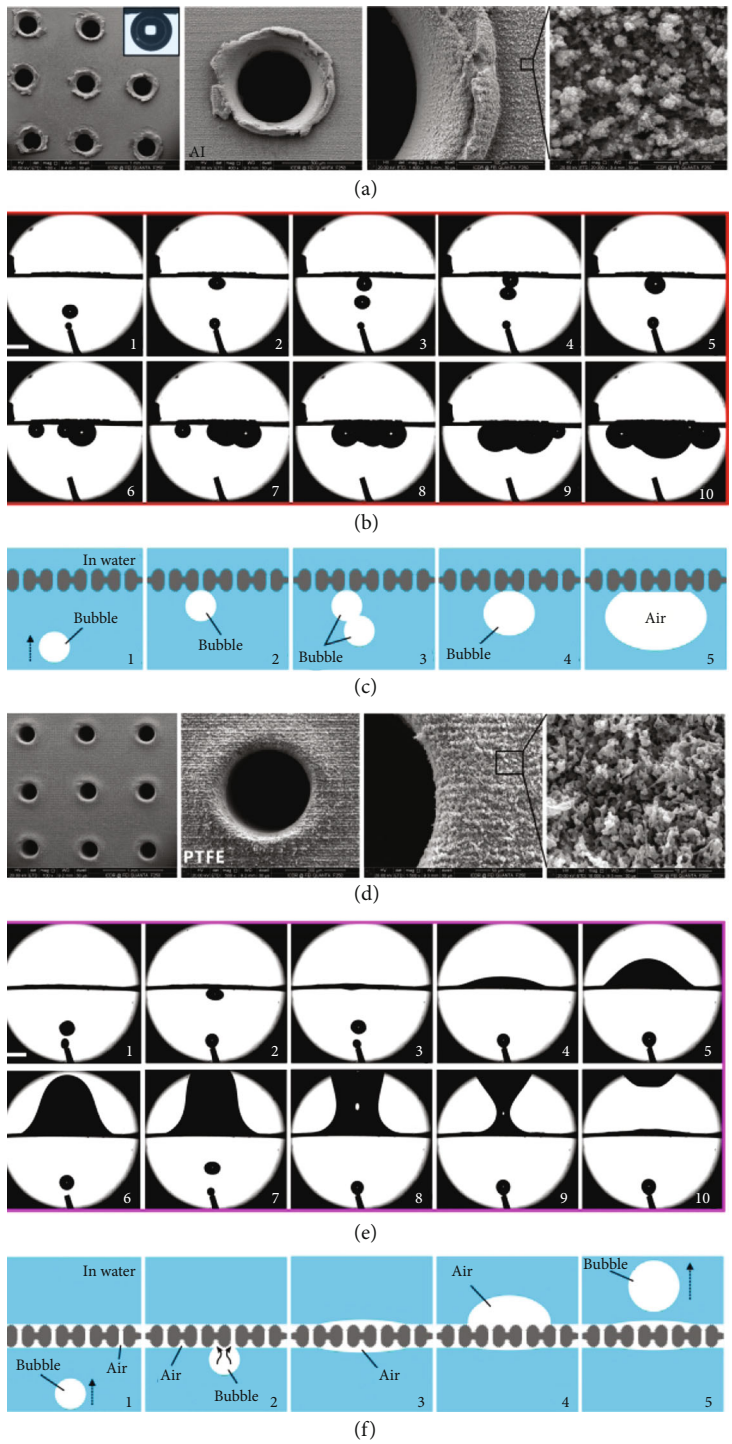

FIGURE 26: Selective passage of bubbles through underwater superaerophobic and superaerophilic porous membranes. (a) Morphology of the underwater superaerophobic porous sheet prepared by femtosecond laser processing. (b) Interception of bubbles by the underwater superaerophobic porous sheet in water. (c) Mechanism of the bubble interception by the underwater superaerophobic porous sheet. (d) Morphology of the underwater superaerophilic porous sheet prepared by femtosecond laser processing. (e) Bubbles passing through the underwater superaerophilic porous sheet in water. (f) Mechanism of the bubble passage through the underwater superaerophilic porous sheet. Reproduced from [121] with the permission.

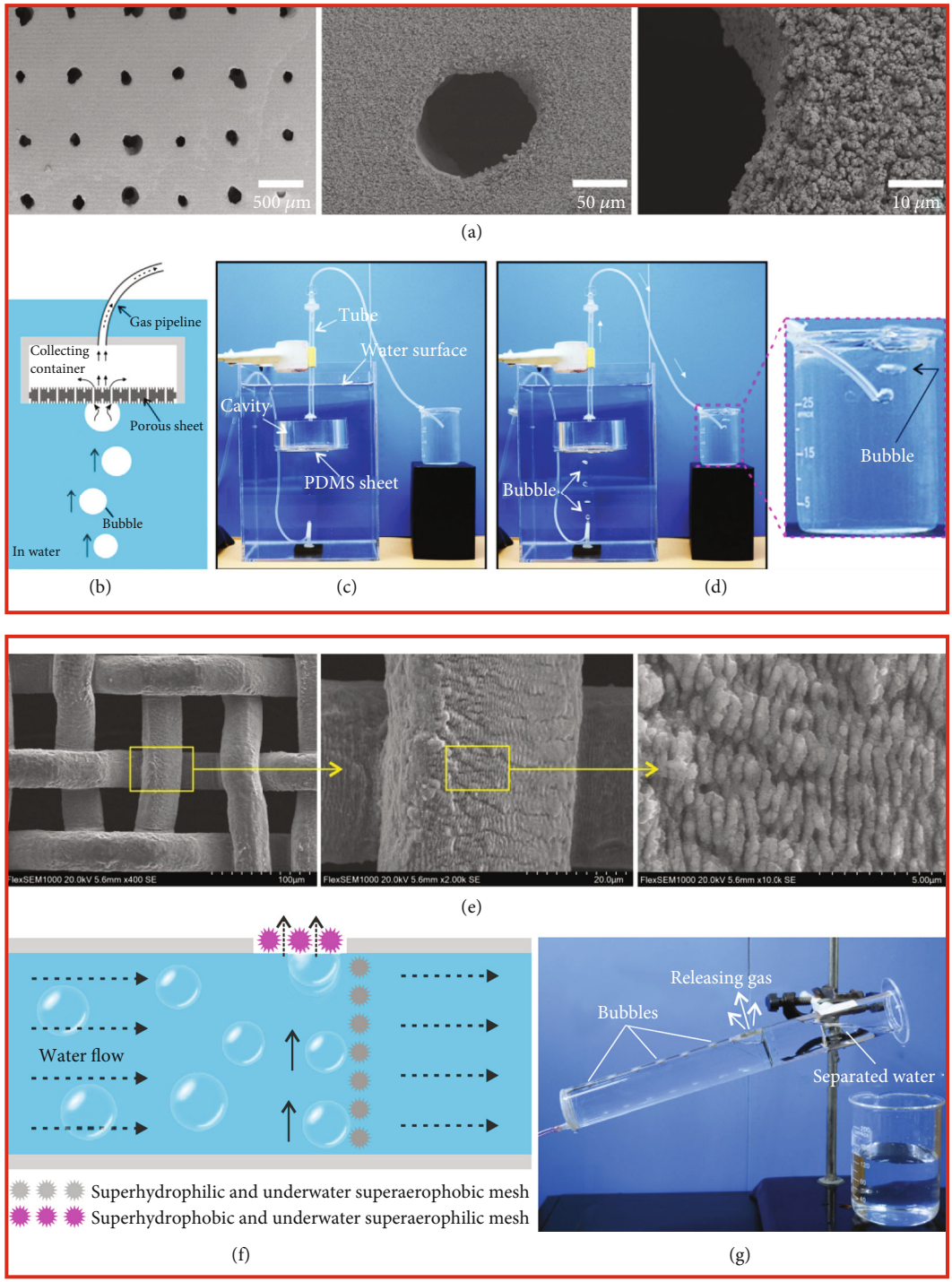

Figure 27: Application examples of the underwater superaerophobic and superaerophilic surfaces fabricated by femtosecond laser. (a–d) Collecting bubbles by a device with an underwater superaerophilic porous sheet as the core component. (e–g) Removing tiny bubbles from water flow in a pipeline by using underwater superaerophobic and superaerophilic meshes. Reproduced from [124, 201] with the permission.

Because of their advantages in manipulating bubbles in liquids, the underwater superaerophobic and superaerophilic surfaces have important applications in the clever use of underwater bubbles and excluding bubble-induced hazards.

6. Slippery Liquid-Infused Porous Surfaces (SLIPS)

6.1. Super-Slippery Property. The *Nepenthes* pitcher plants have very slippery lip edges (Figure 28(a)) [203]. When an

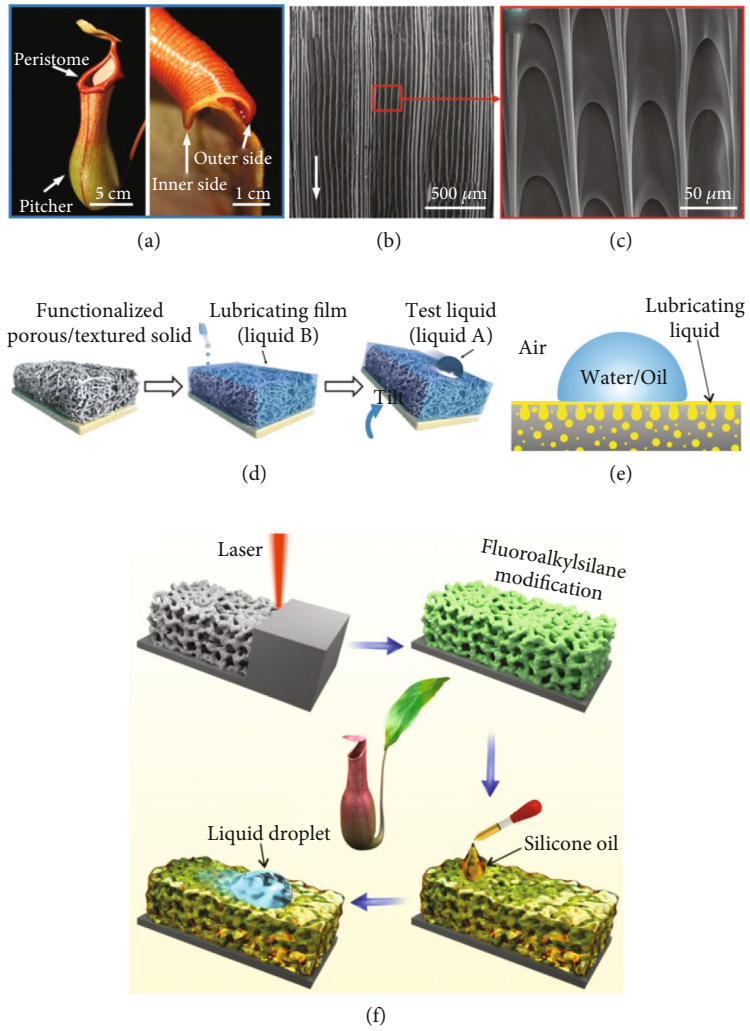

FIGURE 28: Pitcher plant-inspired slippery surface. (a) Photos of pitcher plant. (b, c) Porous microgrooves on the surface of the pitcher plant. (d) Preparation of SLIPS on a functionalized porous Teflon substrate. (e) Wetting state of a liquid droplet on the SLIPS. (f) The preparation process of SLIPS based on the femtosecond laser-induced porous microstructure. Reproduced from [127, 128, 203] with the permission.

insect alights on the edge of a pitcher plant, it has a hard time standing up and easily slides from the edge to the inner bottom of the pitcher plant. The bottom of the pitcher plant is filled with digestive juice, which quickly breaks down the insects into nutrients that help the pitcher plant grow. It is found that microgrooves are neatly arranged on the surface of the lip part of the pitcher plant (Figure 28(b)) [127]. The width of the microgrooves is only several tens of microns. Each microgroove is full of microscale cavities (Figure 28(c)). The microcavities are aligned and overlap each other. The digestive juice volatilized in the cage or water mist in the air can condense on the inner side of the cage lip and can be transported outward in one direction to wet the whole cage lip and keep the entire cage lip wet. As a result, the cavities are filled with fluid, forming a continuous, smooth, and stable interface. The trapped liquid acts as a lubricant layer. The droplets of various liquids can easily slip off the pitcher plant, so the surface of the pitcher plant exhibits excellent liquid repellence. Such liquid-resistant surfaces are generally referred to as "slippery liquid-infused porous surface (SLIPS)" [203].

Wong et al. first prepared such a slippery surface by infusing a low-surface-energy and chemically inert lubricating fluid into a functionalized porous/textured Teflon surface, as shown in Figure 28(d) [203]. The lubricating fluid was locked in the pores of the solid substrate. Therefore, a physically smooth and chemically homogeneous lubricating film is formed on the surface of the Teflon substrate. For a droplet on the artificial SLIPS, it is actually in contact with the lubricating layer. This is a liquid-liquid contact between the SLIPS and the liquid rather than a solid-liquid contact (Figure 28(e)). The trapped lubricating layer dramatically reduces the pinning effect of the liquid contact line on the solid material and makes the SLIPS have excellent repellence to various liquids. Droplets can easily slide down the SLIPS.

To prepare a SLIPS, there are three main basic rules [129, 203]. First of all, the surface of the material should have a porous network microstructure, which allows the lubricating fluid to be firmly locked in the porous substrate

and the fluid in different areas to flow to each other. Secondly, the lubricating fluid is better at wetting the porous structure of the substrate compared with the liquid to be repelled, ensuring that the lubricating fluid will not be squeezed out by foreign liquids and thus lose the slippery characteristic. Finally, the lubricating fluid is insoluble with the liquid to be repelled. Therefore, the preparation of a super-slippery surface usually requires the infusion of lubricating fluid after constructing porous microstructures on the material surface.

Interestingly, the femtosecond laser can directly write porous microstructures on many solid substrates [128]. Based on the laser-induced porous microstructure, Yong et al. proposed a strategy for preparing SLIPS on different substrates, as shown in Figure 28(f) [129]. Firstly, micro/nanoscale pores are generated on the substrate surface by femtosecond laser processing. Secondly, the surface energy of the porous substrate is lowered as much as possible to make the surface appear hydrophobic and oleophilic. The oleophilicity promotes the lubricant infusion, while the hydrophobicity prevents water from displacing the trapped lubricant in the porous structure. Finally, the lubricating fluid is infused into the pores to form a thin lubricating layer on the surface of the solid substrate. A wide range of liquids can slide down the SLIPS.

6.2. SLIPS Based on the Laser-Induced Porous Microstructures

6.2.1. Polymers. Yong et al. found that a porous network microstructure can be easily prepared on a polyamide-6 (PA6, one kind of Nylon) substrate by femtosecond laser direct writing [129]. When the femtosecond laser was focused on the surface of the PA6, the continuous absorption of the laser energy triggered the surface damage of the sample through nonlinear effects. Compared with the traditional ultrafast laser ablation process, gasification of the PA6 substrate also occurred simultaneously with ablation. The laser-irradiated area was in the instantaneous molten state due to the ultrahigh temperature induced by the laser. The generated gas was ejected from the substrate through the molten layer. When the laser focus moved away, the molten state immediately cooled and solidified. Thus, the path of the ejected gas remained in the form of interconnected microholes. Figure 29(a) shows the surface morphology of the PA6 ablated by femtosecond laser. The entire surface is uniformly covered with microscale protrusions and pores. The diameter of the protrusions is 1-5 μm, and the diameter of the pores is only 1 μm. The pores are interconnected, forming a porous network composed of interconnected micropores. The porosity extends from the surface to the interior of the polymer substrate, with a depth of 9.5 μm. The rough porous microstructure enhances the hydrophilicity of the PA6 substrate and reduces the WCA relative to water droplets from $88.5^\circ \pm 3^\circ$ to $50.7^\circ \pm 5^\circ$. The free energy of the porous surface was further reduced by typical fluoroalkyl layer modification. The modified porous surface remained oleophilicity, but it became hydrophobic. The WCA of water droplets on the resultant surface is $129.9^\circ \pm 3.6^\circ$. The modified porous surface still has high adhesion to various liquids. Both water and oil droplets can adhere to the sample, even when placed upright. Finally, the nonvolatile and eco-friendly silicone oil was adopted as the lubricating fluid and infused into the laser-induced micropores. The infusion of lubricating fluid made the PA6 substrate have super-slippery properties. The as-prepared SLIPS allowed the deionized water droplets (Figure 29(b)) and the hexadecane droplets (Figure 29(c)) to slide away unimpeded. The SLIPS also exhibits strong liquid repulsion to a wide range of pure or complex liquids. The liquid drops of drinking water, unfiltered lake water, ink, glycerol, coffee, milk, egg white, egg yolk, and so on could easily slide down from the SLIPS without contamination (Figure 29(d)).

The slippery property of the SLIPS is very stable. The PA6 substrate could maintain liquid-repellent property even after being bent or rubbed 100 times. Three reasons mainly determine the durability of the SLIPS: (1) PA6 is an inherently stable material, (2) the laser-induced porous layer and its substrate are derived from the same material, and (3) the lubricating liquid trapped in the micropores can act as a buffer layer. Surprisingly, once the SLIPS is mechanically damaged by abrasion, scratch, and cut, the surface can restore its liquid-repellent property rapidly (Figure 29(e)). The interconnectivity of the porous network allows the surrounding lubricating liquid to flow spontaneously to the damaged area due to surface tension and capillarity, so the slippery property of the damaged area can be repaired in time. The self-repairing ability makes the SLIPS more suitable for the application environment.

Fang et al. prepared a magnetically controllable SLIPS on an epoxy polymer substrate [130]. The whole surface of the substrate was ablated by the femtosecond laser to form a rough surface microstructure. Then, the femtosecond laser was used to selectively ablate special areas to create an array of uniform microgrooves on the epoxy polymer. The width of the microgrooves is 500 to 800 μm, and the space of the microgroove is 60 μm. The height of the microgrooves is 27.5 ± 0.8 μm at the used laser power of 40 mW. The top of the ridges between the microgrooves and the bottom of the microgrooves are covered with fine rough microstructures. The surface microstructure of the laser-ablated area also contains a large number of microscale and nanoscale pores. Next, the groove-structured sample was modified with fluoroalkylsilane to lower surface energy. Finally, the magnetic ferrofluid was used as the lubricating fluid and infused into the porous microgrooves with a magnetic field. A smooth lubricating film was formed on the sample surface, which completely covered the microgrooves. The sliding behaviors of a water droplet on the as-prepared SLIPS are similar along with the parallel and perpendicular directions to the microgrooves, with a WSA of $2.0 \pm 0.1^\circ$ and $2.6 \pm 0.4^\circ$, respectively. Therefore, the SLIPS has isotropic slippery property. When a magnetic field ($\geq$86 mT) was applied to the SLIPS, the magnetic lubricant in the microgrooves is transferred to the edge of the microgrooves, driven by the magnetic field. Under the action of the magnetic field, the microgroove structure appears on the slippery surface. The water droplet is easy to slide on the SLIPS along

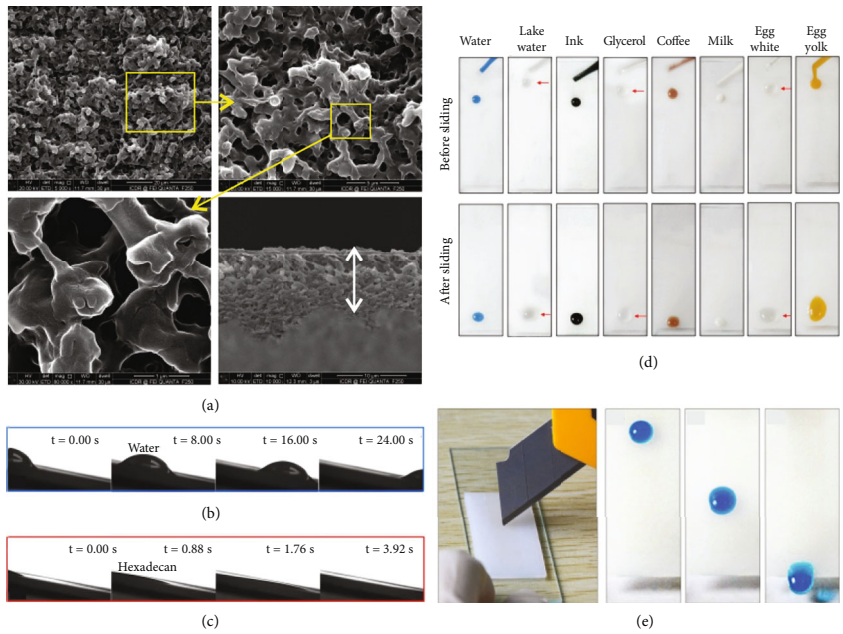

FIGURE 29: Slippery property on the femtosecond laser-structured porous PA6 surface. (a) Porous network microstructure of the PA6 substrate after laser processing. (b) Process of a water droplet sliding down the as-prepared SLIPS. (c) Process of a hexadecane droplet sliding down the as-prepared SLIPS. (d) Drops of various pure or complex liquids sliding down from the SLIPS. (e) The self-repairing slippery property of the SLIPS after cutting damage. Reproduced from [129] with the permission.

the microgrooves (parallel direction) with a WSA of 4.0 ± 0.3°. However, because the droplet is partly inserted into the slippery microgrooves, there is considerable resistance in the perpendicular direction, making it difficult for the droplet to slide along the perpendicular direction. The droplet starts to slide until the slippery surface is tilted by 36.3 ± 3.0°. The sliding behavior indicates that the SLIPS exhibits anisotropic slippery characteristic after applying the magnetic field. Once the magnetic field is removed, the SLIPS can return to its original isotropic slippery state as the ferrofluid flows back to the microgrooves.

Yong et al. also used a femtosecond laser to generate porous network microstructure on the poly(ethylene terephthalate) (PET) substrate [128]. A SLIPS was successfully achieved on the porous PET surface by low-surface-energy modification and the infusion of lubricating fluid. The slippery PET can completely inhibit the growth of C6 glioma cells in addition to its excellent antiliquid ability. Porous network microstructures can also be directly written on the other polymer substrates (e.g., poly(methyl methacrylate), polycarbonate, polyethylene, and polylactic acid) by femtosecond laser [128, 129]. Therefore, combined with femtosecond laser direct writing technology, almost all polymers can be used as substrates to achieve super-slippery properties.

6.2.2. Metals. It is challenging to build porous structures on hard metals. NiTi alloy is an ideal bioengineering material with good shape memory performance, superelasticity, and biocompatibility. This metal is widely used in modern medicine as an interventional medical scaffold. Cheng et al. used the laser pulse train of a femtosecond Bessel laser to prepare a SLIPS on a NiTi alloy substrate [131]. The ordinary Gaussian laser beam was spatially converted into a conical Bessel beam with larger focal field depth and smaller focal spot than the Gaussian beam through an axicon. Each train of femtosecond laser pulses with high frequency could induce a microhole on the sample surface. A series of pores were prepared through a line-by-line laser scanning method on the surface of the implantable NiTi alloy, as shown in Figures 30(a) and 30(b). The diameter of the pores is only 3 μm, but its depth reaches up to ~30 μm. The microholes look very deep, with an aspect ratio of 10. Compared with Gaussian laser, Bessel laser can produce smaller and more uniform microholes because of its features of the extended depth of the focal field and the small focal spot. The formation of the deep porous microstructure is attributed to the combined action of the shaped laser Bessel beam and the pulse train. Before becoming a SLIPS, the surface energy of the porous NiTi alloy needs to be lowered, and lubricating liquid should be injected into the pore structure. To reduce the surface energy of the laser-induced porous microstructure, the sample was simply stored in air for 7 days. Usually, the metals processed by femtosecond laser have a strong adsorption capacity for carbon in the atmosphere. During the air storage process, hydrocarbon groups were gradually grafted onto the porous NiTi surface. As a result, the wettability of the porous NiTi alloy was changed from hydrophilic to hydrophobic by the grafted hydrophobic hydrocarbon groups. The hydrophobic surface shows a WCA of 120° to water droplets. Simple air storage without fluoroalkylsilane is a safer and nontoxic method to ensure the safety of the interventional medical NiTi alloy. As a reagent widely applied in the field of medicine, the nontoxic perfluorodecalin was used as the lubricant and was dripped onto the porous surface of the hydrophobic NiTi

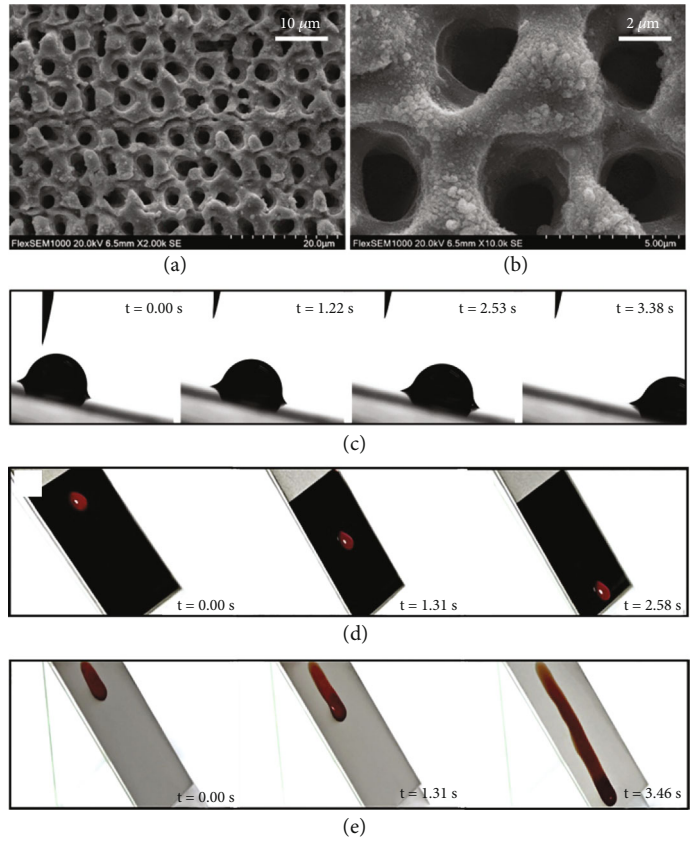

FIGURE 30: Liquid repellence of the SLIPS on NiTi alloy. (a, b) Femtosecond laser-induced porous microstructure on NiTi alloy substrate. (c) Process of a water droplet sliding down the slippery NiTi surface. (d) Blood sliding down the slippery NiTi surface prepared by femtosecond laser processing. (e) Blood sliding down the original untreated NiTi surface. Reproduced from [131] with the permission.

substrate. The lubricant automatically wetted and filled the porous microstructure.

The SLIPS was successfully obtained with the formation of a uniform lubricating layer on the alloy surface. The water droplet on the as-prepared SLIPS has a WCA of 23° and can easily slide down as soon as the sample is slightly tilted (Figure 30(c)), demonstrating excellent water repellence of the SLIPS. The SLIPS can also repel blood. When a drop of blood was dripped on the slippery NiTi surface, the elliptic blood droplet would easily fall off without any residue (Figure 30(d)). In contrast, the blood left a distinct band as it slide across the untreated NiTi alloy (Figure 30(e)). Therefore, the slippery surface can significantly reduce blood adhesion to the NiTi substrate. The SLIPS greatly improved the hemocompatibility of the NiTi alloy, allowing the NiTi alloy to have excellent anticoagulation property, a very low hemolysis rate, and antibacterial property.

Liquid assist is an effective method to induce porous microstructure in femtosecond laser processing. In an alcohol solution, Fang et al. used a femtosecond laser to directly prepare porous microstructures on the surface of stainless steel [132]. After laser treatment, a large number of papillae with a diameter of 1-4 μm and a height of several micrometers were randomly formed on the sample surface. The papillae are surrounded by abundant smaller microholes several micrometers in depth. The interior of these microholes is decorated with many fine nanoscale pores. The structural porosity of the hierarchical porous structure was 45.7%. The porous structure could not be directly produced on stainless steel if the sample was ablated in air. Under laser ablation, the liquid (alcohol) environment plays an important role in forming pores on the sample surface. When the laser pulse is focused on the stainless steel and alcohol interface, high-pressure and high-temperature plasma is generated by nonlinear multiphoton absorption. The focused laser also causes the alcohol to decompose, creating many microbubbles at the solid-liquid interface. Many micropores are formed on the metal surface with the rapid expansion of plasma shock waves and microbubbles. On the other hand, the laser-induced ejected particles are dispersed in the alcohol, preventing them from falling back onto the metal surface and covering the generated microholes. The porous stainless steel was modified with fluoroalkylsilane to reduce surface energy. After modification, the WCA of water droplets on the stainless steel surface was increased to 143° ± 1°. The hydrophobic stainless steel still has high adhesion to water, and water droplets can firmly adhere to the sample surface. Silicone oil as the lubricating liquid was further infused into the hydrophobic porous surface to prepare SLIPS. Water droplets could easily slide down the as-prepared SLIPS, with an inclination of 10°. The SLIPS shows a strong repulsive effect on drinking water,

milk, ink, blood, egg white, and other common compound liquids in daily. The drops of these liquids slide freely on the SLIPS without any residue. Interestingly, alcohol-assisted femtosecond laser ablation can induce micro/nano-scale pores on a variety of metal surfaces, which allows the preparation of slippery structures on broad metal surfaces.

Jiao et al. reported an underwater slippery surface for manipulating bubbles [133]. Rough microgrooves were prepared on an aluminum alloy sheet by femtosecond laser ablation. Next, a silane hydrophobic agent was sprayed on the surface of the groove structure to lower the surface energy of the aluminum alloy and make the sample superhydrophobic. The Fluorinert was then dripped onto the modified microgrooves, where it wetted and entered the porous surface microstructure. In aqueous media, bubbles could transport themselves on the as-prepared slippery surface. It took only 4 s for a 10 μL bubble to advance 4 cm on a ~6° tilted surface. The buoyancy component along the inclined plane provides the main driving force. By designing different shaped slippery zones, the bubbles can be controlled to slide along the designed track. The slippery surface shows a strong ability to control the bubble movement.

6.3. Applications of SLIPS. SLIPS uses a smooth lubricating film to prevent the adhesion of the liquids with different surface tension, viscosity, and chemical composition [128, 129, 132]. Therefore, the slippery surface can be widely applied in microfluidic droplet manipulation, biomedicine, marine biological adsorption, antifreezing, corrosion resistance, scale prevention, and other fields. The SLIPS provides new solutions to many economic, energy, and environmental problems.

6.3.1. Liquid Repellence. Superhydrophobic and superaerophobic surfaces directly use hierarchical surface microstructure to repel liquids, while the microstructure of SLIPSs can lock intermediary fluids. The lubricating cushion retained on the porous surface can play the role of the repulsive surface so that the contact between the foreign liquids and the SLIPS becomes liquid-liquid contact [129, 203]. The SLIPS shows a strong repulsive effect on various liquids. The drops of a wide range of liquids can easily slide down such a surface (Figure 29(d)). The SLIPS also has good stability, especially against pressure. This pressure resistance is not present on ordinary superhydrophobic and superoleophobic surfaces because their liquid repellence is based on the trapped air in the surface microstructure.

6.3.2. Manipulation of Droplets and Bubbles. Excellent liquid repellence allows the slippery surface to manipulate droplets without liquid residue. The liquid adhesion on SLIPS is very low, so it is easy to control the movement of droplets on the slippery surface. Fang et al. mixed the magnetic particles into water droplets [130]. By controlling the magnetic field, the magnetic droplet can be directed to move forward along the designed path (Figure 31(a)). Jiao et al. manipulated bubbles by using the slippery aluminum surface prepared by femtosecond laser [133]. The bubbles can be easily controlled to slide along a designed track on the slippery surface with the assistance of buoyancy in the water (Figure 31(b)). A gas catcher with a large area of the slippery surface was fabricated, which can capture underwater bubbles with an efficiency of more than 95%.

6.3.3. Cell Engineering. The SLIPS is resistant to biological adhesion. Yong et al. found that the femtosecond laser-induced porous microstructure can promote the growth of C6 glioma cells on the PET surface [128]. In contrast, the SLIPS of PET surface prepared by infusing silicon oil into the porous microstructure completely inhibits the growth of C6 glioma cells, as shown in Figure 31(d). The cell-promoting/inhibiting properties of the laser-induced porous and slippery microstructures enable the control of tissue formation.

6.3.4. Biomedical. Cheng et al. prepared SLIPS on implantable NiTi alloy processed by femtosecond laser [131]. The hemocompatibility of NiTi alloy is improved significantly. The SLIPS is highly resistant to blood (Figure 30(d)). Compared with the original NiTi alloy, the adhesion of fibrinogen to the SLIPS is reduced by 12 times (Figure 31(e)). The hemolysis rate of the slippery NiTi alloy also decreases from 4.69% to 1.56%, which is remarkably lower than the Chinese national standard (5%). The SLIPS has an antibacterial property that prevents bacteria from adhering to the NiTi alloy. For example, the antibacterial rate of E. coli bacteria is 98.14%, and that of S. aureus bacteria is 99.32% (Figure 31(f)).

6.3.5. Antifouling. Fang et al. soaked the slippery sheet of stainless steel in the water containing green alga [132]. After 7 days, the slippery area was still clean, whereas the green alga grew well on the flat part of the metal sheet (Figure 31(c)). The results show that the slippery stainless steel has the excellent antifouling performance to the green alga.

7. Repellence to Special Liquids

Different from ordinary water, oils, and bubbles, some special liquids such as polymers and liquid metals also play an important role in material and engineering applications. Recently, the wettability of such special liquids is emerging as a new hot topic in the field of superwettability. Wettability facilitates better control, manipulation, and use of these liquids.

7.1. Underwater Superpolymphobicity. Polymers are also one of the most common materials in our daily life. Polymers are widely used in manufacturing, chemical industry, packaging, construction, food processing, pharmaceutical industry, biological engineering, etc. Some polymers are solid at room temperature, but some are liquid. Liquid polymers are more complex in composition than pure water and oil. In addition, liquid polymers are usually characterized by low fluidity and high viscosity. Polymers also adhere particularly well to solid surfaces and are difficult to be removed. Unlike typical droplets (such as water and oil), some liquid polymers can change to a permanent solid state. For example, the PDMS liquid mixed of prepolymers and curing agent can be cross-linked to induce curing, which causes its shape to

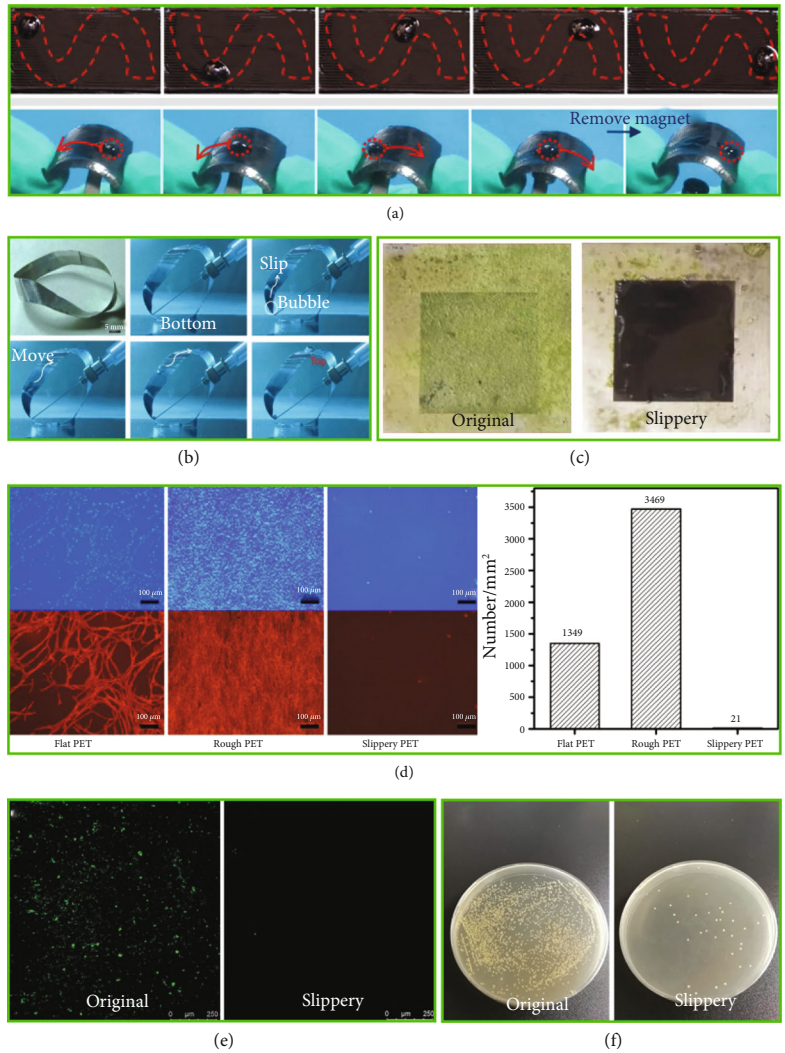

FIGURE 31: Application examples of the SLIPS fabricated based on the femtosecond laser-induced porous microstructures. (a) Controlling the magnetic droplet to slide on the slippery surface by magnetic field. (b) Manipulating bubbles to slide along a designed track on the slippery surface with the assistance of buoyancy in the water. (c) Excellent antifouling performance of the slippery stainless steel to the green alga. (d) Growth of C6 glioma cells on different PET surfaces. (e) Adhesion of fibrinogen to the original and the slippery NiTi alloys. (f) Antibacteria property of the slippery NiTi alloy. Reproduced from [128, 130–133] with the permission.

be fixed. Reducing the adhesion between liquid polymers and solid materials is of great importance in manipulating and using polymers. In various polymer-related applications, it is always a challenge to prevent liquid polymers from adhering to material surfaces.

Recently, Yong et al. used a femtosecond laser to induce micro/nanostructures on a variety of materials and endowed these materials with strong resistance to liquid polymers underwater, including stainless steel, silicon, glass, aluminum, and copper [90, 204–206]. The CA of liquid polymer droplets on these surfaces is greater than 150°, and the droplet can easily roll down. The liquid polymer cannot adhere to the structured surfaces. Such a polymer-repellent property is defined as "underwater superpolymphobicity" [90]. Taking the stainless steel substrate as an example, Figures 32(a)–32(c) show the microstructures of the hydrophilic substrate after femtosecond laser processing [90]. The structured stainless steel surface is characterized by mountain-shaped microstructures, deep microholes, and periodic nanoripples covering the whole surface. The untreated stainless steel shows inherently polymphilicity to in-air liquid polymer droplets with a polymer CA (PCA) of $23 \pm 2°$ (Figure 32(d)). It offers polymphobicity to underwater liquid polymer droplets with PCA of $116 \pm 10°$ (Figure 32(e)). The polymer droplet can firmly attach to the sample surface even though the stainless steel is placed vertically. Regarding the laser-structured surface, it can be fully wetted by water (Figure 32(h)). The PCA of the in-air polymer droplet decreases to $16 \pm 3°$ (Figure 32(f)). Interestingly, a liquid polymer droplet can maintain spherical on the structured surface in water, with a PCA of $156 \pm 3°$ (Figure 32(g)). When a liquid polymer droplet is moved to contact and then leave the structured surface in a water medium, no apparent adhesion occurs at the

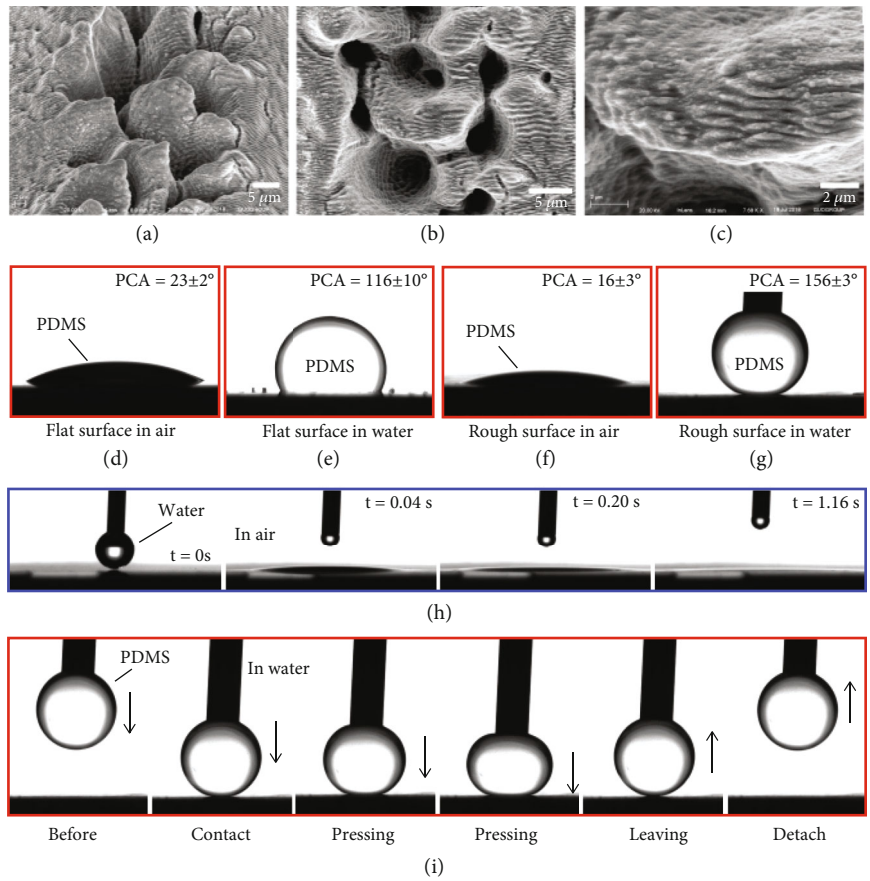

FIGURE 32: Underwater superpolymphobicity of the femtosecond laser-structured stainless steel. (a–c) Hierarchical microstructures of the stainless steel surface after femtosecond laser ablation. (d) In-air droplet and (e) underwater droplet of liquid polymer on the original stainless steel. (f) In-air droplet and (g) underwater droplet of liquid polymer on the laser-structured stainless steel. (h) Releasing a water droplet onto the structured surface. (i) Moving an underwater liquid polymer droplet to contact and then leave the structured stainless steel surface in water. Reproduced from [90] with the permission.

moment of the droplet detaching from the sample surface (Figure 32(i)). The CA hysteresis of the polymer on the sample surface is less than 4°, demonstrating an ultralow adhesion between the underwater liquid polymer and the structured stainless steel. Therefore, the stainless steel surface shows underwater superpolymphobicity after the formation of surface micro/nanostructures by femtosecond laser treatment. The underwater superpolymphobic materials have remarkable repellence to liquid polymers in water.

Like underwater superoleophobicity, underwater superpolymphobicity can be obtained by constructing suitable microstructures on various hydrophilic substrates [204]. The laser-induced microstructures can trap a layer of water over the sample surfaces in water. The trapped water supports a Cassie contact state between underwater liquid polymer and the structured surface, thus allowing the material to repel liquid polymers [90]. The properties of polymer repellence can be used to reduce the adhesion of polymers to material surfaces, design polymer shapes, and separate polymers from water [90, 204–208]. Underwater superpolymphobicity will have significant potential applications in polymer production, packaging, casting industry, polymer molding, 3D printing, and other fields related to polymers.

7.2. Supermetalphobicity. Liquid metals have important potential applications in the field of liquid robots, flexible circuits, and so on [209–212]. The core technology to achieve these applications is how to control the shape and adhesion of the liquid metal and even obtain complex liquid-metal patterns. In addition to the basic properties of metals, liquid metals also have the property of liquids, such as fluidity. Liquid metals tend to stick to solid surfaces. The high adhesion between liquid metal and solid surface makes it difficult to control the shape of liquid metal and prepare fine liquid-metal patterns. Making a solid surface repel liquid metal is important to the promising applications of liquid metals.

Yong et al. investigated the wetting behavior of liquid metal droplets on the femtosecond laser-processed surfaces with different micro/nanostructures [213]. They found that the wettability of liquid metal on a rough solid surface is completely different from that of water droplets. Superhydrophobicity and superhydrophilicity are achieved on silicon and PDMS substrates by using a femtosecond laser to prepare microstructures on the sample surfaces and appropriate chemical modification. It is found that not only the superhydrophobic surface but also the superhydrophilic

surface shows the excellent repulsive ability to the liquid metal. The droplets of liquid metal have metal CA (MCA) of higher than 150° on the structured surfaces and can easily roll off the solid surfaces, indicating strong repellence of the laser-treated substrates to liquid metals. This property of liquid-metal repellence is named "supermetalphobicity". The experimental results and contact-model analysis show that surface microstructure plays a decisive role in endowing a solid surface with supermetalphobicity, while surface chemistry has relatively little influence on the realization of supermetalphobicity. The liquid metal surface is often coated with a thin layer of oxide metal, leaving the liquid metal in solid/solid contact with the structured solid surface. Therefore, as long as the micro/nanostructures are on the solid surface, the contact area between liquid metal and solid substrate can be reduced, thus reducing the adhesion of solid surface to liquid metal.

The preparation of supermetalphobic microstructure can effectively promote the progress of liquid-metal materials in flexible circuit and liquid robot applications [135, 214–217]. For example, Zhang et al. prepared micro/nanoscale surface structures on a soft PDMS film by femtosecond laser ablation (Figure 33(a)) [214]. The laser-induced microstructure makes the PDMS surface greatly repel liquid metal. The drop of liquid metal on the resultant surface has a MCA of 159.7° and a metal SA (MSA) of 4.0° (Figure 33(b)). The adhesive force between the liquid metal and the supermetalphobic surface was reduced by at least 266 times compared to untreated flat PDMS substrate. Therefore, liquid metal can adhere to the untreated PDMS surface but is difficult to adhere to the laser-structured liquid-metal-repellent area. This unique property can be used to fabricate various flexible circuits. As shown in Figure 33(c), the PDMS substrate can be selectively ablated by femtosecond laser, leaving the untreated rest area to form patterns. When the liquid metal is printed on the PDMS surface, it only covers the smooth patterns and cannot be on the laser-ablated area. Therefore, various patterns of liquid metal can be obtained, whose shapes are consistent with the designed pattern (Figure 33(d)). The as-prepared liquid-metal patterns can be used as flexible conductors in the circuit. In this way, various flexible circuits can be designed. Figure 33(e) shows a flexible microheater fabricated based on the liquid-metal pattern. When an input current is applied to the as-prepared circuit, the device can generate heat (Figure 33(f)). Figure 33(g) is a flexible microstrip patch antenna consisting of a liquid-metal pattern. The working frequency is measured to be 2.6 GHz, agreeing well with the designed requirement (Figure 33(h)). Even though the microheater and antenna were bent, they remained original functions by taking advantage of the strong ductility and great flexibility of the liquid metal.

The concepts of underwater superpolymphobicity and supermetalphobicity are just put forward in recent years, so the related research is still very limited now. Although we only briefly introduce such properties in this section, the underwater superpolymphobicity and supermetalphobicity are fascinating for manipulating polymers and liquid metals. The researches related to the wettabilities of polymers and liquid metals will sprout like bamboo shoots after a spring rain.

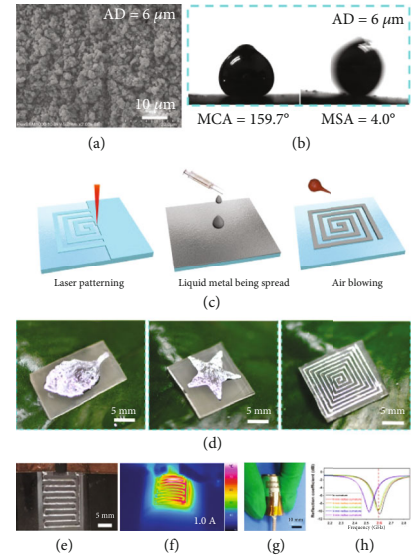

FIGURE 33: Flexible circuit prepared based on the liquid-metal pattern on the femtosecond laser-textured PDMS substrate. (a) Laser-induced microstructure on PDMS substrate. (b) Wettability of liquid metal droplet on the laser-structured surface. (c) Preparation of liquid-metal pattern on the laser-textured surface. (d) Different liquid-metal patterns. (e, f) Flexible microheater for heating. (g, h) Flexible microstrip patch antenna with a working frequency of 2.6 GHz. Reproduced from [214] with the permission.

8. Conclusions and Outlook

This review systematically summarizes the realizations and applications of the superwettability achieved by femtosecond laser. Inspired by nature, superwetting microstructure can be easily prepared on the surface of solid materials by femtosecond laser processing. Superhydrophilicity can be obtained by forming a hierarchical microstructure on a hydrophilic substrate, which causes water to thoroughly wet the material surface. Superhydrophobicity is a synergistic effect between surface microstructure and low-surface-energy chemistry. To achieve superhydrophobicity, it is necessary to use a femtosecond laser to directly construct the hierarchical microstructures on the hydrophobic substrate or build microstructure on the hydrophilic substrate followed by low-surface-energy modification. Superhydrophobic materials greatly repel aqueous solutions. The reentrant microstructure is the key to realizing superamphiphobicity. The superamphiphobic surfaces also have superoleophobicity as well as superhydrophobicity. Unlike the preparation of superamphiphobic surfaces, underwater superoleophobic surfaces can be easily fabricated by generating microstructure on a hydrophilic substrate. Both types of superoleophobic surfaces have a strong repellence to oils and oily liquids, but superamphiphobic materials work in the air while underwater superoleophobic materials work in the water. Femtosecond laser-induced superhydrophilic microstructures usually show superaerophobicity,

and the superhydrophobic microstructures show superaerophilicity in a water medium. The underwater superaerophobic surfaces can repel bubbles so that bubbles are difficult to adhere to the material surface in water. In contrast, bubbles can easily spread over underwater superaerophilic surfaces and be absorbed by solid surfaces. The femtosecond laser can directly write porous microstructures on many solid substrates. The lubricating fluid is further filled into the laser-induced pores to form a thin lubricating layer on the surface of the solid substrate. The as-prepared SLIPSs show excellent repellence against various pure or composite liquids. The emerging superpolymphobicity and supermetalphobicity are also briefly introduced. The laser-induced microstructures that repel underwater liquid polymers or liquid metals can be used to manipulate and pattern polymers and liquid metals. The concepts of underwater superpolymphobicity and supermetalphobicity were put forward only in the past two years. In addition to the detailed preparation methods, the rich applications of these superwetting surfaces are illustrated. The unique surface wettability enables the femtosecond laser-processed materials to have rich practical applications in antiliquids, self-cleaning, anti-icing/fogging/snowing, antifouling, oil/water separation, anticorrosion, drag reduction, water harvesting, manipulation of liquid droplets, liquid patterning, microfluidics, lab chip, cell engineering, buoyancy enhancement, and so on.

The features of ultrashort pulse width and ultrahigh peak energy enable the femtosecond laser to become an effective tool to control the wettability of solid materials. Femtosecond laser microfabrication shows many advantages in the realization of superwettability compared to traditional methods. Firstly and foremost, the femtosecond laser can be used to process a wide range of materials without relying on special substrates. A femtosecond laser can ablate almost any material. Secondly, this technology is very flexible. The laser-ablated position can be precisely controlled by the control program. A variety of patterns can be easily prepared without using expensive masks, thus achieving complex design of surface wettability. Thirdly, the process of femtosecond laser treatment is very simple. Different hierarchical microstructures can be directly formed on the surface of the solid substrate by one-step ablation. The same ablation process can be extended to various substrates. Fourthly, the morphology of the surface microstructure can be simply adjusted by laser parameters (e.g., laser power, pulse width, repetition frequency, and polarization), processing parameters (focal length, scanning speed, and scanning space), and processing manners. Therefore, the wettability of the laser-ablated surface can be easily controlled. Finally, this is a physical and mechanical method of preparation that does not rely on toxic reagents, chemical reactions, and hazardous operations. These advantages make femtosecond laser a great success in the preparation of multifunctional surfaces with unique superwettability.

Although femtosecond laser has achieved a variety of superwettability over the past decade, there are still challenges that constrain the development of this field (femtosecond laser-induced superwettability). These limitations are also the current problems faced by femtosecond laser microfabrication. Firstly, femtosecond laser machining is a time-consuming process. The processing efficiency needs to be significantly optimized and improved towards industrial applications. This problem can potentially be solved with high-power laser systems and more efficient scanning methods such as automatic parallel processing. Secondly, the complex and uneven surface machining is also a problematic point of femtosecond laser processing. To ensure that the laser beam is always focused on the uneven surface, the substrate should follow the focus position of the laser beam and be moved multidimensional in time. The ranging and positioning optical paths also need to be coupled to the laser processing system. Thirdly, durability is critical for the application of superwetting materials. The preparation of superwetting surfaces with resistance to friction, high temperature, and acid/alkali corrosion is still the focus of current research. The robust superwetting materials can work for a long time in various harsh environments. Last but not least, the application examples of the femtosecond laser-induced artificial superwetting materials are still in the laboratory stage. These materials and applications should be brought to market as soon as possible.

Although the technology of femtosecond laser controlling surface wettability is still limited by the defect of low machining efficiency, its strong flexibility and the ability to process most given materials are irreplaceable by other micromanufacturing technologies. With more superwetting surfaces being designed and prepared and new applications emerging, this research direction will have a promising future. We believe that the large-scale, commercial application of the femtosecond laser-induced superwetting materials is not far off.

Conflicts of Interest

There are no conflicts of interest to declare.

Acknowledgments

This work is supported by the National Science Foundation of China under the Grant nos. 61875158 and 61905188, the National Key Research and Development Program of China under the Grant no. 2017YFB1104700, the International Joint Research Laboratory for Micro/Nano Manufacturing and Measurement Technologies, and the Fundamental Research Funds for the Central Universities.

References

[1] M. Liu, S. Wang, and L. Jiang, "Nature-inspired superwettability systems," *Nature Reviews Materials*, vol. 2, no. 7, p. 17036, 2017.

[2] M. Liu, Y. Zheng, J. Zhai, and L. Jiang, "Bioinspired superantiwetting interfaces with special liquid-solid adhesion," *Accounts of Chemical Research*, vol. 43, no. 3, pp. 368–377, 2010.

[3] K. Liu, X. Yao, and L. Jiang, "Recent developments in bioinspired special wettability," *Chemical Society Reviews*, vol. 39, no. 8, pp. 3240–3255, 2010.

[4] X. Yao, Y. Song, and L. Jiang, "Applications of bio-inspired special wettable surfaces," *Advanced Materials*, vol. 23, no. 6, pp. 719–734, 2011.

[5] F. Chen, D. S. Zhang, Q. Yang et al., "Bioinspired wetting surface via laser microfabrication," *ACS Applied Materials & Interfaces*, vol. 5, no. 15, pp. 6777–6792, 2013.

[6] B. Su, Y. Tian, and L. Jiang, "Bioinspired interfaces with superwettability: from materials to chemistry," *Journal of the American Chemical Society*, vol. 138, no. 6, pp. 1727–1748, 2016.

[7] J. N. Wang, Y. L. Zhang, Y. Liu, W. Zheng, L. P. Lee, and H. B. Sun, "Recent developments in superhydrophobic graphene and graphene-related materials: from preparation to potential applications," *Nanoscale*, vol. 7, no. 16, pp. 7101–7114, 2015.

[8] H. Teisala, M. Tuominen, and J. Kuusipalo, "Superhydrophobic coatings on cellulose-based materials: fabrication, properties, and applications," *Advanced Materials Interfaces*, vol. 1, no. 1, p. 1300026, 2014.

[9] A. Milionis, E. Loth, and I. S. Bayer, "Recent advances in the mechanical durability of superhydrophobic materials," *Advances in Colloid and Interface Science*, vol. 229, pp. 57–79, 2016.

[10] W. Zhang, D. Wang, Z. Sun, J. Song, and X. Deng, "Robust superhydrophobicity: mechanisms and strategies," *Chemical Society Reviews*, vol. 50, no. 6, pp. 4031–4061, 2021.

[11] B. Bhushan, "Biomimetics: lessons from nature-an overview," *Philosophical Transactions of the Royal Society A: Mathematical, Physical and Engineering Sciences*, vol. 367, no. 1893, pp. 1445–1486, 2009.

[12] T. Darmanin and F. Guittard, "Superhydrophobic and superoleophobic properties in nature," *Materials Today*, vol. 18, no. 5, pp. 273–285, 2015.

[13] E. Stratakis, J. Bonse, J. Heitz et al., "Laser engineering of biomimetic surfaces," *Materials Science and Engineering: R: Reports*, vol. 141, article 100562, 2020.

[14] W. Barthlott and C. Neinhuis, "Purity of the sacred lotus, or escape from contamination in biological surfaces," *Planta*, vol. 202, no. 1, pp. 1–8, 1997.

[15] L. Feng, S. Li, Y. Li et al., "Super-hydrophobic surfaces: from natural to artificial," *Advanced Materials*, vol. 14, no. 24, pp. 1857–1860, 2002.

[16] X. Gao and L. Jiang, "Water-repellent legs of water striders," *Nature*, vol. 432, no. 7013, p. 36, 2004.

[17] Y. Zheng, X. Gao, and L. Jiang, "Directional adhesion of superhydrophobic butterfly wings," *Soft Matter*, vol. 3, no. 2, pp. 178–182, 2007.

[18] X. Gao, X. Yan, X. Yao et al., "The dry-style antifogging properties of mosquito compound eyes and artificial analogues prepared by soft lithography," *Advanced Materials*, vol. 19, no. 17, pp. 2213–2217, 2007.

[19] M. Liu, S. Wang, Z. Wei, Y. Song, and L. Jiang, "Bioinspired design of a superoleophobic and low adhesive water/solid interface," *Advanced Materials*, vol. 21, no. 6, pp. 665–669, 2009.

[20] J. Yong, F. Chen, J. Huo et al., "Green, biodegradable, underwater superoleophobic wood sheet for efficient oil/water separation," *ACS Omega*, vol. 3, no. 2, pp. 1395–1402, 2018.

[21] A. R. Parker and C. R. Lawrence, "Water capture by a desert beetle," *Nature*, vol. 414, no. 6859, pp. 33-34, 2001.

[22] J. Ju, H. Bai, Y. Zheng, T. Zhao, R. Fang, and L. Jiang, "A multi-structural and multi-functional integrated fog collection system in cactus," *Nature Communications*, vol. 3, no. 1, p. 1247, 2012.

[23] Y. Zheng, H. Bai, Z. Huang et al., "Directional water collection on wetted spider silk," *Nature*, vol. 463, no. 7281, pp. 640–643, 2010.

[24] Y. Si, Z. Dong, and L. Jiang, "Bioinspired designs of superhydrophobic and superhydrophilic materials," *ACS Central Science*, vol. 4, no. 9, pp. 1102–1112, 2018.

[25] T. Jiang, Z. Guo, and W. Liu, "Biomimetic superoleophobic surfaces: focusing on their fabrication and applications," *Journal of Materials Chemistry A*, vol. 3, no. 5, pp. 1811–1827, 2015.

[26] J. Yong, Q. Yang, X. Hou, and F. Chen, "Relationship and interconversion between superhydrophilicity, underwater superoleophilicity, underwater Superaerophilicity, Superhydrophobicity, underwater Superoleophobicity, and underwater superaerophobicity: a mini-review," *Frontiers in Chemistry*, vol. 8, p. 808, 2020.

[27] S. Das, S. Kumar, S. K. Samal, S. Mohanty, and S. K. Nayak, "A review on superhydrophobic polymer nanocoatings: recent development and applications," *Industrial and Engineering Chemistry Research*, vol. 57, no. 8, pp. 2727–2745, 2018.

[28] Z. Xue, M. Liu, and L. Jiang, "Recent developments in polymeric superoleophobic surfaces," *Journal of Polymer Science Part B: Polymer Physics*, vol. 50, no. 17, pp. 1209–1224, 2012.

[29] Y. Tian, B. Su, and L. Jiang, "Interfacial material system exhibiting superwettability," *Advanced Materials*, vol. 26, no. 40, pp. 6872–6897, 2014.

[30] L. Wen, Y. Tian, and L. Jiang, "Bioinspired super-wettability from fundamental research to practical applications," *Angewandte Chemie, International Edition*, vol. 54, no. 11, pp. 3387–3399, 2015.

[31] J. Jeevahan, M. Chandrasekaran, G. B. Joseph, R. B. Durairaj, and G. Mageshwaran, "Superhydrophobic surfaces: a review on fundamentals, applications, and challenges," *Journal of Coating Technology and Research*, vol. 15, no. 2, pp. 231–250, 2018.

[32] H. Bellanger, T. Darmanin, E. Taffin de Givenchy, and F. Guittard, "Chemical and physical pathways for the preparation of superoleophobic surfaces and related wetting theories," *Chemical Reviews*, vol. 114, no. 5, pp. 2694–2716, 2014.

[33] Z. Zhu, S. Zheng, S. Peng, Y. Zhao, and Y. Tian, "Superlyophilic interfaces and their applications," *Advanced Materials*, vol. 29, no. 45, p. 1703120, 2017.

[34] D. Wang, Q. Sun, M. J. Hokkanen et al., "Design of robust superhydrophobic surfaces," *Nature*, vol. 582, no. 7810, pp. 55–59, 2020.

[35] Y. Lu, S. Sathasivam, J. Song, C.-R. Crick, C.-J. Carmalt, and I.-P. Parkin, "Robust self-cleaning surfaces that function when exposed to either air or oil," *Science*, vol. 347, no. 6226, pp. 1132–1135, 2015.

[36] S. Nishimoto and B. Bhushan, "Bioinspired self-cleaning surfaces with superhydrophobicity, superoleophobicity, and superhydrophilicity," *RSC Advances*, vol. 3, no. 3, pp. 671–690, 2013.

[37] P. Ragesh, V. Anand Ganesh, S.-V. Nair, and A.-S. Nair, "A review on "Self-cleaning and multifunctional materials","

Journal of Materials Chemistry A, vol. 2, no. 36, pp. 14773–14797, 2014.

[38] J. Yong, F. Chen, Q. Yang et al., "Femtosecond laser weaving superhydrophobic patterned PDMS surfaces with tunable adhesion," *Journal of Physical Chemistry C*, vol. 117, no. 47, pp. 24907–24912, 2013.

[39] M. Wang, C. Chen, J. Ma, and J. Xu, "Preparation of superhydrophobic cauliflower-like silica nanospheres with tunable water adhesion," *Journal of Materials Chemistry*, vol. 21, no. 19, pp. 6962–6967, 2011.

[40] Z. Xue, Y. Cao, N. Liu, L. Feng, and L. Jiang, "Special wettable materials for oil/water separation," *Journal of Materials Chemistry A*, vol. 2, no. 8, pp. 2445–2460, 2014.

[41] B. Wang, W. Liang, Z. Guo, and W. Liu, "Biomimetic superlyophobic and super-lyophilic materials applied for oil/water separation: a new strategy beyond nature," *Chemical Society Reviews*, vol. 44, no. 1, pp. 336–361, 2015.

[42] R.-K. Gupta, G.-J. Dunderdale, M.-W. England, and A. Hozumi, "Oil/water separation techniques: a review of recent progresses and future directions," *Journal of Materials Chemistry A*, vol. 5, no. 31, pp. 16025–16058, 2017.

[43] J. Yong, J. Huo, F. Chen, Q. Yang, and X. Hou, "Oil/water separation based on natural materials with super-wettability: recent advances," *Physical Chemistry Chemical Physics*, vol. 20, no. 39, pp. 25140–25163, 2018.

[44] K.-W. Kwon, S.-S. Choi, S.-H. Lee et al., "Label-free, microfluidic separation and enrichment of human breast cancer cells by adhesion difference," *Lab on a Chip*, vol. 7, no. 11, pp. 1461–1468, 2007.

[45] A. Vitale, M. Quaglio, S.-L. Marasso, A. Chiodoni, M. Cocuzza, and R. Bongiovanni, "Direct photolithography of perfluoropolyethers for solvent-resistant microfluidics," *Langmuir*, vol. 29, no. 50, pp. 15711–15718, 2013.

[46] M.-J. Kreder, J. Alvarenga, P. Kim, and J. Aizenberg, "Design of anti-icing surfaces: smooth, textured or slippery?," *Nature Reviews Materials*, vol. 1, no. 1, pp. 1–15, 2016.

[47] J. Lv, Y. Song, L. Jiang, and J. Wang, "Bio-inspired strategies for anti-icing," *ACS Nano*, vol. 8, no. 4, pp. 3152–3169, 2014.

[48] E. Stratakis, A. Ranella, and C. Fotakis, "Biomimetic micro/nanostructured functional surfaces for microfluidic and tissue engineering applications," *Biomicrofluidics*, vol. 5, no. 1, article 013411, 2011.

[49] L. Shen, B. Wang, J. Wang, J. Fu, C. Picart, and J. Ji, "Asymmetric free-standing film with multifunctional anti-bacterial and self-cleaning properties," *ACS Applied Materials & Interfaces*, vol. 4, no. 9, pp. 4476–4483, 2012.

[50] J. Genzer and K. Efimenko, "Recent developments in superhydrophobic surfaces and their relevance to marine fouling: a review," *Biofouling*, vol. 22, no. 5, pp. 339–360, 2006.

[51] S. Zhang, J. Huang, Z. Chen, and Y. Lai, "Bioinspired special wettability surfaces: from fundamental research to water harvesting applications," *Small*, vol. 13, no. 3, p. 1602992, 2017.

[52] Y. Su, L. Chen, Y. Jiao et al., "Hierarchical hydrophilic/hydrophobic/bumpy Janus membrane fabricated by femtosecond laser ablation for highly efficient fog harvesting," *ACS Applied Materials & Interfaces*, vol. 13, no. 22, pp. 26542–26550, 2021.

[53] V. Jokinen, L. Sainiemi, and S. Franssila, "Complex droplets on chemically modified silicon nanograss," *Advanced Materials*, vol. 20, no. 18, pp. 3453–3456, 2008.

[54] E. Vazirinasab, R. Jafari, and G. Momen, "Application of superhydrophobic coatings as a corrosion barrier: a review," *Surface and Coatings Technology*, vol. 341, pp. 40–56, 2018.

[55] G. Barati Darband, M. Aliofkhazraei, S. Khorsand, S. Sokhanvar, and A. Kaboli, "Science and engineering of superhydrophobic surfaces: review of corrosion resistance, chemical and mechanical stability," *Arabian Journal of Chemistry*, vol. 13, no. 1, pp. 1763–1802, 2020.

[56] J. Songok, M. Tuominen, H. Teisala et al., "Paper-based microfluidics: fabrication technique and dynamics of capillary-driven surface flow," *ACS Applied Materials & Interfaces*, vol. 6, no. 22, pp. 20060–20066, 2014.

[57] S. Wang, T. Wang, P. Ge et al., "Controlling flow behavior of water in microfluidics with a chemically patterned anisotropic wetting surface," *Langmuir*, vol. 31, no. 13, pp. 4032–4039, 2015.

[58] F. Shi, J. Niu, J. Liu et al., "Towards understanding why a superhydrophobic coating is needed by water striders," *Advanced Materials*, vol. 19, no. 17, pp. 2257–2261, 2007.

[59] C. Lee, C.-H. Choi, and C.-J. Kim, "Superhydrophobic drag reduction in laminar flows: a critical review," *Experiments in Fluids*, vol. 57, no. 12, p. 176, 2016.

[60] J. Yong, Q. Yang, F. Chen et al., "A bioinspired planar superhydrophobic microboat," *Journal of Micromechanics and Microengineering*, vol. 24, no. 3, article 035006, 2014.

[61] Z. Zhan, M. ElKabbash, J. L. Cheng, J. Zhang, S. Singh, and C. Guo, "Highly floatable superhydrophobic metallic assembly for aquatic applications," *ACS Applied Materials & Interfaces*, vol. 11, no. 51, pp. 48512–48517, 2019.

[62] Q. Gong and W. Zhao, "Ultrafast science to capture ultrafast motions," *Ultrafast Science*, vol. 2021, article 9765859, 2 pages, 2021.

[63] Y. Kobayashi, C. Heide, H. K. Kelardeh et al., "Polarization flipping of even-order harmonics in monolayer transition-metal dichalcogenides," *Ultrafast Science*, vol. 2021, article 9820716, pp. 1–9, 2021.

[64] T. C. Chong, M. H. Hong, and L. P. Shi, "Laser precision engineering: from microfabrication to nanoprocessing," *Laser & Photonics Reviews*, vol. 4, no. 1, pp. 123–143, 2010.

[65] A. Y. Vorobyev and C. Guo, "Direct femtosecond laser surface nano/microstructuring and its applications," *Laser & Photonics Reviews*, vol. 7, no. 3, pp. 385–407, 2013.

[66] K. Sugioka and Y. Cheng, "Ultrafast lasers–reliable tools for advanced materials processing," *Light: Science & Applications*, vol. 3, no. 4, article e149, 2014.

[67] K. Sugioka and Y. Cheng, "Femtosecond laser three-dimensional micro- and nanofabrication," *Applied Physics Reviews*, vol. 1, no. 4, article 041303, 2014.

[68] J. Yong, F. Chen, Q. Yang, and X. Hou, "Femtosecond laser controlled wettability of solid surfaces," *Soft Matter*, vol. 11, no. 46, pp. 8897–8906, 2015.

[69] J. Yong, F. Chen, Q. Yang, Z. Jiang, and X. Hou, "A review of femtosecond-laser-induced underwater superoleophobic surfaces," *Advanced Materials Interfaces*, vol. 5, no. 7, p. 1701370, 2018.

[70] Y. Zhang, Y. Jiao, C. Li et al., "Bioinspired micro/nanostructured surfaces prepared by femtosecond laser direct writing for multi-functional applications," *International Journal of Extreme Manufacturing*, vol. 2, no. 3, article 032002, 2020.

[71] J. Yong, Q. Yang, C. Guo, F. Chen, and X. Hou, "A review of femtosecond laser-structured superhydrophobic or

underwater superoleophobic porous surfaces/materials for efficient oil/water separation," *RSC Advances*, vol. 9, no. 22, pp. 12470–12495, 2019.

[72] F. Xia and L. Jiang, "Bio-inspired, smart, multiscale interfacial materials," *Advanced Materials*, vol. 20, no. 15, pp. 2842–2858, 2008.

[73] J. Yong, F. Chen, Q. Yang, J. Huo, and X. Hou, "Superoleophobic surfaces," *Chemical Society Reviews*, vol. 46, no. 14, pp. 4168–4217, 2017.

[74] G. Wen, Z. Guo, and W. Liu, "Biomimetic polymeric superhydrophobic surfaces and nanostructures: from fabrication to applications," *Nanoscale*, vol. 9, no. 10, pp. 3338–3366, 2017.

[75] M. Cao and L. Jiang, "Superwettability integration: concepts, design and applications," *Surface Innovations*, vol. 4, no. 4, pp. 180–194, 2016.

[76] S. Wang and L. Jiang, "Definition of superhydrophobic states," *Advanced Materials*, vol. 19, no. 21, pp. 3423-3424, 2007.

[77] Y. Si and Z. Guo, "Superhydrophobic nanocoatings: from materials to fabrications and to applications," *Nanoscale*, vol. 7, no. 14, pp. 5922–5946, 2015.

[78] R. N. Wenzel, "Resistance of solid surfaces to wetting by water," *Industrial and Engineering Chemistry*, vol. 28, no. 8, pp. 988–994, 1936.

[79] A. B. D. Cassie and S. Baxter, "Wettability of porous surfaces," *Transactions of the Faraday Society*, vol. 40, pp. 546–551, 1944.

[80] B. N. Chichkov, C. Momma, S. Nolte, F. von Alvensleben, and A. Tünnermann, "Femtosecond, picosecond and nanosecond laser ablation of solids," *Applied Physics A: Materials Science & Processing*, vol. 63, no. 2, pp. 109–115, 1996.

[81] S. Küper and M. Stuke, "Ablation of UV-transparent materials with femtosecond UV excimer laser pulses," in *MRS Online Proceedings Library (OPL)*, vol. 129, pp. 375–384, Boston, Massachusetts, 1988.

[82] M. Y. Shen, C. H. Crouch, J. E. Carey, and E. Mazur, "Femtosecond laser-induced formation of submicrometer spikes on silicon in water," *Applied Physics Letters*, vol. 85, no. 23, pp. 5694–5696, 2004.

[83] D. Zhang, B. Ranjan, T. Tanaka, and K. Sugioka, "Underwater persistent bubble-assisted femtosecond laser ablation for hierarchical micro/nanostructuring," *International Journal of Extreme Manufacturing*, vol. 2, no. 1, article 015001, 2020.

[84] X.-Q. Liu, B.-F. Bai, Q.-D. Chen, and H.-B. Sun, "Etching-assisted femtosecond laser modification of hard materials," *Opto-Electronic Advances*, vol. 2, no. 9, article 190021, pp. 19002101–19002114, 2019.

[85] J. Yong, F. Chen, Q. Yang et al., "Rapid fabrication of large-area concave microlens arrays on PDMS by a femtosecond laser," *ACS Applied Materials & Interfaces*, vol. 5, no. 19, pp. 9382–9385, 2013.

[86] K. K. C. Lee, P. R. Herman, T. Shoa, M. Haque, J. D. W. Madden, and V. X. D. Yang, "Microstructuring of polypyrrole by maskless direct femtosecond laser ablation," *Advanced Materials*, vol. 24, no. 9, pp. 1243–1246, 2012.

[87] S. E. Kirkwood, A. C. Van Popta, Y. Y. Tsui, and R. Fedosejevs, "Single and multiple shot near-infrared femtosecond laser pulse ablation thresholds of copper," *Applied Physics A: Materials Science & Processing*, vol. 81, no. 4, pp. 729–735, 2005.

[88] D. Zhang and K. Sugioka, "Hierarchical microstructures with high spatial frequency laser induced periodic surface structures possessing different orientations created by femtosecond laser ablation of silicon in liquids," *Opto-Electronic Advances*, vol. 2, no. 3, article 190002, pp. 19000201–19000218, 2019.

[89] J. Yong, F. Chen, M. Li et al., "Remarkably simple achievement of superhydrophobicity, superhydrophilicity, underwater superoleophobicity, underwater superoleophilicity, underwater superaerophobicity, and underwater superaerophilicity on femtosecond laser ablated PDMS surfaces," *Journal of Materials Chemistry A*, vol. 5, no. 48, pp. 25249–25257, 2017.

[90] J. Yong, S. C. Singh, Z. Zhan, M. EIKabbash, F. Chen, and C. Guo, "Femtosecond-Laser-Produced Underwater "Superpolymphobic" Nanorippled Surfaces: Repelling Liquid Polymers in Water for Applications of Controlling Polymer Shape and Adhesion," *ACS applied nano Materials*, vol. 2, no. 11, pp. 7362–7371, 2019.

[91] D. B. Wolfe, J. B. Ashcom, J. C. Hwang, C. B. Schaffer, E. Mazur, and G. M. Whitesides, "Customization of poly(dimethylsiloxane) stamps by micromachining using a femtosecond-pulsed laser," *Advanced Materials*, vol. 15, no. 1, pp. 62–65, 2003.

[92] J. Bonse, S. Baudach, J. Krüger, W. Kautek, and M. Lenzner, "Femtosecond laser ablation of silicon-modification thresholds and morphology," *Applied Physics A: Materials Science & Processing*, vol. 74, no. 1, pp. 19–25, 2002.

[93] J. Yong, Q. Yang, J. Huo, X. Hou, and F. Chen, "Underwater gas self-transportation along the femtosecond laser-written open superhydrophobic surface microchannels (<100 μm) for gas/bubble manipulation," *International Journal of Extreme Manufacturing*, vol. 4, p. 110255, 2022.

[94] X. Bai, Q. Yang, Y. Fang et al., "Anisotropic, adhesion-switchable, and thermal-responsive superhydrophobicity on the femtosecond laser-structured shape-memory polymer for droplet manipulation," *Chemical Engineering Journal*, vol. 400, article 125930, 2020.

[95] J. Yong, F. Chen, Q. Yang, U. Farooq, and X. Hou, "Photoinduced switchable underwater superoleophobicity-superoleophilicity on laser modified titanium surfaces," *Journal of Materials Chemistry A*, vol. 3, no. 20, pp. 10703–10709, 2015.

[96] A. Y. Vorobyev and C. Guo, "Metal pumps liquid uphill," *Applied Physics Letters*, vol. 94, no. 22, article 224102, 2009.

[97] A. Y. Vorobyev and C. Guo, "Laser turns silicon superwicking," *Optics Express*, vol. 18, no. 7, pp. 6455–6460, 2010.

[98] A. Y. Vorobyev and C. Guo, "Water sprints uphill on glass," *Journal of Applied Physics*, vol. 108, no. 12, article 123512, 2010.

[99] T. Baldacchini, J. E. Carey, M. Zhou, and E. Mazur, "Superhydrophobic surfaces prepared by microstructuring of silicon using a femtosecond laser," *Langmuir*, vol. 22, no. 11, pp. 4917–4919, 2006.

[100] V. Zorba, E. Stratakis, M. Barberoglou et al., "Biomimetic artificial surfaces quantitatively reproduce the water repellency of a lotus leaf," *Advanced Materials*, vol. 20, no. 21, pp. 4049–4054, 2008.

[101] J. Yong, Q. Yang, F. Chen et al., "Stable superhydrophobic surface with hierarchical mesh-porous structure fabricated by a femtosecond laser," *Applied Physics A: Materials Science & Processing*, vol. 111, no. 1, pp. 243–249, 2013.

[102] J. Yong, Q. Yang, F. Chen et al., "A simple way to achieve superhydrophobicity, controllable water adhesion, anisotropic sliding, and anisotropic wetting based on femtosecond-laser-induced line-patterned surfaces," *Journal of Materials Chemistry A*, vol. 2, no. 15, pp. 5499–5507, 2014.

[103] J. Yong, Y. Fang, F. Chen et al., "Femtosecond laser ablated durable superhydrophobic PTFE films with micro-through-holes for oil/water separation: Separating oil from water and corrosive solutions," *Applied Surface Science*, vol. 389, pp. 1148–1155, 2016.

[104] X. Bai, Q. Yang, Y. Fang et al., "Superhydrophobicity-memory surfaces prepared by a femtosecond laser," *Chemical Engineering Journal*, vol. 383, article 123143, 2020.

[105] A.-M. Kietzig, S. G. Hatzikiriakos, and P. Englezos, "Patterned superhydrophobic metallic surfaces," *Langmuir*, vol. 25, no. 8, pp. 4821–4827, 2009.

[106] B. Wu, M. Zhou, J. Li, X. Ye, G. Li, and L. Cai, "Superhydrophobic surfaces fabricated by microstructuring of stainless steel using a femtosecond laser," *Applied Surface Science*, vol. 256, no. 1, pp. 61–66, 2009.

[107] A. Y. Vorobyev and C. Guo, "Multifunctional surfaces produced by femtosecond laser pulses," *Journal of Applied Physics*, vol. 117, no. 3, article 033103, 2015.

[108] J. Yong, F. Chen, Q. Yang et al., "Femtosecond laser induced hierarchical ZnO superhydrophobic surfaces with switchable wettability," *Chemical Communications*, vol. 51, no. 48, pp. 9813–9816, 2015.

[109] M. Zhou, H. F. Yang, B. J. Li et al., "Forming mechanisms and wettability of double-scale structures fabricated by femtosecond laser," *Applied Physics A: Materials Science & Processing*, vol. 94, no. 3, pp. 571–576, 2009.

[110] M. S. Ahsan, F. Dewanda, M. S. Lee, H. Sekita, and T. Sumiyoshi, "Formation of superhydrophobic soda-lime glass surface using femtosecond laser pulses," *Applied Surface Science*, vol. 265, pp. 784–789, 2013.

[111] Y. Lin, J. Han, M. Cai et al., "Durable and robust transparent superhydrophobic glass surfaces fabricated by a femtosecond laser with exceptional water repellency and thermostability," *Journal of Materials Chemistry A*, vol. 6, no. 19, pp. 9049–9056, 2018.

[112] X. Liu, H. Gu, M. Wang et al., "3D printing of bioinspired liquid superrepellent structures," *Advanced Materials*, vol. 30, no. 22, p. 1800103, 2018.

[113] J. Han, M. Cai, Y. Lin et al., "3D re-entrant nanograss on microcones for durable superamphiphobic surfaces via laser-chemical hybrid method," *Applied Surface Science*, vol. 456, pp. 726–736, 2018.

[114] J. Yong, F. Chen, Q. Yang et al., "Bioinspired underwater superoleophobic surface with ultralow oil-adhesion achieved by femtosecond laser microfabrication," *Journal of Materials Chemistry A*, vol. 2, no. 23, pp. 8790–8795, 2014.

[115] G. Li, Z. Zhang, P. Wu et al., "One-step facile fabrication of controllable microcone and micromolar silicon arrays with tunable wettability by liquid-assisted femtosecond laser irradiation," *RSC Advances*, vol. 6, no. 44, pp. 37463–37471, 2016.

[116] J. Zhang, F. Chen, Q. Yang et al., "A widely applicable method to fabricate underwater superoleophobic surfaces with low oil-adhesion on different metals by a femtosecond laser," *Applied Physics A: Materials Science & Processing*, vol. 123, no. 9, p. 594, 2017.

[117] G. Li, Y. Lu, P. Wu et al., "Fish scale inspired design of underwater superoleophobic microcone arrays by sucrose solution assisted femtosecond laser irradiation for multifunctional liquid manipulation," *Journal of Materials Chemistry A*, vol. 3, no. 36, pp. 18675–18683, 2015.

[118] J. Yong, F. Chen, Q. Yang et al., "Bioinspired transparent underwater superoleophobic and anti-oil surfaces," *Journal of Materials Chemistry A*, vol. 3, no. 18, pp. 9379–9384, 2015.

[119] J. Yong, F. Chen, Q. Yang et al., "Femtosecond laser controlling underwater oil-adhesion of glass surface," *Applied Physics A: Materials Science & Processing*, vol. 119, no. 3, pp. 837–844, 2015.

[120] J. Huo, Q. Yang, F. Chen et al., "Underwater transparent miniature "Mechanical hand" based on femtosecond laser-induced controllable oil-adhesive patterned glass for oil droplet manipulation," *Langmuir*, vol. 33, no. 15, pp. 3659–3665, 2017.

[121] J. Yong, F. Chen, Y. Fang et al., "Bioinspired design of underwater superaerophobic and superaerophilic surfaces by femtosecond laser ablation for anti- or capturing bubbles," *ACS Applied Materials & Interfaces*, vol. 9, no. 45, pp. 39863–39871, 2017.

[122] J. Yong, S. C. Singh, Z. Zhan, F. Chen, and C. Guo, "How to obtain six different superwettabilities on a same microstructured pattern: relationship between various superwettabilities in different solid/liquid/gas systems," *Langmuir*, vol. 35, no. 4, pp. 921–927, 2019.

[123] J. Yong, S. C. Singh, Z. Zhan, J. Huo, F. Chen, and C. Guo, "Reducing adhesion for dispensing tiny water/oil droplets and gas bubbles by femtosecond laser-treated needle nozzles: superhydrophobicity, superoleophobicity, and superaerophobicity," *ChemNanoMat*, vol. 5, no. 2, pp. 241–249, 2019.

[124] J. Yong, F. Chen, J. Huo et al., "Femtosecond laser induced underwater superaerophilic and superaerophobic PDMS sheets with through microholes for selective passage of air bubbles and further collection of underwater gas," *Nanoscale*, vol. 10, no. 8, pp. 3688–3696, 2018.

[125] J. Huo, J. Yong, F. Chen, Q. Yang, Y. Fang, and X. Hou, "Trapped air-induced reversible transition between underwater superaerophilicity and superaerophobicity on the femtosecond laser-ablated superhydrophobic PTFE surfaces," *Advanced Materials Interfaces*, vol. 6, no. 17, p. 1900262, 2019.

[126] J. Yong, S. C. Singh, Z. Zhan, F. Chen, and C. Guo, "Substrate-independent, fast, and reversible switching between underwater superaerophobicity and aerophilicity on the femtosecond laser-induced superhydrophobic surfaces for selectively repelling or capturing bubbles in water," *ACS Applied Materials & Interfaces*, vol. 11, no. 8, pp. 8667–8675, 2019.

[127] H. Chen, P. Zhang, L. Zhang et al., "Continuous directional water transport on the peristome surface of *Nepenthes alata*," *Nature*, vol. 532, no. 7597, pp. 85–89, 2016.

[128] J. Yong, J. Huo, Q. Yang et al., "Femtosecond laser direct writing of porous network microstructures for fabricating superslippery surfaces with excellent liquid repellence and anti-cell proliferation," *Advanced Materials Interfaces*, vol. 5, no. 7, p. 1701479, 2018.

[129] J. Yong, F. Chen, Q. Yang et al., "NepenthesInspired design of self-repairing omniphobic slippery liquid infused porous surface (SLIPS) by femtosecond laser direct writing," *Advanced Materials Interfaces*, vol. 4, no. 20, p. 1700552, 2017.

[130] Y. Fang, J. Liang, X. Bai et al., "Magnetically controllable isotropic/anisotropic slippery surface for flexible droplet manipulation," *Langmuir*, vol. 36, no. 50, pp. 15403–15409, 2020.

[131] Y. Cheng, Q. Yang, Y. Lu et al., "A Femtosecond Bessel laser for preparing a nontoxic slippery liquid-infused porous surface (SLIPS) for improving the hemocompatibility of NiTi alloys," *Biomaterials Science*, vol. 8, no. 23, pp. 6505–6514, 2020.

[132] Y. Fang, J. Yong, Y. Cheng, Q. Yang, X. Hou, and F. Chen, "Liquid infused slippery stainless steel surface prepared by alcohol-assisted femtosecond laser ablation," *Advanced Materials Interfaces*, vol. 8, no. 5, p. 2001334, 2021.

[133] Y. Jiao, X. Lv, Y. Zhang et al., "Pitcher plant-bioinspired bubble slippery surface fabricated by femtosecond laser for buoyancy driven bubble self-transport and efficient gas capture," *Nanoscale*, vol. 11, no. 3, pp. 1370–1378, 2019.

[134] J. Wang, G. Cai, S. Li, D. Gao, J. Xiong, and P. S. Lee, "Printable superelastic conductors with extreme stretchability and robust cycling endurance enabled by liquid-metal particles," *Advanced Materials*, vol. 30, no. 16, p. 1706157, 2018.

[135] C. Zhang, Q. Yang, C. Shan et al., "Tuning a surface superrepellent to liquid metal by a femtosecond laser," *RSC Advances*, vol. 10, no. 6, pp. 3301–3306, 2020.

[136] T. Darmanin and F. Guittard, "Recent advances in the potential applications of bioinspired superhydrophobic materials," *Journal of Materials Chemistry A*, vol. 2, no. 39, pp. 16319–16359, 2014.

[137] P. Roach, N. J. Shirtcliffe, and M. I. Newton, "Progess in superhydrophobic surface development," *Soft Matter*, vol. 4, no. 2, pp. 224–240, 2008.

[138] C.-H. Xue and J.-Z. Ma, "Long-lived superhydrophobic surfaces," *Journal of Materials Chemistry A*, vol. 1, no. 13, pp. 4146–4161, 2013.

[139] K. Liu and L. Jiang, "Bio-inspired self-cleaning surfaces," *Annual Review of Materials Research*, vol. 42, no. 1, pp. 231–263, 2012.

[140] M. Barberoglou, V. Zorba, E. Stratakis et al., "Bio-inspired water repellent surfaces produced by ultrafast laser structuring of silicon," *Applied Surface Science*, vol. 255, no. 10, pp. 5425–5429, 2009.

[141] D. Zhang, F. Chen, Q. Yang et al., "A simple way to achieve pattern-dependent tunable adhesion in superhydrophobic surfaces by a femtosecond laser," *ACS Applied Materials & Interfaces*, vol. 4, no. 9, pp. 4905–4912, 2012.

[142] D. Zhang, F. Chen, Q. Yang, J. Si, and X. Hou, "Mutual wetting transition between isotropic and anisotropic on directional structures fabricated by femotosecond laser," *Soft Matter*, vol. 7, no. 18, pp. 8337–8342, 2011.

[143] F. Chen, D. Zhang, Q. Yang et al., "Anisotropic wetting on microstrips surface fabricated by femtosecond laser," *Langmuir*, vol. 27, no. 1, pp. 359–365, 2011.

[144] J. Yong, Q. Yang, F. Chen et al., "Superhydrophobic PDMS surfaces with three-dimensional (3D) pattern-dependent controllable adhesion," *Applied Surface Science*, vol. 288, pp. 579–583, 2014.

[145] J. Yong, F. Chen, Q. Yang et al., "Controllable adhesive superhydrophobic surfaces based on PDMS microwell arrays," *Langmuir*, vol. 29, no. 10, pp. 3274–3279, 2013.

[146] J. Yong, Q. Yang, F. Chen et al., "Bioinspired superhydrophobic surfaces with directional adhesion," *RSC Advances*, vol. 4, no. 16, pp. 8138–8143, 2014.

[147] Y. Fang, J. Yong, F. Chen et al., "Bioinspired fabrication of bi/tridirectionally anisotropic sliding superhydrophobic PDMS surfaces by femtosecond laser," *Advanced Materials Interfaces*, vol. 5, no. 6, p. 1701245, 2018.

[148] Y. Fang, J. Yong, F. Chen et al., "Durability of the tunable adhesive superhydrophobic PTFE surfaces for harsh environment applications," *Applied Physics A*, vol. 122, no. 9, p. 827, 2016.

[149] N. Zheng, G. Fang, Z. Cao, Q. Zhao, and T. Xie, "High strain epoxy shape memory polymer," *Polymer Chemistry*, vol. 6, no. 16, pp. 3046–3053, 2015.

[150] B. Q. Y. Chan, Z. W. K. Low, S. J. W. Heng, S. Y. Chan, C. Owh, and X. J. Loh, "Recent advances in shape memory soft materials for biomedical applications," *ACS Applied Materials & Interfaces*, vol. 8, no. 16, pp. 10070–10087, 2016.

[151] X. Bai, J. Yong, C. Shan, Y. Fang, X. Hou, and F. Chen, "Remote, selective, and in situ manipulation of liquid droplets on a femtosecond laser-structured superhydrophobic shape-memory polymer by near-infrared light," *Science China Chemistry*, vol. 64, no. 5, pp. 861–872, 2021.

[152] https://en.wikipedia.org/wiki/Icing_conditions.

[153] X. Gong, X. Gao, and L. Jiang, "Recent progress in bionic condensate microdrop self-propelling surfaces," *Advanced Materials*, vol. 29, no. 45, p. 1703002, 2017.

[154] S.-J. Pan, A.-K. Kota, J.-M. Mabry, and A. Tuteja, "Superomniphobic surfaces for effective chemical shielding," *Journal of the American Chemical Society*, vol. 135, no. 2, pp. 578–581, 2013.

[155] S. C. Singh, M. ElKabbash, Z. Li et al., "Solar-trackable super-wicking black metal panel for photothermal water sanitation," *Nature Sustainability*, vol. 3, no. 11, pp. 938–946, 2020.

[156] W. Liu, P. Fan, M. Cai et al., "An integrative bioinspired venation network with ultra-contrasting wettability for large-scale strongly self-driven and efficient water collection," *Nanoscale*, vol. 11, no. 18, pp. 8940–8949, 2019.

[157] R. Pan, H. Zhang, and M. Zhong, "Triple-scale superhydrophobic surface with excellent anti-icing and icephobic performance via ultrafast laser hybrid fabrication," *ACS Applied Materials & Interfaces*, vol. 13, no. 1, pp. 1743–1753, 2021.

[158] A. Wang, L. Jiang, X. Li et al., "Low-adhesive superhydrophobic surface-enhanced Raman spectroscopy substrate fabricated by femtosecond laser ablation for ultratrace molecular detection," *Journal of Materials Chemistry B*, vol. 5, no. 4, pp. 777–784, 2017.

[159] A. Ranella, M. Barberoglou, S. Bakogianni, C. Fotakis, and E. Stratakis, "Tuning cell adhesion by controlling the roughness and wettability of 3D micro/nano silicon structures," *Acta Biomaterialia*, vol. 6, no. 7, pp. 2711–2720, 2010.

[160] W. Zheng, J. Huang, S. Li et al., "Advanced materials with special wettability toward intelligent oily wastewater remediation," *ACS Applied Materials & Interfaces*, vol. 13, no. 1, pp. 67–87, 2021.

[161] F. Ren, G. Li, Z. Zhang et al., "A single-layer Janus membrane with dual gradient conical micropore arrays for self-driving fog collection," *Journal of Materials Chemistry A*, vol. 5, no. 35, pp. 18403–18408, 2017.

[162] K. Yin, H. Du, X. Dong, C. Wang, J.-A. Duan, and J. He, "A simple way to achieve bioinspired hybrid wettability surface with micro/nanopatterns for efficient fog collection," *Nanoscale*, vol. 9, no. 38, pp. 14620–14626, 2017.

[163] A. Tuteja, W. Choi, M. Ma et al., "Designing superoleophobic surfaces," *Science*, vol. 318, no. 5856, pp. 1618–1622, 2007.

[164] A. Tuteja, W. Choi, J. M. Mabry, G. H. McKinley, and R. E. Cohen, "Robust omniphobic surfaces," *Proceedings of the National Academy of Sciences of the United States of America*, vol. 105, no. 47, pp. 18200–18205, 2008.

[165] R. Helbig, J. Nickerl, C. Neinhuis, and C. Werner, "Smart skin patterns protect springtails," *PLoS One*, vol. 6, no. 9, p. 25105, 2011.

[166] S. Dong, X. Zhang, Q. Li et al., "Springtail-inspired superamphiphobic ordered nanohoodoo arrays with quasi-doubly reentrant structures," *Small*, vol. 16, no. 19, p. 2000779, 2020.

[167] G.-T. Yun, W.-B. Jung, M. S. Oh et al., "Springtail-inspired superomniphobic surface with extreme pressure resistance," *Science Advances*, vol. 4, no. 8, p. eaat4978, 2018.

[168] Z. Chu and S. Seeger, "Superamphiphobic surfaces," *Chemical Society Reviews*, vol. 43, no. 8, pp. 2784–2798, 2014.

[169] H. Liu, Y. Wang, J. Huang, Z. Chen, G. Chen, and Y. Lai, "Bioinspired surfaces with superamphiphobic properties: concepts, synthesis, and applications," *Advanced Functional Materials*, vol. 28, no. 19, p. 1707415, 2018.

[170] A.-K. Kota, G. Kwon, and A. Tuteja, "The design and applications of superomniphobic surfaces," *NPG Asia Materials*, vol. 6, no. 7, article e109, 2014.

[171] B. Zhang, Y. Zeng, J. Wang, Y. Sun, J. Zhang, and Y. Li, "Superamphiphobic aluminum alloy with low sliding angles and acid-alkali liquids repellency," *Materials & Design*, vol. 188, article 108479, 2020.

[172] X. Han, J. Peng, S. Jiang, J. Xiong, Y. Song, and X. Gong, "Robust superamphiphobic coatings based on raspberry-like hollow SnO2Composites," *Langmuir*, vol. 36, no. 37, pp. 11044–11053, 2020.

[173] Y. Cai, L. Lin, Z. Xue, M. Liu, S. Wang, and L. Jiang, "Filefish-inspired surface design for anisotropic underwater oleophobicity," *Advanced Functional Materials*, vol. 24, no. 6, pp. 809–816, 2014.

[174] L.-P. Xu, J. Zhao, B. Su et al., "An ion-induced low-oil-adhesion organic/inorganic hybrid film for stable superoleophobicity in seawater," *Advanced Materials*, vol. 25, no. 4, pp. 606–611, 2013.

[175] X. Liu, J. Zhou, Z. Xue et al., "Clam's shell inspired high-energy inorganic coatings with underwater low adhesive superoleophobicity," *Advanced Materials*, vol. 24, no. 25, pp. 3401–3405, 2012.

[176] Z. Wang, L. Zhu, W. Li, and H. Liu, "Bioinspired in situ growth of conversion films with underwater superoleophobicity and excellent self-cleaning performance," *ACS Applied Materials & Interfaces*, vol. 5, no. 21, pp. 10904–10911, 2013.

[177] Y.-Q. Liu, Y.-L. Zhang, X.-Y. Fu, and H.-B. Sun, "Bioinspired underwater superoleophobic membrane based on a graphene oxide coated wire mesh for efficient oil/water separation," *ACS Applied Materials & Interfaces*, vol. 7, no. 37, pp. 20930–20936, 2015.

[178] D. Wu, S. Wu, Q. Chen et al., "Facile creation of hierarchical PDMS microstructures with extreme underwater superoleophobicity for anti-oil application in microfluidic channels," *Lab on a Chip*, vol. 11, no. 22, pp. 3873–3879, 2011.

[179] J. Zhou, A. V. Ellis, and N. H. Voelcker, "Recent developments in PDMS surface modification for microfluidic devices," *Electrophoresis*, vol. 31, no. 1, pp. 2–16, 2010.

[180] M. Li, Q. Yang, J. Yong et al., "Underwater superoleophobic and anti-oil microlens array prepared by combing femtosecond laser wet etching and direct writing techniques," *Optics Express*, vol. 27, no. 24, pp. 35903–35913, 2019.

[181] Y. Cheng, Q. Yang, Y. Fang, J. Yong, F. Chen, and X. Hou, "Underwater anisotropic 3D superoleophobic tracks applied for the directional movement of oil droplets and the microdroplets reaction," *Advanced Materials Interfaces*, vol. 6, no. 10, p. 1900067, 2019.

[182] G. Li, H. Fan, F. Ren et al., "Multifunctional ultrathin aluminum foil: oil/water separation and particle filtration," *Journal of Materials Chemistry A*, vol. 4, no. 48, pp. 18832–18840, 2016.

[183] K. Yin, D. Chu, X. Dong, C. Wang, J.-A. Duan, and J. He, "Femtosecond laser induced robust periodic nanoripple structured mesh for highly efficient oil-water separation," *Nanoscale*, vol. 9, no. 37, pp. 14229–14235, 2017.

[184] J. Yong, Q. Yang, F. Chen et al., "Using an "underwater superoleophobic pattern" to make a liquid lens array," *RSC Advances*, vol. 5, no. 51, pp. 40907–40911, 2015.

[185] C. Yu, P. Zhang, J. Wang, and L. Jiang, "Superwettability of gas bubbles and its application: from bioinspiration to advanced materials," *Advanced Materials*, vol. 29, no. 45, p. 1703053, 2017.

[186] J. E. George, S. Chidangil, and S. D. George, "Recent progress in fabricating superaerophobic and superaerophilic surfaces," *Advanced Materials Interfaces*, vol. 4, no. 9, p. 1601088, 2017.

[187] X. Liu, F. Yang, J. Guo, J. Fu, and Z. Guo, "New insights into unusual droplets: from mediating the wettability to manipulating the locomotion modes," *Chemical Communications*, vol. 56, no. 94, pp. 14757–14788, 2020.

[188] X. Tang, Y. Tian, X. Tian et al., "Design of multi-scale textured surfaces for unconventional liquid harnessing," *Materials Today*, vol. 43, pp. 62–83, 2021.

[189] J. Huo, Q. Yang, J. Yong et al., "Underwater superaerophobicity/superaerophilicity and unidirectional bubble passage based on the femtosecond laser-structured stainless steel mesh," *Advanced Materials Interfaces*, vol. 7, no. 14, p. 1902128, 2020.

[190] Y. Hu, W. Qiu, Y. Zhang et al., "Channel-controlled Janus membrane fabricated by simultaneous laser ablation and nanoparticles deposition for underwater bubbles manipulation," *Applied Physics Letters*, vol. 114, no. 17, article 173701, 2019.

[191] J. Yong, F. Chen, W. Li et al., "Underwater superaerophobic and superaerophilic nanoneedles-structured meshes for water/bubbles separation: removing or collecting gas bubbles in water," *Global Challenges*, vol. 2, no. 4, p. 1700133, 2018.

[192] J. Song, Z. Liu, X. Wang et al., "High-efficiency bubble transportation in an aqueous environment on a serial wedge-shaped wettability pattern," *Journal of Materials Chemistry A*, vol. 7, no. 22, pp. 13567–13576, 2019.

[193] R. S. Seymour and S. K. Hetz, "The diving bell and the spider: the physical gill ofArgyroneta aquatica," *The Journal of Experimental Biology*, vol. 214, no. 13, pp. 2175–2181, 2011.

[194] F. van Breugel and M. H. Dickinson, "Superhydrophobic diving flies (Ephydra hians) and the hypersaline waters of mono lake," *Proceedings of the National Academy of Sciences of the United States of America*, vol. 114, no. 51, pp. 13483–13488, 2017.

[195] W. Barthlott, T. Schimmel, S. Wiersch et al., "The Salvinia paradox: superhydrophobic surfaces with hydrophilic pins for air retention under water," *Advanced Materials*, vol. 22, no. 21, pp. 2325–2328, 2010.

[196] Z. Liu, H. Zhang, Y. Han et al., "Superaerophilic wedge-shaped channels with precovered air film for efficient sub-aqueous Bubbles/Jet transportation and continuous oxygen supplementation," *ACS Applied Materials & Interfaces*, vol. 11, no. 26, pp. 23808–23814, 2019.

[197] Z. Li, C. Cao, Z. Zhu, J. Liu, W. Song, and L. Jiang, "Superaerophilic materials are surprising catalysts: wettability-induced excellent hydrogenation activity under ambient H2 Pressure," *Advanced Materials Interfaces*, vol. 5, no. 22, p. 1801259, 2018.

[198] C. Tu, Q. Yang, Y. Chen et al., "Anisotropic spreading of bubbles on superaerophilic straight trajectories beneath a slide in water," *Water*, vol. 12, no. 3, p. 798, 2020.

[199] C. Chen, L. A. Shi, Z. Huang et al., "Microhole-arrayed PDMS with controllable wettability gradient by one-step femtosecond laser drilling for ultrafast underwater bubble unidirectional self-transport," *Advanced Materials Interfaces*, vol. 6, no. 12, p. 1900297, 2019.

[200] J. Huo, X. Bai, J. Yong et al., "How to adjust bubble's adhesion on solid in aqueous media: Femtosecond laser- ablated patterned shape-memory polymer surfaces to achieve bubble multi- manipulation," *Chemical Engineering Journal*, vol. 414, article 128694, 2021.

[201] J. Yong, J. Zhuang, X. Bai et al., "Water/gas separation based on the selective bubble-passage effect of underwater superaerophobic and superaerophilic meshes processed by a femtosecond laser," *Nanoscale*, vol. 13, no. 23, pp. 10414–10424, 2021.

[202] S. Zhu, J. Li, S. Cai et al., "Unidirectional transport and effective collection of underwater CO2Bubbles utilizing ultrafast-laser-ablated Janus foam," *ACS Applied Materials & Interfaces*, vol. 12, no. 15, pp. 18110–18115, 2020.

[203] T. S. Wong, S. H. Kang, S. K. Y. Tang et al., "Bioinspired self-repairing slippery surfaces with pressure-stable omniphobicity," *Nature*, vol. 477, no. 7365, pp. 443–447, 2011.

[204] J. Yong, Q. Yang, X. Hou, and F. Chen, "Underwater superpolymphobicity: concept, achievement, and applications," *Nano Select*, vol. 2, no. 6, pp. 1011–1022, 2021.

[205] J. Yong, Z. Zhan, S. C. Singh, F. Chen, and C. Guo, "Femtosecond laser-structured underwater "Superpolymphobic" surfaces," *Langmuir*, vol. 35, no. 28, pp. 9318–9322, 2019.

[206] J. Yong, Z. Zhan, S. C. Singh, F. Chen, and C. Guo, "Microfluidic channels fabrication based on underwater superpolymphobic microgrooves produced by femtosecond laser direct writing," *ACS Applied Polymer Materials*, vol. 1, no. 11, pp. 2819–2825, 2019.

[207] J. Yong, X. Bai, Q. Yang, X. Hou, and F. Chen, "Filtration and removal of liquid polymers from water (polymer/water separation) by use of the underwater superpolymphobic mesh produced with a femtosecond laser," *Journal of Colloid and Interface Science*, vol. 582, pp. 1203–1212, 2021.

[208] J. Yong, Q. Yang, J. Huo, X. Hou, and F. Chen, "Superwettability-based separation: from oil/water separation to polymer/water separation and bubble/water separation," *Nano Select*, vol. 2, no. 8, pp. 1580–1588, 2021.

[209] L. Sheng, Z. He, Y. Yao, and J. Liu, "Transient state machine enabled from the colliding and coalescence of a swarm of autonomously running Liquid Metal motors," *Small*, vol. 11, no. 39, pp. 5253–5261, 2015.

[210] M. G. Mohammed and R. Kramer, "All-printed flexible and stretchable electronics," *Advanced Materials*, vol. 29, no. 19, p. 1604965, 2017.

[211] M. D. Dickey, "Stretchable and soft electronics using Liquid Metals," *Advanced Materials*, vol. 29, no. 27, p. 1606425, 2017.

[212] B. J. Carey, J. Z. Ou, R. M. Clark et al., "Wafer-scale two-dimensional semiconductors from printed oxide skin of liquid metals," *Nature Communications*, vol. 8, no. 1, p. 14482, 2017.

[213] J. Yong, C. Zhang, X. Bai et al., "Designing "Supermetalphobic" surfaces that greatly repel liquid metal by femtosecond laser processing: does the surface chemistry or microstructure play a crucial role?," *Advanced Materials Interfaces*, vol. 7, no. 6, p. 1901931, 2020.

[214] J. Zhang, K. Zhang, J. Yong et al., "Femtosecond laser preparing patternable liquid-metal-repellent surface for flexible electronics," *Journal of Colloid Science*, vol. 578, pp. 146–154, 2020.

[215] J. Zhang, J. Yong, C. Zhang et al., "Liquid metal-based reconfigurable and repairable electronics designed by a femtosecond laser," *ACS Applied Electronic Materials*, vol. 2, no. 8, pp. 2685–2691, 2020.

[216] C. Zhang, Q. Yang, J. Yong et al., "Guiding magnetic liquid metal for flexible circuit," *International Journal of Extreme Manufacturing*, vol. 3, no. 2, article 025102, 2021.

[217] H. Wu, L. Zhang, S. Jiang et al., "Ultrathin and high-stress-resolution liquid-metal-based pressure sensors with simple device structures," *ACS Applied Materials & Interfaces*, vol. 12, no. 49, pp. 55390–55398, 2020.